

Wireless Power Transfer

by

Fernando Moreno

A Thesis Presented in Partial Fulfillment  
of the Requirements for the Degree  
Master of Science

Approved April 2015 by the  
Graduate Supervisory Committee:

Rodolfo Diaz, Chair  
James Aberle  
Michael Kozicki

ARIZONA STATE UNIVERSITY

May 2015

## ABSTRACT

A new loop configuration capable of reducing power radiation magnitudes lower than conventional loops has been developed. This configuration is demonstrated for the case of two coaxial loops of 0.1 meter radius coupled via the magnetic reactive field. Utilizing electromagnetism theory, techniques from antenna design and a new near field design initiative, the ability to design a magnetic field has been investigated by using a full wave simulation tool. The method for realization is initiated from first order physics model, ADS and onto a full wave situation tool for the case of a non-radiating helical loop. The exploration into the design of a magnetic near field while mitigating radiation power is demonstrated using an real number of twists to form a helical wire loop while biasing the integer twisted loop in a non-conventional moebius termination. The helix loop setup as a moebius loop convention can also be expressed as a shorted antenna scheme. The 0.1 meter radius helix antenna is biased with a 1MHz frequency that categorized the antenna loop as electrically small. It is then demonstrated that helical configuration reduces the electric field and mitigates power radiation into the far field. In order to compare the radiated power reduction performance of the helical loop a shielded loop is used as a baseline for comparison. The shielded loop system of the same geometric size and frequency is shown to have power radiation expressed as -46.1 dBm. The power radiated mitigation method of the helix loop reduces the power radiated from the two loop system down to -98.72 dBm.

## DEDICATION

This dedication is to identify all of those who encouraged me in my pursuit of a higher education. Thanks for encouraging me to keep going no matter what came. I want to thank my mother Margaret De Alejandro Moreno for everything she did to encourage me in the pursuit of a higher education. Thank you mom, I really appreciate you. I want to thank my father Fernando Urbano Moreno for also encouraging me in pursuit of a higher education. Thank you dad, I really appreciate you. I want to thank my grandmother Felipa De Alejandro for teaching me in life that I need to go to school so I can “catch money”. May God continually give her rest in Heaven. I also want to thank my sisters and brother for encouraging me to succeed in life. Thank you Rochelle, Bessie and Daniel for being such great siblings. To my son, whom I love, and pray to God that he makes good choices in life to avoid working as hard as I had to for this education. Work hard, be honest, and most of all my Son, fear God. The footsteps of the righteous are established by the Lord, and the Lord delights in his way (Psalms 37:23).

## ACKNOWLEDGMENTS

This Thesis would never have been written if not for the abilities and leadership of Dr. Rodolfo E. Diaz through the decade of undergraduate, graduate and industry interactions. Thank you Rudy, I really appreciate you. To Dr. James Aberle, thank you very much for talking me into entering graduate school and also for sponsoring me to begin graduate school early, before I graduated, with my undergraduate degree. Thank you James, I really appreciate you. Finally, thank you Dr. Kozicki for being such a humble mentor and giving me a path to pursue this thesis. Thank you Michael, I really appreciate you.

## TABLE OF CONTENTS

	Page
LIST OF TABLES.....	vi
LIST OF FIGURES.....	vii
CHAPTER	
1 INTRODUCTION.....	1
Organization.....	1
2 BASELINE PROPERTIES OF A POWERTRANSFER SYSTEM: LARGE AND	
Small Loop System.....	3
Description of Power Transfer System Relevant Theory.....	3
The Impedance and Admittance Matrix.....	4
Mutual Impedance of the Two Loop System.....	6
Mutual Inductance.....	6
Magneto-Statics Approach.....	7
Magneto-Statics Inductance Equations.....	7
Hz/Bz on the Axis of Loop.....	7
Mutual Inductance Using Elliptical Functions.....	8
Magnetic Dipole Approach.....	8
Electrodynamics - Flux Section Small Loop As Source.....	9
Considerations for Computational Calculations.....	11
Flux Results From Each Method.....	11
Discussion.....	16
3 POWER TRANSFER PROPERTIES OF THE TWO LOOP SYSTEM.....	18

CHAPTER	Page
Background for Application.....	18
Application of Transducer Theory.....	19
Ohmic Loss and Impedance Assumed at Feed.....	20
Radiation Resistance and Radiation Conductance .....	21
Impedance/Conductance Models .....	23
Self Capacitance ( $Z_{11}$ or $Z_{22}$ ).....	23
Self Inductance/Self Impedance ( $Z_{11}$ or $Z_{22}$ ) .....	23
Mutual Impedance by Reaction Integral.....	24
Connecting a Load to Loop 2: Derivation for $Z_{IN}$ .....	26
Real Power Transfer Parameters for Transducer Efficiency.....	28
Tuning For Power Transfer Efficiency Under Resonance Condition.....	30
Resonance Tuning Conditions .....	31
Verification of Mathcad Models Using Ads Simulations .....	31
Efficiency Comparisons of Loop Tuning with a 10-OHM Battery Load.....	51
Efficiency Comparisons of Loop Tuning with a 300-OHM Battery Load.....	54
Efficiency Comparisons Discussion .....	57
Discussion.....	59
<b>4 SHIELDED LOOP POWER TRANSFER PROPERTIES TWO LOOP</b>	
<b>SYSTEM.....</b>	<b>61</b>
Introduction Background for Shielded Loops .....	61
Two Loop Coupling System Methodology .....	63
HFSS S-Matrix Untuned Shielded Loop Results .....	65

CHAPTER	Page
HFSS Wireless Power Transfer Models Untuned Loops.....	68
Post Processing Of Shielded Loop HFSS Simulation.....	70
Discussion.....	70
<b>5 HELIX LOOP INVESTIGATION OF THE TWO LOOP SYSTEM .....</b>	<b>72</b>
Introduction Background For Helix Loops.....	72
HFSS Setup.....	72
HFSS Tetrahedral Defaults .....	73
HFSS Poly-Line Setup for Field Plotting .....	73
Single Flat Loop .....	74
Contour Plots of Single Flat Loop by Electrically Small Phenomenon .....	75
Single Loop Helix Of 4-Cycles.....	81
Contour Plots Of Single Helical Loop By Electrically Small Phenomenon .....	83
Helix Loop Of 4-Cycles .....	89
Contour Plot Of Helix Loop By Electrically Small Phenomenon .....	91
Discussion.....	96
<b>6 PERFORMANCE CHARACTERISTICS FOR A TWO LOOP SYSTEM.....</b>	<b>98</b>
Introduction Of Loop Comparison.....	98
Shielded Loop Power Transfer .....	99
Shielded Loop Power Radiation .....	100
Four Cycle Helix Loop Power Transfer .....	100
Four Cycle Helix Loop Power Radiation .....	102
Zero Cycle Helix Loop Power Transfer .....	102

CHAPTER	Page
Zero Cycle Helix Loop Power Radiation .....	104
Discussion Of Wireless Power Transfer Systems .....	104
7 WIRELESS POWER TRANSFER CONCLUSION .....	106
Introduction Chapter Summary.....	106
Baseline Properties Of Power Transfer System Summary .....	106
Power Transfer Properties Of Two Loops Summary .....	107
Shielded Loop Power Transfer Properties Summary .....	108
Helix Loop Investigation Summary.....	108
Conclusion A Two Loop System.....	109
REFERENCES.....	111
APPENDIX	
A WIRELESS POWER TRANSFER MODELS.....	113



## LIST OF TABLES

Table	Page
1. Mathcad Simulations Compared to Respective Ads Simulations .....	50
2. Percent Error Between Mathcad and Ads Results .....	50
3. Power Transfer Efficiency for Each Turning Circuit .....	51
4. S-Parameters of Two Shielded Loops With Neck Feeds 180 Degrees Apart .....	69
5. Wireless Power Transfer Model S-Paramters of the Two Loops.....	69
6. Percent Error S-Paramteris for Two Methods of the Two Loops .....	70
7. Performance Summor of Wireless Power Transfer Characteristics.....	105

## LIST OF FIGURES

Figure	Page
1. Magneto Static Flux Along The Axis Of A Loop .....	12
2. Elliptical Function Flux Along The Axis Of The Loops .....	13
3. Magneto Static B-Field Of A Magnetic Dipole .....	14
4. Magneto Dynamic B-Field Of A Magnetic Dipole .....	15
5. Magneto Statics, Elliptical, Static Dipole, Dynamic Dipole.....	16
6. Schelkunoff Admittance Circuit Model Of A Loop Antenna .....	22
7. S-S Equivalent Circuit To Simulate The Power Transfer Loop To Loop.....	32
8. Current On Source Loop Of S-S Tuning Configuration With A 10 Ohm Load .....	33
9. Current On Receiver Loop Of S-S Tuning Configuration With A 10 Ohm Load ....	33
10. Voltage On Receiver Loop Of S-S Tuning Configuration With A 10 Ohm Load ...	34
11. Ads Graphical Power Calculation .....	35
12. Real Power On Source Loop Of S-S Tuning Configuration With A 10 Ohm .....	36
13. Real Power On Receiver Loop Of S-S Tuning Configuration With A 10 Ohm Load.....	36
14. S-P Equivalent Tuning Circuit For Power Transfer Of The Source Loop To The Receiver Loop As Designed In Ads.....	37
15. Current On Source Loop Of S-P Tuning Configuration With A 10 Ohm Load Plotted Against Frequency .....	37
16. Current On Receiver Loop Of S-P Tuning Configuration With A 10 Ohm Load Plotted Against Frequency .....	39

Figure	Page
17. Voltage On Receiver Loop Of S-P Tuning Configuration With A 10 Ohm Load Plotted Against Frequency .....	39
18. Real Power On Source Loop Of S-P Tuning Configuration With A 10 Ohm Load Plotted Against Frequency .....	40
19. Real Power On Receiver Loop Of S-P Tuning Configuration With A 10 Ohm Load Plotted Against Frequency .....	41
20. P-S Equivalent Tuning Circuit For Power Transfer Of The Source Loop To The Receiver Loop As Designed In Ads .....	42
21. Current On Source Loop Of P-S Tuning Configuration With A 10 Ohm Load Plotted Against Frequency .....	42
22. Current On Receiver Loop Of P-S Tuning Configuration With A 10 Ohm Load Plotted Against Frequency .....	43
23. Voltage On Receiver Loop Of P-S Tuning Configuration With A 10 Ohm Load Plotted Against Frequency .....	44
24. Real Power On Source Loop Of P-S Tuning Configuration With A 10 Ohm Load Plotted Against Frequency .....	44
25. Real Power On Receiver Loop Of P-S Tuning Configuration With A 10 Ohm Load Plotted Against Frequency .....	45
26. P-P Equivalent Tuning Circuit For Power Transfer Of The Source Loop To The Receiver Loop As Viewed In Ads .....	46
27. Current On Source Loop Of P-P Tuning Configuration With A 10 Ohm Load Plotted Against Frequency .....	46

Figure	Page
28. Current On Receiver Loop Of P-P Tuning Configuration With A 10 Ohm Load Plotted Against Frequency .....	47
29. Voltage On Receiver Loop Of P-P Tuning Configuration With A 10 Ohm Load...	48
30. Real Power On Source Loop Of P-P Tuning Configuration With A 10 Ohm Load Plotted Against Frequency .....	48
31. Real Power On Receiver Loop Of P-P Tuning Configuration With A 10 Ohm Load Plotted Against Frequency .....	49
32. S-S Tuning Configuration With A 10 Ohm Load In Graphical And Vector Format.....	52
33. S-P Tuning Configuration With A 10 Ohm Load In Graphical And Vector Format.....	53
34. P-S Tuning Configuration With A 10 Ohm Load In Graphical Representation.....	53
35. P-P Tuning Configuration With A 10 Ohm Load In Graphical Representation .....	54
36. S-S Tuning Configuration With A 300 Ohm Load In Graphical And Vector Format.....	55
37. S-P Tuning Configuration With A 300 Ohm Load In Graphical And Vector Format.....	56
38. P-S Tuning Configuration With A 300 Ohm Load In Graphical Representation.....	56
39. P-P Tuning Configuration With A 300 Ohm Load In Graphical Representation.....	57
40. A Single 50- $\Omega$ Copper Shielded Loop Of 0.1m Radius .....	61
41. A Single 50- $\Omega$ Copper Shielded Loop Of 0.1m Radius Depicting The First Half And Neck As Rg-58 Coaxial Cable .....	62

Figure	Page
42. A Single 50-Ω Copper Shielded Loop Of 0.1m Radius Depicting Center Conductor United With A Solid Object Of Rg-58 Coaxial Cable Dimensions, With The General Outside Figure Appearance, While B Shows The Outside Coaxial Cable Being Transparent To Highlight The Inner Conductor .....	62
43. A) A Single 50-Ω Copper Shielded Loop Of 0.1m Radius Depicting The Neck Feed Composed Of Rg-58 Coaxial Cable Dimensions, With B) An Enlargement Of The Feed/Neck Location .....	64
44. Two Shielded Loops With Neck Feeds 180 Degrees Opposite Of Each Other.....	64
45. A) Single Shielded Loop Results And B) Its Physical Configuration .....	66
46. A) Two Shielded Loop Results And B) The Physical Configuration Showing Orientation Of The Neck Feeds.....	67
47. A) The Simulation Results And B) The Physical Configuration Of The Two Shielded Loops With Neck Feeds 180 Degrees Apart .....	68
48. H-Field Vectors For Single Loop Conductor .....	74
49. H-Field Vs Distance Of Single Loop Along Z-Axis .....	75
50. Single Flat Loop Conductor Hxy Complex Magnitude Field Overlay For A 1v-100mhz Source .....	76
51. Single Flat Loop Conductor Hxz Complex Magnitude Field Overlay For A 1v-100mhz Source .....	77
52. Single Flat Loop Conductor Hyz Complex Magnitude Field Overlay .....	78
53. Single Flat Loop Conductor Exy Complex Magnitude Field Overlay For A 1v-100mhz Source .....	79

Figure	Page
54. Single Flat Loop Conductor Exz Complex Magnitude Field Overlay For A 1v- 100mhz Source .....	80
55. Single Flat Loop Conductor Eyz Complex Magnitude Field Overlay .....	81
56. H-Field Vectors For Single Loop 4-Cycles Conductor .....	82
57. H-Field Vs Distance Of Single Loop Helix 4-Cycles Conductor Along The Z-Axis.....	83
58. Single Loop 4-Cycles Conductor Hxy Complex Magnitude Field Overlay .....	84
59. Single Loop 4-Cycles Conductor Hxz Complex Magnitude Field Overlay .....	85
60. Single Loop 4-Cycles Conductor Hyz Complex Magnitude Field Overlay .....	86
61. Single Loop 4-Cycles Conductor Exy Complex Magnitude Field Overlay .....	87
62. Single Loop 4-Cycles Conductor Exz Complex Magnitude Field Overlay .....	88
63. Single Loop 4-Cycles Conductor Eyz Complex Magnitude Field Overlay .....	89
64. H-Field Vectors For Helix Loop Of 4-Cycles Conductor .....	90
65. H-Field Vs Distance Helix Loop Of 4-Cycles Conductor Along The Z-Axis .....	90
66. Helix Loop Of 4-Cycles Conductor Hxy Complex Magnitude Field Overlay .....	91
67. Helix Loop Of 4-Cycles Conductor Hxz Complex Magnitude Field Overlay .....	92
68. Helix Loop Of 4-Cycles Conductor Hyz Complex Magnitude Field Overlay .....	93
69. Helix Loop Of 4-Cycles Conductor Exy Complex Magnitude Field Overlay .....	94
70. Helix Loop Of 4-Cycles Conductor Exz Complex Magnitude Field Overlay .....	95
71. Helix Loop Of 4-Cycles Conductor Eyz Complex Magnitude Field Overlay .....	96
72. Hfss Setup For Two Shielded Loops. Loop 1 Is The Lower Shielded Loop And Loop 2 Is The Upper Shielded Loop .....	100

Figure	Page
73. Hfss Setup Of Shielded Loops .....	100
74. Hfss Setup For Two Four Cycle Helical Loops. Loop 1 Is The Lower Four Cycle Helical Loop And Loop 2 Is The Upper Four Cycle Helical Loop .....	101
75. Four Cycle Helical Loops Connected To Twinax Sources In A Moebius Termination .....	101
76. Four Cycle Helical Loop With Moebius Termination To A Twinax Source .....	102
77. Zero Cycle Helical Loops Terminated To Twinax Sources.....	103
78. Zero Cycle Helical Loops Terminated To Twinax Sources... ..	103

## CHAPTER 1

### INTRODUCTION

Wireless power transfer has been explored for decades since the beginning of the Tesla claim to transmit power wirelessly. It is well known that small amount of power can be transmitted wirelessly with the far field radiation. For powering devices such as rechargeable batteries for electronics, the power transfer must be explored for efficient charging. Conventional loops of one to  $N^{th}$  turns have been explored and optimized for modern electronics.

Advancement in modern tactical electronics for soldiers has become prevalent in modern warfare. Hostile environment have become increasingly dangerous for operators to complete missions covertly due to the opposition gaining access to radio frequency analysis that can detect radiation from electronic powering stations. The need to recharge a soldier's electronic equipment without adding wires and procedures for charge has become desirable.

Eliminating power radiation for wireless charging has not become feasible with advancement in designing of the reactive magnetic field. In order to build an optimal system, the first step requires a investigation into power radiation mitigation or virtual elimination that will protect the where about of the operator have made a technological advancement.

The Helical loop terminated in a moebius connection is proposed for developing a wireless power transfer technology that mitigates power radiation through the canceling of E-fields. Therefore, a hypothesis to be tested is proposed as: Can we reduce radiation



and preserve coupling by going to a higher order “pole” version of the standard current loop? Currently no other technology is offered as a step toward a solution.

## 1.2 Organization

Chapter 2 provides a detailed analysis for developing a closed loop solution in loop antenna wireless power transfer. From that analysis, Chapter 3 describes the four models that are developed for investigating and validating schemes used in tuning the antennas with resistive loads. The first order models results are compared against equivalent circuit simulations in ADS. Chapter 4 introduces the shielded loops as a possible solution to wireless power transfer. Chapter 5 pilots the investigation into a helical configuration that is exploited later in chapter 6. Finally, chapter 6 steps in the direction developing a baseline simulation of tuned shielded loop to loop coupling using a full wave modeling tool. Power transfer and power radiated performance is compared for a shielded loop to shielded loop system, helix loop to helix loop. The hypothesis is addressed with two configurations. Finally, recommendations for future work are given at the end of chapter 6.

## CHAPTER 2

### BASELINE PROPERTIES OF A POWER TRANSFER SYSTEM: LARGE AND SMALL LOOP SYSTEM

#### 2.1 Description of power transfer system relevant theory

It is known that two loops within the Near Field distances of each other have power transfer capabilities via magnetic induction [4, 10]. For this investigation it was considered that two loops of one turn with the transfer of power originating from a “large radius” source loop to a “small radius” receiver loop. Specifically, the source loop shall have a radius of 0.1 meters, while the receiver loop will be 1/10<sup>th</sup> of the source loop; 0.01 meters. Both loops are considered to be suspended in free space with no external interactions (e.g. no ground plane interaction). Both loops are assumed shorted loops. The power transferred between the respective loops will then be evaluated by considering the amount of Power transferred from the source loop  $P_{in}$ . Assuming 1 ampere generated from the source, the Power equations can be used for calculating the power being transmitted from the generator and source loop. Next, radiated power and power to load is considered. The amount of radiated power lost is determined by considering the radiation resistance seen by the source combined with the receiver and then calculating how much is radiated away. The power to load calculation will consider the Ohmic Resistance of the metal of the loops. At this time no extra load resistance will be assumed and hence the load is considered to be only the Ohmic Resistance of the receiver loop. Once it was calculated all impedances, voltages and currents of the system it was determined the power transfer efficiency of the described two-loop system.

#### 2.2 Transducer Section

### 2.2.1 The Impedance and Admittance Matrix

The transducer theory shows that the Voltages of both loops and current of receiver can be calculated if a realization is known for the impedances  $Z_{11}$ ,  $Z_{22}$ ,  $Z_{12}$ , and  $Z_{21}$  of our system [9, 10]. For the reciprocal circuit, the non-diagonal impedance matrix coefficients are symmetric

$$Z_{21} = Z_{12} \quad (1)$$

Two coupled antennas can be modeled as a transducer as long as the gaps between their respective input terminals are small [9, 10]. Additionally, a transducer exhibits linear behavior if the voltages across each pair of terminals are linear functions of the currents.

Therefore for our two loop system

$$V_1 = Z_{11} I_1 + Z_{12} I_2 \quad (2)$$

$$V_2 = Z_{21} I_1 + Z_{22} I_2 \quad (3)$$

Where

$V_1$  is the voltage across the terminals of Loop 1,

$V_2$  is the voltage across the terminals of Loop 2,

$I_1$  is the current through Loop 1,

$I_2$  is the current through Loop 2,

$Z_{11}$  is the (self) impedance of Loop 1,  $Z_{11} = \frac{V_1}{I_1}$  in the absence of loop 2.

$Z_{12}$  is the mutual impedance of Loop 1 to Loop 2.  $Z_{12} = \frac{V_2}{I_1}$  The voltage induced in loop 2 due to the current in loop 1.

$Z_{22}$  is the (self) impedance of Loop 2,  $Z_{22} = \frac{V_2}{I_2}$  in the absence of loop 1.

$Z_{21}$  is the mutual impedance of Loop 2 to Loop 1.  $Z_{21} = \frac{V_1}{I_2}$  The voltage induced in loop 1 due to the current in loop 2.

Shown in matrix form

$$\begin{bmatrix} V_1 \\ V_2 \end{bmatrix} = \begin{bmatrix} Z_{11} & Z_{12} \\ Z_{21} & Z_{22} \end{bmatrix} \times \begin{bmatrix} I_1 \\ I_2 \end{bmatrix} \quad (4)$$

Where, given the currents, the total voltages can be calculated. For a given voltage, the inverse of impedance is the admittance and thus if  $z$  is a 2x2 matrix it can be defined as the corresponding admittance matrix as follows. Let,

$$Z = \begin{bmatrix} a & b \\ c & d \end{bmatrix} \quad (5)$$

$$Y = \left( \frac{1}{ad-bc} \right) \times \begin{bmatrix} d & -b \\ -c & a \end{bmatrix} \quad (6)$$

Resulting in:

$$Y = \left( \frac{1}{Z_{11}Z_{22}-Z_{12}Z_{21}} \right) \times \begin{bmatrix} Z_{22} & -Z_{12} \\ -Z_{21} & Z_{11} \end{bmatrix} \quad (7)$$

Now, let  $D$  be the following expression:

$$D = (Z_{11}Z_{22} - Z_{12}Z_{21}) \quad (8)$$

Equation (6) above can now be rewritten in terms of the admittance matrix

$$\begin{bmatrix} I_1 \\ I_2 \end{bmatrix} = \begin{bmatrix} \frac{Z_{22}}{D} & \frac{-Z_{12}}{D} \\ \frac{-Z_{21}}{D} & \frac{Z_{11}}{D} \end{bmatrix} \times \begin{bmatrix} V_1 \\ V_2 \end{bmatrix} \quad (9)$$

or

$$\begin{bmatrix} I_1 \\ I_2 \end{bmatrix} = \begin{bmatrix} Y_{11} & Y_{12} \\ Y_{21} & Y_{22} \end{bmatrix} \times \begin{bmatrix} V_1 \\ V_2 \end{bmatrix} \quad (10)$$

with  $Y_{xx} = \frac{Z_{xx}}{D}$ .

Finally, the currents can be expressed as

$$I_1 = Y_{11}V_1 + Y_{12}V_2 \quad (11)$$

$$I_2 = Y_{21}V_1 + Y_{22}V_2 \quad (12)$$

So that, given the voltages the currents can be calculated.

### 2.2.2 Mutual Impedance of the Two Loop System

By extension from Magneto statics it can be known as defining the relationship between

Mutual Impedance and Mutual Inductance as

$$L_{12} = \frac{Z_{12}}{j\omega} \quad (13)$$

and

$$L_{21} = \frac{Z_{21}}{j\omega} \quad (14)$$

where

$\omega$  is the angular frequency and

$L_{xy}$  is the mutual inductance.

### 2.3 Mutual Inductance

As suggested by the last two equations it can be expected that the mutual impedance problem to be reduced to the mutual inductance Magneto statics problem at low frequencies. Therefore, different classic approximations help identify the important parameters and serve as sanity checks. The investigation can begin by solving the mutual inductance of the two loop system. The Magneto statics Biot-Savart approach, the

Magneto-Statics Elliptical function approach, and the Magneto-Statics Magnetic Dipole approach. These should agree with the antenna Electrodynamics approach as frequency goes to zero. Each solution obtained from the resulting method will then be reviewed and compared for their accuracy and specific conditions required for the solution to work.

### 2.3.1 Magneto-Statics Approach

Mutual Inductance (Mutual Impedance) of two loops using the Magneto-Statics approach will first be considered. At 1MHz, a large loop of 0.1 meter radius is considered electrically small [10, 11]. This constitutes Magneto-Statics characteristic behavior.

#### 2.3.1.1 Magneto-Statics Inductance equations

##### 2.3.1.1.1 $H_z/B_z$ on the axis of loop

By applying the Biot-Savart law [4] along the axis of a loop of radius  $r$ , the z-component is obtained

$$B_z = \frac{\mu_0}{4\pi} \frac{2\pi R^2 I}{(z^2 + R^2)^{\frac{3}{2}}} \quad (15)$$

By assuming the smaller loop ( $1/10^{\text{th}}$  radius of the larger loop) is small enough that the flux through it is uniform, one can simply multiply  $B_z$  by the area of the small loop and divide by current to get the inductance of the large loop source projected onto the small loop receiver.

$$M_{large\_loop} = \frac{B_z A_{small\_loop}}{I_{large\_loop}} \quad (16)$$

where,

$M_{large\_loop}$  is the Mutual Inductance of the two loop system.

$A_{small\_loop}$  is the area of the small loop with radius  $r$  and

$I_{large\_loop}$  is the current of the large loop.

### 2.3.1.1.2 Mutual Inductance using elliptical functions

Elliptical functions of the first and second kind can be used for calculating the Mutual Inductance of two loops without the uniform flux approximation. As shown in Ramo, Whinnery and Van Duzer [11] the final result for mutual inductance of coaxial loops

$$M = \mu\sqrt{ab} \left[ \left( \frac{2}{k} - k \right) K(k) - \frac{2}{k} E(k) \right] \quad (17)$$

Where,

$a$  is the radius of loop 1.

$b$  is the radius of loop 2.

$$k^2 = \frac{4ab}{d^2 + (a+b)^2}$$

$d$  is distance between coaxial loops.

$$E(k) = \int_0^{\pi/2} \sqrt{1 - k^2 \sin^2 \phi} \, d\phi$$

$$K(k) = \int_0^{\pi/2} \frac{d\phi}{\sqrt{1 - k^2 \sin^2 \phi}}$$

### 2.3.1.1.3 Magnetic Dipole approach

The next Mutual Inductance calculation is realized by considering duality and the Magneto-Static solution for a Magnetic Dipole in free space [11]. Consider a loop that is relatively small compared to the other loop of the system, 1/10th the size of the large loop for the present two loop system. The small loop can then be modeled as a magnetic dipole.

It follows that the  $\theta$ -component and the  $r$ -component of the total B-field are the dipole fields of a loop.

$$B_{\theta} = \frac{\mu\rho}{4\pi r^3} \sin \theta \quad (18)$$

$$B_r = \frac{\mu\rho}{2\pi r^3} \cos \theta \quad (19)$$

#### 2.3.1.1.4 Electrodynamics - Flux Section small loop as source

Now to compliment the magneto statics approaches the focus is shifted to the electrodynamic approach [11]. To begin, consider a Co-Axial system and calculate the Mutual Inductance as a function of separation between the loops.

The Planar case takes the same two loops lying on a plane, and again separated as a function of distance. Both scenarios assume the small loop is a magnetic dipole and use the electrodynamic fields of a magnetic dipole in spherical coordinates for calculating the B field in space. Then, by projecting the B field flux through the area of the larger receiver loop, the inductance can be calculated. For calculating the total flux,  $\int B \cdot ds$  crossing the large loop the integral is carried out as a discrete sum. That is, the flux can be calculated by dividing up the large loop cross section into small squares each with the same unit area. By summing all flux contributions captured by each of the unit areas within the larger receiver loop area, a final total flux passing through the larger loop can be tabulated.

Then:

$$M_{12} = \frac{\oint B_2 \cdot dS_1}{I_2} = \frac{\psi_{12}}{I_2} \quad (20)$$

and by reciprocity

$$M_{21} = \frac{\Psi_{21}}{I_1} \quad (21)$$



$$\Psi_{21} = \iint (\mathbf{B}_{21}) \cdot \hat{\mathbf{z}} R dR d\phi \quad (22)$$

The dipole field of the loops is obtained using duality as follows:

Consider the Electric Field of a dipole in spherical coordinates  $E_\theta$  and  $E_r$  [12].

$$E_\theta = \frac{1}{4\pi} e^{-jk_0 r} \left( \frac{j\omega\mu}{r} + \sqrt{\frac{\mu}{\epsilon}} \frac{1}{r^2} + \frac{1}{j\omega\epsilon r^3} \right) \sin(\theta) \quad (23)$$

$$E_r = \frac{1}{2\pi} e^{-jk_0 r} \left( \sqrt{\frac{\mu}{\epsilon}} \frac{1}{r^2} + \frac{1}{j\omega\epsilon r^3} \right) \cos(\theta) \quad (24)$$

Where the distance  $r = \sqrt{x^2 + y^2 + z^2}$  is the distance from the Cartesian origin.

If the Electric Dipole moment is,

$$\rho_e = qh \quad (25)$$

and it is known that

$$I = j\omega q \quad (26)$$

then, substituting  $q$  into Electric Dipole moment is it realized as

$$\rho_e = \left( \frac{I}{j\omega} \right) h \quad (27)$$

The static Magnetic Dipole is moment is defined as:

$$\rho_m = IS = I\pi r^2 = I\pi a_{sm}^2 \quad (28)$$

Therefore, the AC Magnetic Dipole of the current moment is simply  $j\omega\mu I\pi a^2 = I_m \cdot l$ .

Therefore by duality

$$B_\theta = \frac{j\omega\mu^2 I\pi a_{sm}^2}{4\pi} e^{-j \cdot k_0 \cdot r} \left( \frac{j \cdot \omega \cdot \epsilon}{r} + \frac{1}{\eta r^2} + \frac{1}{j\omega\mu r^3} \right) \sin(\theta) \quad (29)$$

$$B_r = \frac{j\omega\mu^2 I\pi a_{sm}^2}{2\pi} e^{-jk_0 r} \left( \frac{1}{\eta r^2} + \frac{1}{j\omega\mu r^3} \right) \cos(\theta) \quad (30)$$

Simplifying,

$$B_{\theta} = \frac{j\omega\mu^2 I a_{sm}^2}{4} e^{-jk_0 r} \left( \frac{j\omega\epsilon}{r} + \frac{1}{\eta r^2} + \frac{1}{j\omega\mu r^3} \right) \sin(\theta) \quad (31)$$

$$B_r = \frac{j\omega\mu^2 I a_{sm}^2}{2} e^{-jk_0 r} \left( \frac{1}{\eta r^2} + \frac{1}{j\omega\mu r^3} \right) \cos(\theta) \quad (32)$$

For ease of programming, the cosine is replaced with the respective x, y, and z components as follows.

$$\cos(\theta) = \frac{z}{r} \quad (33)$$

$$\sin(\theta) = \pm \sqrt{1 - \left(\frac{z}{r}\right)^2} \quad (34)$$

Recalculating, the B-field components become

$$B_{\theta} = \frac{j\omega\mu^2 I a_{sm}^2}{4} e^{-jk_0 r} \left( \frac{j\omega\epsilon}{r} + \frac{1}{\eta r^2} + \frac{1}{j\omega\mu r^3} \right) \pm \sqrt{1 - \left(\frac{z}{r}\right)^2} \quad (35)$$

$$B_r = \frac{j\omega\mu^2 I a_{sm}^2}{2} e^{-jk_0 r} \left( \frac{1}{\eta r^2} + \frac{1}{j\omega\mu r^3} \right) \frac{z}{r} \quad (36)$$

The flux calculation total  $\int B \cdot ds$  approach is performed as before by equally dividing the large loop cross sectional area into multiple small unit areas. The Mutual Inductance of the two loops system is then calculated by dividing the total flux captured by the total current of the source loop.

### 2.3.1.2 Considerations for Computational Calculations

The MathCAD sheet is included in the Appendix.

### 2.3.2 Flux Results from each Method

All flux results assume a source loop of radius 0.1m that is positioned coaxially with a secondary loop 1/10<sup>th</sup> the radius of the source loop. Mutual inductance versus separation

distance is shown for all four approaches. Where, mutual inductance units are in henrys and separation in units of meters. The first graph is the Magneto-Statics approach.

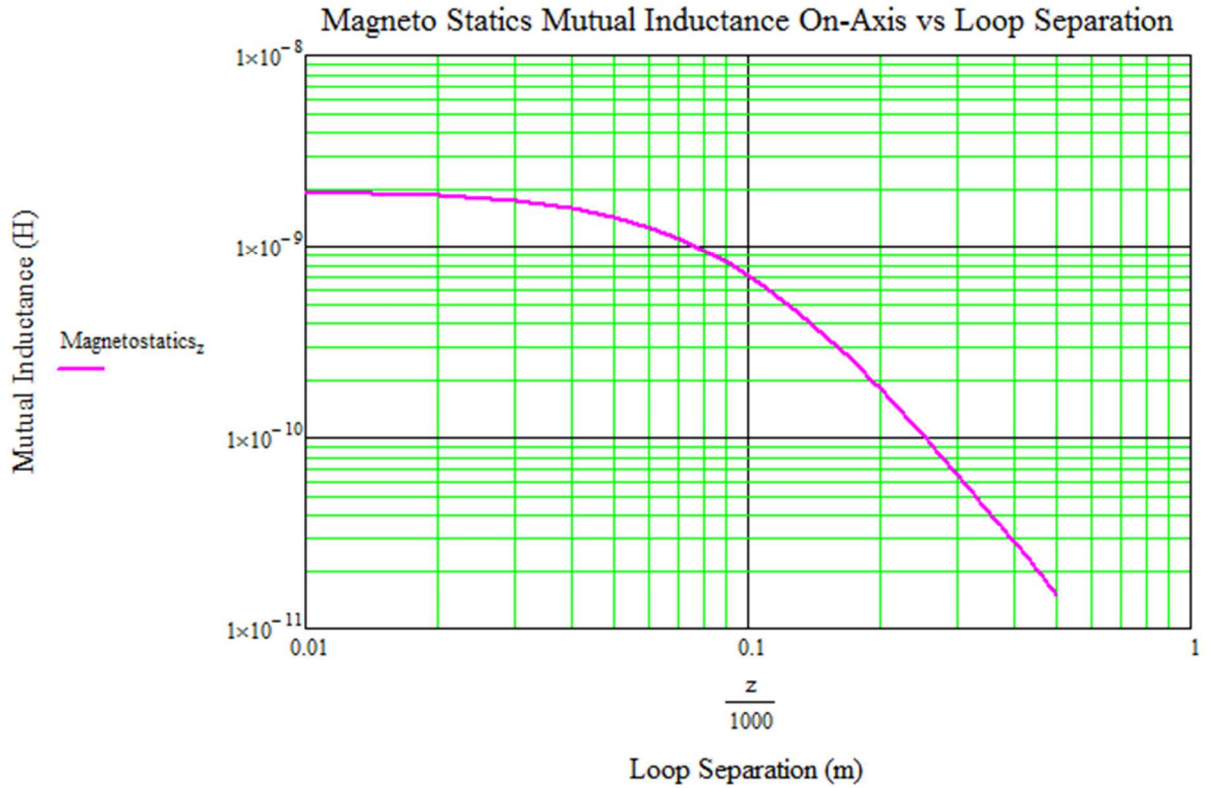


Figure 1. Magneto Static flux along the axis of a loop.

The Magneto Statics solution is used as high fidelity results for comparing other methods as a baseline solution.

The second method is the graphical results using the Neumann approach and Elliptical functions.

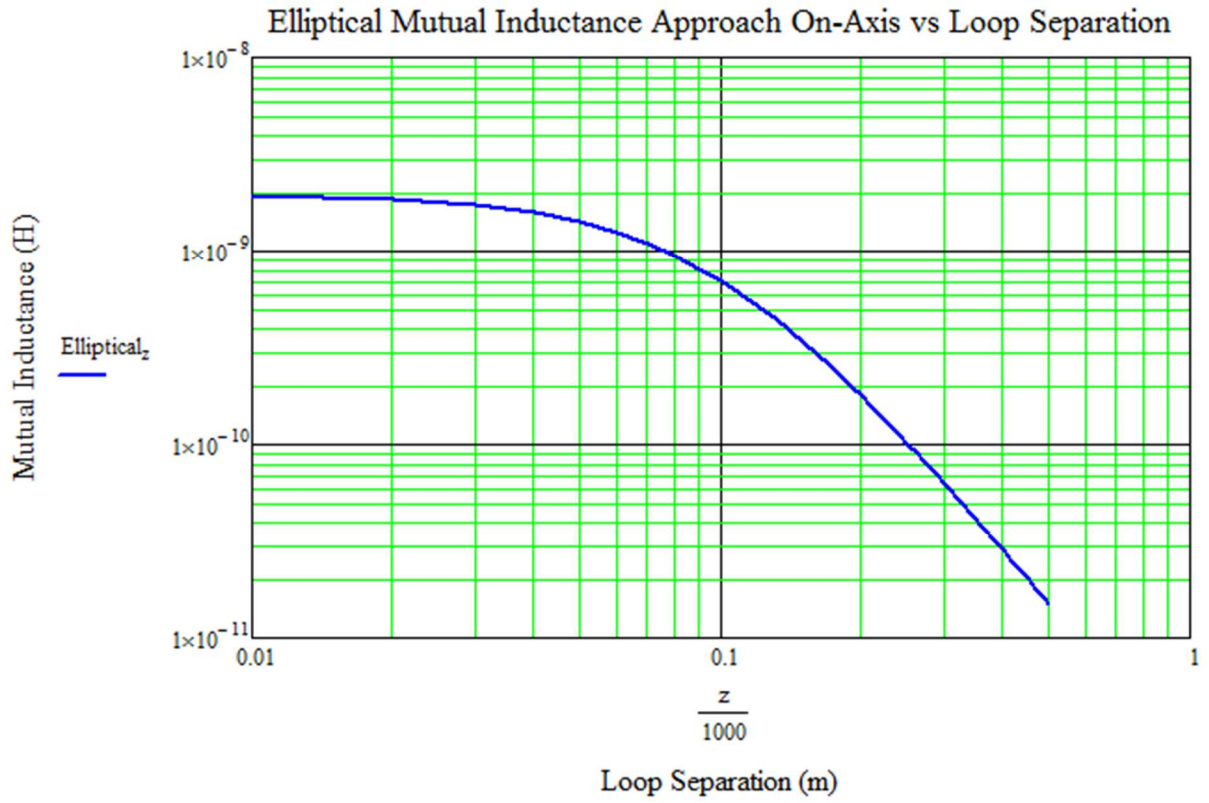


Figure 2. Elliptical Function flux along the axis of the loops.

The elliptical solution is commonly used in literature and can be readily compared to the magneto statics solution.

The third method is the graphical results using the Magneto Static B-fields of a magnetic dipole.

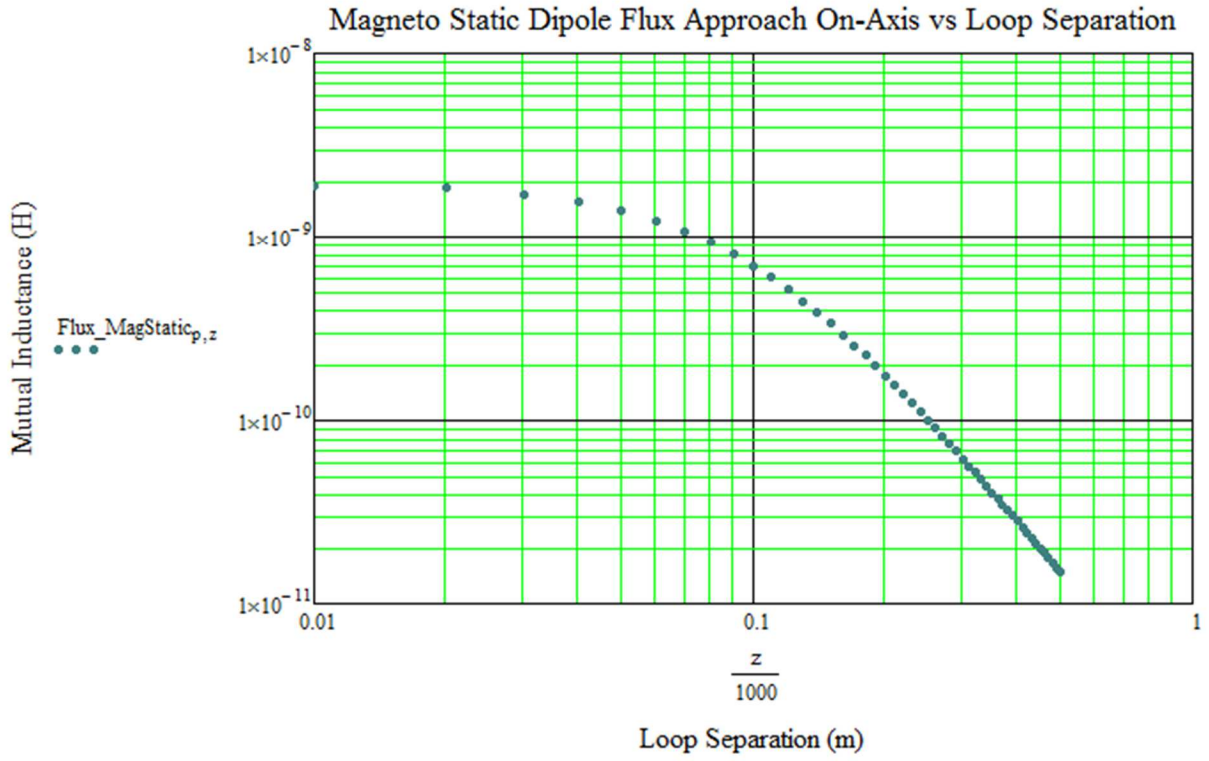


Figure 3. Magneto Static B-field of a magnetic dipole.

From electro static dipole solution and duality, it is shown that magneto static dual magnetic dipole exhibits high fidelity.

The fourth method is the graphical results using the Magneto Dynamic B-fields of a magnetic dipole.

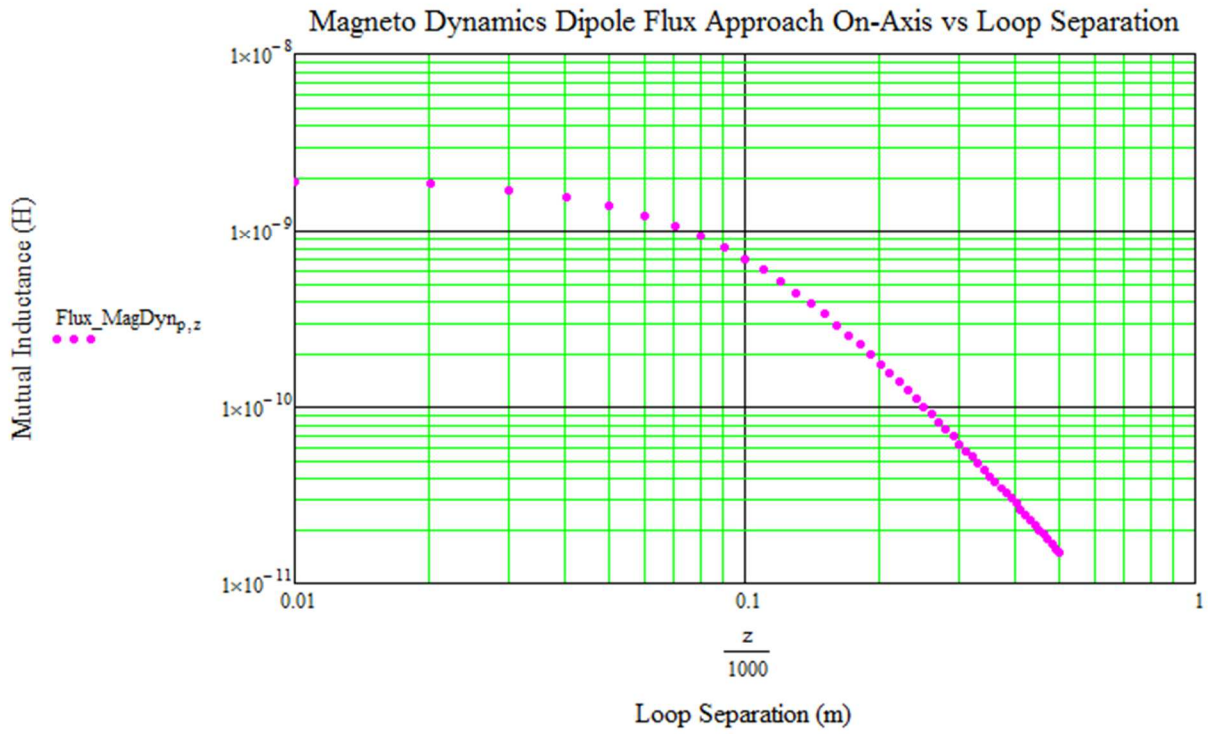


Figure 4. Magneto Dynamic B-field of a magnetic dipole

Finally, comparisons of all approaches are combined on one graph for comparison.

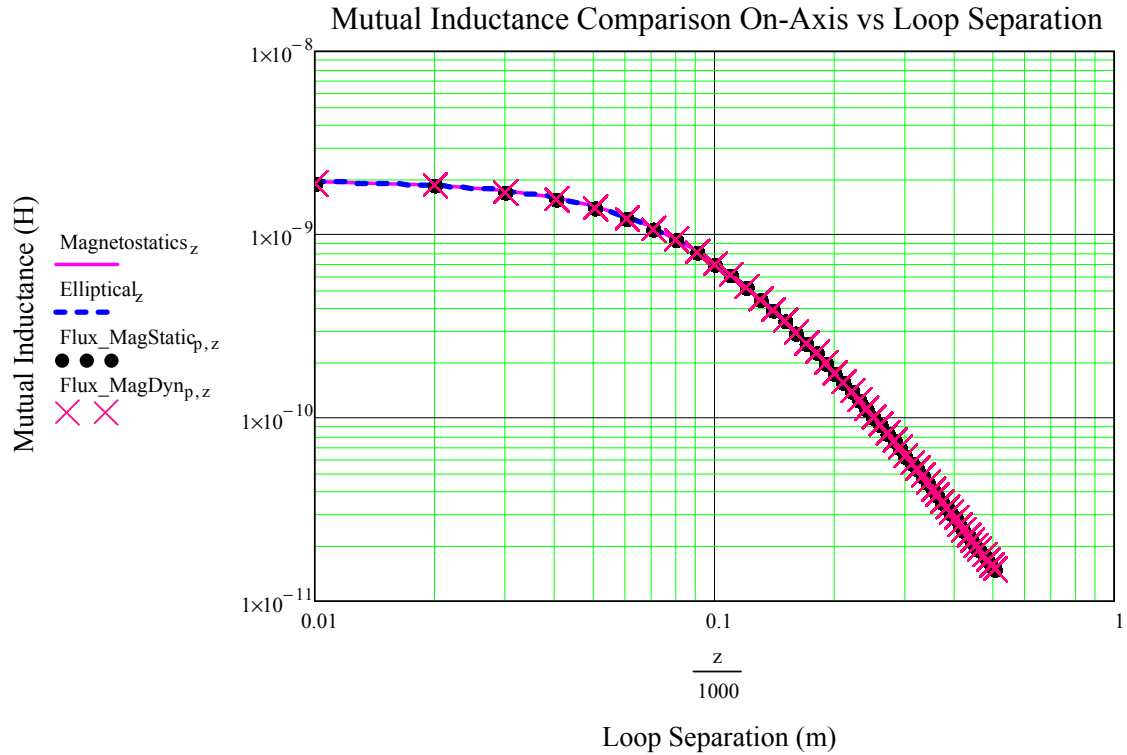


Figure 5. Magneto Statics, Elliptical, Magneto Static dipole and Magneto Dynamic dipole.

## 2.4 Discussion

The mathematical investigation of two conventional loop each of one turn is used for understanding the transfer of power originating from a “large radius” source loop to a “small radius” receiver loop. The source loop shall have a radius of 0.1 meters, while the receiver loop will be 1/10<sup>th</sup> of the source loop; 0.01 meters. Both loops are considered to be suspended in free space with no external interactions (e.g. no ground plane interaction). Both loops are assumed shorted loops and no extra load resistance was assumed. Transducer theory is then used to determine the mutual impedance, and therefore the mutual inductance. Mutual inductance is calculated and compared by using

duality and approached such as the Magneto statics Biot-Savart law, elliptical functions, magneto-static dipole and the electrodynamics approach. The mutual inductance of the transducer is used to calculate the coupling coefficient. In conclusion, the electrodynamics method used to calculate the mutual inductance and coupling coefficient is validated by comparing three additional different approaches.



## CHAPTER 3

### POWER TRANSFER PROPERTIES OF THE TWO LOOP SYSTEM

#### 3.1 Background for application

This investigation is directed towards medical and military applications. For the power radiated, consider a medical application in which there are sensitive electronic sensors and electronics that provide life supporting therapy for the respective patient. These medical systems can be negatively impacted by a significantly radiating disruptive power source. This could negatively affect the monitoring or life support equipment for patients and may also impact critical data collection and/or transmission needed for life supporting treatment, and thus unintended radiation of significant magnitude could lead to conditions ranging from, at best, undesirable (e.g. data loss) to catastrophic implications (e.g. sensor failure or corruption of medical device).

Considering a military application, the user may be outfitted with sophisticated electronic equipment and/or sensory electronics that require access to a wireless power transfer charging system during an important military operation. Furthermore, the hostile environment of the soldier may require wireless recharge usage that demands no detectability. Additionally, the soldier must not generate any significant electromagnetic emissions that could give the enemy any information of the presence or knowledge of the operation. Even minor radiation emission could catastrophically lead to losses or jeopardize the objective. Therefore, it is imperative that no detectable emission or radiation be generated during use.

### 3.2 Application of transducer theory.

For this investigation we consider two loops of identical size, and being electrically small, which is defined as [7]

$$2\pi r \ll \lambda \quad (1)$$

with  $r$  equal to the loop radius and  $\lambda$  equal to the wavelength of the respective electromagnetic radiation, and therefore constrained to near field coupling, which is defined as a distance  $< \lambda$ . For simplicity, it will be assumed the loop current is constant in amplitude and phase at all points on the loop. As a consequence of the constant loop current assumption, any results for the loops greater than several meters in diameter are not valid above 5MHz. Additionally, the radius  $\rho_0$  of the wire conductor is assumed small compared to the radius of the loop. Using Linear Transducer theory [9, 10], from chapter 2 the impedance matrix, equations 2 and 3 below are reproduced,

$$V_1 = Z_{11} I_1 + Z_{12} I_2 \quad (2)$$

$$V_2 = Z_{21} I_1 + Z_{22} I_2 \quad (3)$$

and shown in matrix form in equation 4

$$\begin{bmatrix} V_1 \\ V_2 \end{bmatrix} = \begin{bmatrix} Z_{11} & Z_{12} \\ Z_{21} & Z_{22} \end{bmatrix} \times \begin{bmatrix} I_1 \\ I_2 \end{bmatrix} \quad (4)$$

and then equation 5 expressed in terms of current and admittance

$$\begin{bmatrix} I_1 \\ I_2 \end{bmatrix} = \begin{bmatrix} Y_{11} & Y_{12} \\ Y_{21} & Y_{22} \end{bmatrix} \times \begin{bmatrix} V_1 \\ V_2 \end{bmatrix} \quad (5)$$

Finally, the matrix is expressible as equations 13 and 14 from chapter 2.

$$I_1 = Y_{11} V_1 + Y_{12} V_2 \quad (6)$$

$$I_2 = Y_{21} V_1 + Y_{22} V_2 \quad (7)$$

The Power seen entering into loop 1 is then:

$$P_{in} = I_1 V_1 \quad (8)$$

### 3.2.1 Ohmic Loss and Impedance assumed at feed

It is assumed the receiver loop is made of copper, with a conductivity of  $\sigma = 5.8 \times 10^7$  Siemens. For the wireless power harvesting from the source loop by the receiver loop to be investigated, the power captured by the copper loop material is determined by binding the energy harvested to the receiver loop of the system. The loop will experience magnetic flux which in turn generates a current and a voltage. For the copper receiver loop it is known the reactive power is not as useful for calculations as real power calculated in watts. Therefore, we shall focus our calculations on real power with units of watts which will lead to the calculation of generated power at the receiver loop. This approach will allow the realization of numerical data useful in modeling the transferring of power to a load or battery of a system that requires electrical energy.

The real power dissipated due to Ohmic loss is

$$P_{loss} = I^2 R_{ohmic} \quad (9)$$

Looking at the power equation due to Ohmic resistance loss, it is apparent that the current in the second loop is highly dependent on the Ohmic resistance and hence, the resistance component that the electromagnetic wave sees while traveling along the wire is called the surface resistance. The alternating current (AC) resistance of the loop's wire depends on the skin depth [12]. Defining the surface resistance as

$$R_s = \frac{1}{\sigma \delta} \quad (10)$$

Where

$\sigma$  is the conductance and

$\delta$  is the skin depth of the copper wire.

The skin depth for the wire loop is expressed as such [12]:

$$\delta = \sqrt{\frac{2}{2\pi f \mu_0 \sigma}} \quad (11)$$

Therefore, at high frequencies ( $\delta < \rho_0$ ) the resistance calculation for a round wire, in  $\Omega$  per unit length ( $\Omega/m$ ) is

$$R_{hf} = \frac{R_s}{2\pi r_0} \quad (12)$$

Such that

$$R_{wire} = R_{hf} \cdot 2\pi R_{loop} \quad (13)$$

The frequencies of interest are selected under the assumptions of literature [6] that shows desired characteristics of uniform current distribution. It is known that the effect of non-uniform current distributions, in which as stated  $2\pi r \ll \lambda$  [6], at the approximate frequencies above 5MHz become significant. Additionally, the radiated power becomes significant and the electrically small limits of the loops become increasingly critical.

### 3.2.2 Radiation resistance and Radiation conductance

Calculating radiation resistance is dependent on antenna geometry, material composition and frequency [1]. Typically, the radiation resistance is required for describing the radiated power relative to the antenna and frequency in use. The well-known radiation resistance for a loop antenna impedance model is derived by considering the  $E_\varphi$  field at large distances from the loop [9, 10]:

$$E_\varphi = \frac{\eta \beta^2 I S}{4\pi r} e^{-j\beta r} \sin \theta \quad (14)$$

where,

$\eta = 377\Omega$  is the impedance of free space

$\beta$  is the wave number  $k_0 = \omega\sqrt{\epsilon\mu}$

$I$  is the current of the loop

$S$  is the area of the loop

$r$  is the radial distance from source center outwards

$\theta$  is the angle ranging from zero to  $\pi$ ,

while the radiated power can be solved as

$$P = \int_0^{2\pi} \int_0^\pi r^2 E_\varphi E_\varphi^* \sin \theta d\theta d\varphi = \frac{\eta}{12\pi} (\beta^2 S)^2 I I^* \quad (15)$$

The radiation resistance of the loop is then

$$R = \frac{\eta}{6\pi} (\beta^2 S)^2 = 320\pi^4 \frac{S^2}{\lambda^4} \cong 31,000 \frac{S^2}{\lambda^4} \quad (16)$$

Equation 16 holds valid for radiation resistance of the loop investigation assuming the approach is to use an impedance, series-based, circuit model. However, the approach that will be used here will be to consider an admittance circuit model developed by Schelkunoff, as shown below [9, 10].

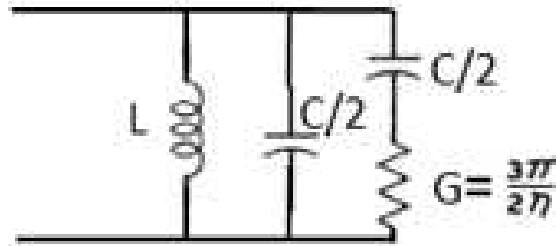


Figure 6. Schelkunoff admittance circuit model of a loop antenna.

For realizing the radiation conductance, [9, 10] it can be shown that the conductance is calculated as follows:

$$G_{radiation} = \frac{3\pi}{2\eta} \quad (17)$$

This is significantly different than radiation resistance, in which the radiation resistance depends on  $S$  and  $\lambda$ . Whereas, the radiation conductance is a constant.

### 3.2.3. Impedance/Conductance Models

For the impedance of the loop itself, we reference Schelkunoff's admittance model of an elementary loop antenna [9, 10] which contains inductive and capacitance loading in parallel, and conductance loading in series with the capacitive loading.

#### 3.2.4.1 Self Capacitance ( $Z_{11}$ or $Z_{22}$ )

The capacitance of the circuit is the distributed capacitive loading seen between opposite sides of the loop due to the charge associated with the current in the loop. Schelkunoff gives the shunt capacitance as

$$C_{loop} = \frac{1}{3} C_{av} b \pi \quad (18)$$

Where,

$b$  is the radius of the loop.

$C_{av}$  is the average value of the capacitance between the two halves of the loop per unit length along the circumference better modeled as a shorted two wire line:

$$C_{av} = \frac{\pi \epsilon}{\log b/a} \quad (19)$$

with

$b$  equal to the radius of the loop and

$a$  equal to the radius of the wire.

#### 3.2.4.2 Self Inductance/Self Impedance ( $Z_{11}$ or $Z_{22}$ )

The total distributed inductance of a small single loop can be calculated by adding both the internal inductance ( $L_i$ ) and the inductance due to the copper wire loop ( $L_{loop}$ ). All inductive contributions are then combined into one lumped inductance. The first inductive metric is derived from the internal inductance [1].

$$L_i = \frac{b}{\omega a} \sqrt{\frac{\omega \mu_0}{2\sigma}} \quad (20)$$

where,

$b$  is the radius of the loop

$a$  is the radius of the wire and

$\omega$  is the angular frequency of the EM radiation.

Additionally, the inductance due to the loop is derived as [1]:

$$L_{loop} = \frac{\mu_0 b}{\pi} \int_{\log}^{\pi} \left( \frac{2b}{a} \sin \psi \right) d\psi = \mu_0 b \log \frac{b}{a} \quad (21)$$

where  $\psi$  is the angle of the radius from the center of the loop to the outer perimeter of the circular conductor. We can use the Static Electromagnetic calculations and thus use the results to calculate the electrodynamics metrics respective to the system's application frequency.

### 3.3.1 Mutual Impedance by Reaction Integral

The mutual impedances between the loops modeled as antennas can be calculated following Schelkunoff using the Reaction Theorem. Therefore we can express the Mutual Impedance as [12]

$$Z_{12} = \frac{V_{12}}{I_2} = \frac{V_{ocb}}{I_b} \quad (22)$$

where,

*Subscript 1* is referenced to loop 1

*Subscript 2* is reference to loop 2

*Subscript a* is referencing loop 1,

and therefore *subscript b* references loop 2.

$V_{ocb}$  is the open – circuit voltage at terminal a induced by the field of antenna b.

Using the reciprocity theorem we can therefore express  $V_{ocb}$  as the following expression:

$$V_{ocb} = \int E_a \cdot J_b dV \quad (23)$$

where,

$E_a$  is the field produced by the antenna  $a$  at the position of antenna  $b$ , with antenna  $b$  removed

$J_b$  is the source current of antenna  $b$ .

Therefore the expression for Mutual Impedance is:

$$\pm Z_{12} = \frac{V_{ocb}}{I_b} = \frac{1}{I_b} \int E_{a0} \cdot J_b dV \quad (24)$$

Furthermore, if the current is confined to a wire, the volume integral simplifies to an integral along the wire and it can be shown that the Mutual Impedance becomes

$$-Z_{12} = \frac{1}{I_1 I_2} \int E_2 \cdot I_1(\xi) d\xi \quad (25)$$

Where,

$\xi$  is the distance variable along the wire.

### 3.3.2 Input impedance $Z_{in}$

$Z_{in}$  of a linear transducer can be obtained if the receiver antenna is Short-Circuited.

That is, we let  $V_2=0$  in equation 3

$$V_1 = Z_{11} I_1 + Z_{12} I_2 \quad (26)$$

$$V_2 = Z_{21} I_1 + Z_{22} I_2 \quad (27)$$

and by solving for the ratio  $\frac{V_1}{I_1}$  of the transducer system matrix we can define the input

impedance seen from loop 1 as it interacts with loop 2. Thus

$$Z_{in} = Z_{11} - \frac{Z_{12}^2}{Z_{22}} \quad (28)$$



### 3.3.3.1 Connecting a Load to Loop 2: Derivation for $Z_{in}$

The receiver loop must have power storing capability for harvesting the energy/power from the source loop. By assuming a battery attached to the loop, the impedance looking in from the (assumed) voltage supply of the source loop will be impacted by the impedance loading due to the battery. Hence, from a source perspective, the input impedance will be dependent on the battery load. Therefore, derivation due to a battery load must be derived.

Transducer theory is valid as long as the gaps between the two respective antennas (that form a transducer) input terminals are small [9, 10]. Additionally, a transducer is linear if the voltages across each pair of terminals are linear functions of the respective currents. In the given case of two loops in proximity, they may be modeled as a Linear Transducer, e.g. using equations 26 and 27 above, and the matrix form given by equation 4 above.

For connecting a load  $Z_L$  onto port 2, it is assumed

$$V_2 = -Z_L I_2 \quad (29)$$

where the negative sign is due to the positive direction for  $I_2$  being directed into the two-port instead of into the load. Equation 27 now becomes

$$-Z_L I_2 = Z_{21} I_1 + Z_{22} I_2 \quad (30)$$

Equation 30 is solved for  $I_2$  as a function of  $I_1$  and then we can replace  $I_2$  by solving Equation 26 for  $I_2$  and using this expression, leaving  $V_1, V_2$  and  $I_2$  as functions of  $I_1$  as is noted below:

$$I_2 = -\frac{Z_{21}}{Z_L + Z_{22}} I_1 \quad (31)$$

$$V_1 = Z_{11}I_1 - \frac{Z_{12}Z_{21}}{Z_L + Z_{22}}I_1 \quad (32)$$

$$V_1 = \left( Z_{11} - \frac{Z_{12}Z_{21}}{Z_L + Z_{22}} \right) I_1 = Z_{in}I_1 \quad (33)$$

Input impedance  $Z_{in}$  and the two-port's effect on the input circuit are expressed as a two terminal loop of impedance, given by:

$$Z_{in} = Z_{11} - \frac{Z_{12}Z_{21}}{Z_L + Z_{22}} \quad (34)$$

It is assumed the transducer model is supplied with a transmission line voltage source connected by a transformer which is designed to match the real part of  $Z_{in}$ . The transmission line impedance is recognized as  $Z_0$  while the impedance looking *in* from the perspective of the transmission line is  $Z_{in}$ . It can be shown that by setting  $Z_L = Z_{in}$ , the reflection coefficient can be calculated for modeling the transmission line source wave interaction with the transducer. The Reflection Coefficient [3] is expressed as

$$\Gamma = \frac{Z_L - Z_0}{Z_L + Z_0} \quad (35)$$

With the reflection coefficient, the voltage and then the current at Loop 1 can be calculated using the voltage-reflection and current-reflection relationship expressed as

$$V(z) = V_0^+ [e^{-j\beta z} + \Gamma e^{j\beta z}] \quad (36)$$

$$I(z) = \frac{V_0^+}{Z_0} [e^{-j\beta z} - \Gamma e^{j\beta z}] \quad (37)$$

If the distance  $z$  along the transmission line to loop 1 is electrically small ( $d \ll \lambda$ ), the voltage-reflection and current-reflection relationships of a transmission line reduce to

$$V(\sim 0) = V_0^+ [1 + \Gamma] \quad (38)$$

and

$$I(\sim 0) = \frac{V_0^+}{Z_0} [1 - \Gamma] \quad (39)$$

where it is recognized that for very small electrical lengths of  $z$ , the exponential reduces to 1:  $e^{\pm j\beta z} \cong 1$ .

Realizing the Voltage and Current on loop 1 (source loop) using equations 38 and 39, we can combine them with the self-impedances and mutual impedances of the transducer theory matrix and solve for the voltage and current of loop 2. Finally, given known values for the various transducer matrix variables, we can calculate the real power across the system.

### 3.3.3.2 Real Power Transfer Parameters for Transducer Efficiency

To obtain real power transfer metrics we first need to define the real power supplied by transmission line source, the real power loss due to reflection and the real power transmitted to the transducer model. The real power transmitted to the transducer model is the real power that is initially seen by the source loop and therefore distributed among the system of the transducer model. Real power is known as the power lost due to Ohmic resistance.

The real power supplied by the transmission line source may be expressed as incident power as follows:

$$P_{inc} = \frac{|V_{src}|^2}{Re(Z_0)} \quad (40)$$

where,

$P_{inc}$  is the power incident wave from the transmission line source,

$V_{src}$  is the source voltage connected to the transmission line and

$Z_0$  is the characteristic impedance of the transmission line source.

The incident power wave will then hit the boundary of the transmission line and the two loop system, that is the first loop known as the source loop coupled to the second loop. The wave will then undergo a reflection and transmission split in real power and in which the reflected power is expressed as:

$$P_{refl} = \frac{|V_{src}|^2 \cdot |\Gamma|^2}{Re(Z_0)} \quad (41)$$

Where

$P_{refl}$  is the power reflected from incident wave due to any impedance mismatch.

The real power that reaches the first loop (source) is expressed as follows:

$$P_{tr} = \frac{|V_{src}|^2}{Re(Z_0)} \cdot (1 - |\Gamma|^2) \quad (42)$$

Where,

$P_{tr}$  is the power transmitted from the incident wave and is dependent upon any impedance mismatch. Knowing the power that is sourced from the transmission line, the efficiency in terms of percentage may be defined as the real power that is delivered to the battery load, divided by the incident real power, multiplied by 100. The percent efficiency of the transducer configuration is thus expressed as:

$$Eff = \left( \frac{P_{batt}}{P_{inc}} \right) \cdot 100 \quad (43)$$

Where,

$P_{batt}$  is the power dropped across the battery load and

$P_{inc}$  is the power incident from the transmission line source.

Therefore, using efficiency as a figure of merit, we can investigate both series and parallel tuning approaches for the primary and secondary loops as to which gives the optimal power transfer characteristics of the transducer system.

### 3.3.3.3 Tuning for Power Transfer Efficiency under Resonance Condition

At 1 MHz, there is significant inductive loading to the self-impedance for each loop. Because this inductive loading reduces efficiency it is necessary to minimize the reactance seen in the system. By adding the conjugate capacitance to the inductive impedance of a circuit, the reactive component can be reduced to nearly non-significant value. This technique results in a resonance condition where only the real part of the impedance is seen by the source. For each loop we have the option to tune the reactance in series or parallel with the inductive reactance of the loop. Using the inductive calculations that were previously derived we can solve for the tuning capacitance that is needed to cancel the reactive component of the impedance and achieve a resonance condition.

For series tuning of one loop,

$$\frac{1}{j\omega C_{tune}} = j\omega L_{loop} \quad (44)$$

where,

$C_{tune}$  is the tuning capacitance required to cancel the inductive reactance of the loop and  $L_{loop}$  is the inductive reactance due to the current in the loop.

Solving for the capacitance needed to cancel the inductive reactance, one obtains:

$$C_{s\_tune} = \frac{1}{\omega^2 L_{loop}} \quad (45)$$

Similarly for parallel tuning we can express the capacitance relationship as:

$$\frac{1}{j\omega C_{tune}} = R + j\omega L_{loop} \quad (46)$$

and thus solving for the capacitance needed to cancel the inductive reactance, we obtain:

$$C_{p\_tune} = \frac{1}{R^2 + (\omega L_{loop})^2} \quad (47)$$

Note that the tuning capacitance is dependent on both inductance reactance and resistance. When the resistance is significant when compared to the inductance reactance, the tuning capacitance will be impacted by both resistance and reactance. Hence, the secondary loop with a load of significant resistance will impact the parallel capacitance tuning. It is well understood that the resonance condition is required for maximum power transfer efficiency. Regarding series and parallel tuning, this thesis will investigate the different tuning combinations to realize the best use case. We can then determine the best tuning strategy for maximum power transfer or maximum efficiency at a given distance from a source loop to a receiver loop.

### 3.3.3.4 Resonance Tuning Conditions

A total of four separate tuning strategies will be investigated. The strategy will be to tune each loop separate from the other loop in either a series or a parallel configuration. The four configurations are as follows: Series-Series, Series-Parallel, Parallel-Series and Parallel-Parallel, which will be abbreviated as S-S, S-P, P-S and P-P, respectively.

#### 3.3.4.1 Verification of MathCAD models using Advanced Design System Simulations

The four MathCAD models labeled as S-S, S-P, P-S and P-P need to be validated. The Mutual Inductance is related to the coupling coefficient  $k$  and can be expressed as

$$k = \frac{M}{\sqrt{L_1 L_2}} \quad (48)$$

Where,

$M$  is the Static Mutual Inductance between loops 1 and 2.

$L_1$  is the Static Inductance of loop 1.

$L_2$  is the Static Inductance of loop 2.

By calculating the coupling coefficient  $k$  and applying an equivalent circuit schematic of the two loop system in simulation software Advanced Design System (ADS) by Agilent Technologies, we can simulate the circuit and then compare the results obtained using the MathCAD model results. The coupling coefficient can be inserted into the Mutual Coupling token used in ADS for mutual inductance and using an AC simulation token we can initiate a series of simulations in order to obtain currents and voltages to be compared to the respective MathCAD model for validity. In the first set of simulations, a coupling coefficient  $k$  of 0.199 from the S-S model was used in conjunction with a load of 10-Ohms to represent a low impedance battery, solely for model development and validation purposes. Figure 7 below shows the initial S-S simulation circuit.

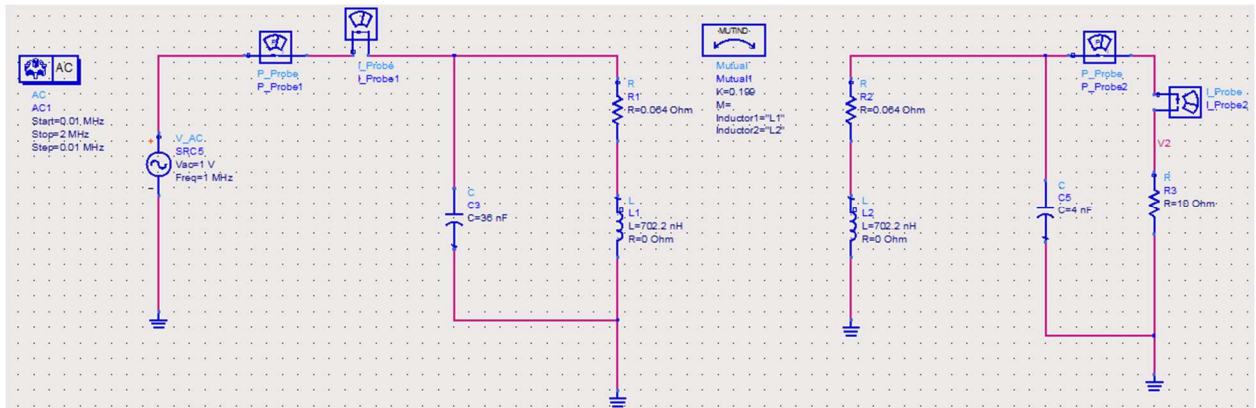


Figure 7. S-S equivalent tuning circuit to simulate the power transfer of the source loop to the receiver loop.

The simulation results for S-S AC simulation are shown in figure 8 below: For the resonant current in the source loop it can be shown there is an agreement in magnitude of the ADS circuit simulation and the MathCAD model. It is shown that the narrow band resonant response characteristic is depicted as expected.

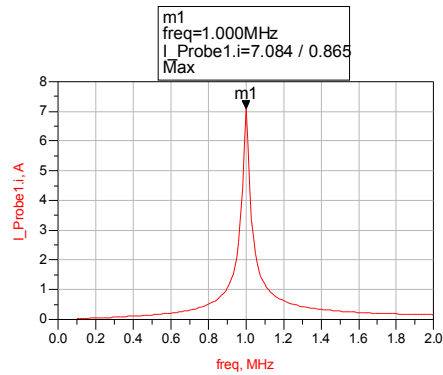


Figure 8. Current on source loop of S-S tuning configuration with a 10 ohm load, plotted in ADS versus frequency.

The MathCAD S-S model of the current on the source loop was calculated as:

$$I_{150} = 7.101$$

while the ADS simulation circuit model gave a magnitude of 7.084 Amperes.

For the resonant current in the receiver loop we can see an agreement in magnitude of the ADS circuit simulation and the MathCAD model, with the ADS results noted in figure 9. It is shown that the narrow band resonant response characteristic is depicted as expected.

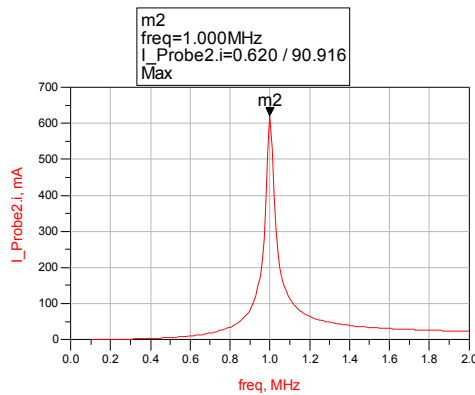




Figure 9. Current on receiver loop of S-S tuning configuration with a 10 ohm load plotted in ADS versus frequency.

The MathCAD S-S model of the current on the receiver loop was calculated as:

$$I_{2_{50}} = -2.669 \times 10^{-9} - 0.619i$$

while the ADS simulation circuit model gave a magnitude of 0.620 Amperes.

For the resonant voltage in the receiver loop we can see an agreement in magnitude of the ADS circuit simulation, plotted in figure 10 and the MathCAD model. It is shown that the narrow band resonant response characteristic is depicted as expected.

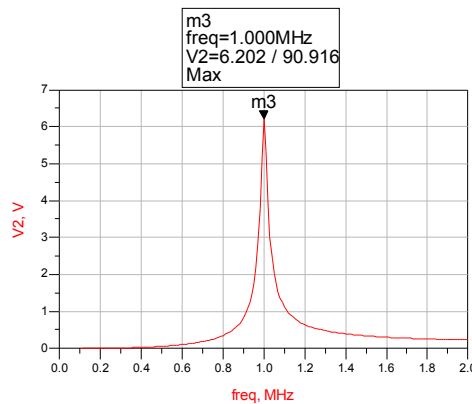


Figure 10. Voltage on receiver loop of S-S tuning configuration with a 10 ohm load plotted versus frequency.

The MathCAD S-S model of the voltage on the receiver loop battery load was calculated as:

$$V_{2_{50}} = 2.687 \times 10^{-8} + 6.233i$$

while the ADS simulation circuit model gave a magnitude of 6.202 Volts.

It is shown in Figure 11 below that for the resonant real power simulations it is calculated by ADS with a  $\frac{1}{2}$  factor whereas the MathCAD models do not use a  $\frac{1}{2}$  factor to calculate real power.

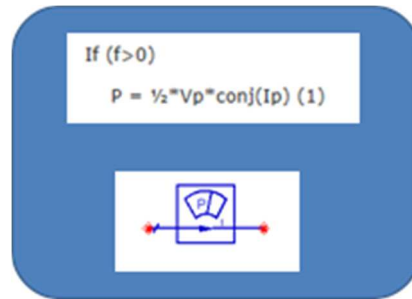


Figure 11. ADS graphical power calculation

Hence, in the source loop we can see an agreement of the ADS circuit simulation, shown in figure 12 below, and the MathCAD model. It is shown that the narrow band resonant response characteristic is depicted as expected.

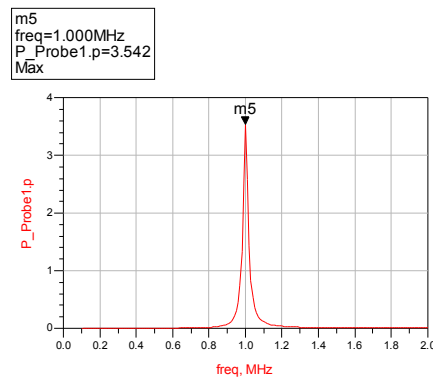


Figure 12. Real power on source loop of S-S tuning configuration with a 10 ohm load plotted in ADS versus frequency.

while the MathCAD S-S model of the real power in watts of the source loop is calculated as:

$$Ptr_{50} = 7.101$$

The ADS simulation circuit model gave a magnitude of 3.542 Watts. When multiplied by two to recover the one-half gives 7.804 Watts.

For the resonant real power in the receiver loop we can see an agreement of the ADS circuit simulation, as shown in figure 13 below, and the MathCAD model. It is shown that the narrow band resonant response characteristic is depicted as expected.

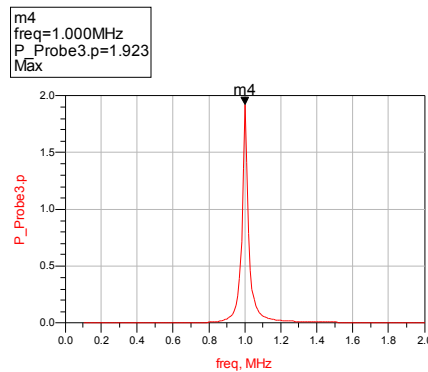


Figure 13. Real power on receiver loop of S-S tuning configuration with a 10 ohm load plotted against frequency.

The MathCAD S-S model of the real power on the receiver loop battery load was calculated as:

$$P_{batt_{50}} = 3.836$$

The ADS simulation circuit model gave a magnitude of 1.923Watts. When multiplied by two to recover the one-half gives 3.846 Watts.

Next, the receiver loop was changed from a series tuned circuit to a parallel tuned circuit.

The initial S-P simulation circuit is shown in figure 14 below.

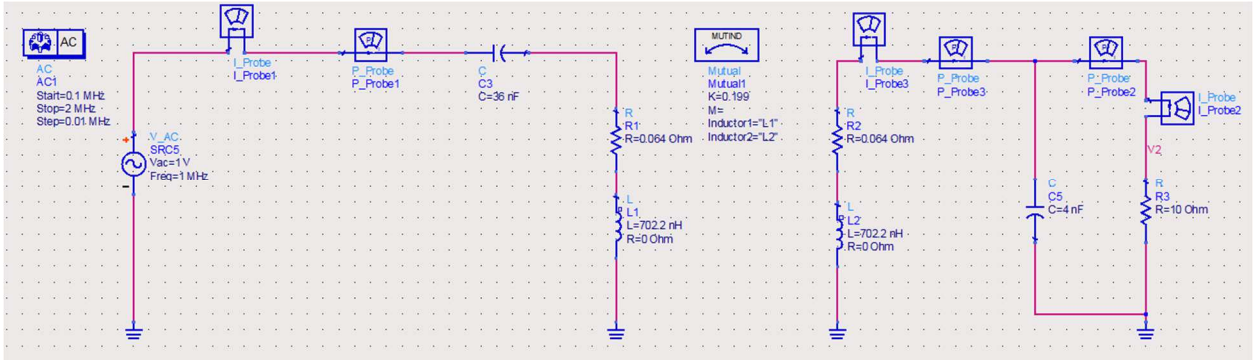


Figure 14. S-P equivalent tuning circuit for power transfer of the source loop to the receiver loop as designed in ADS.

The simulation results for S-P AC simulation are as follows. For the resonant current in the source loop it can be shown there is an agreement with the ADS circuit simulation, as displayed in figure 15 below, and the MathCAD model. It is shown that the narrow band resonant response characteristic is depicted as expected.

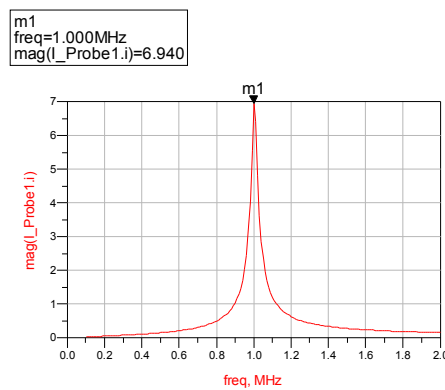


Figure 15. Current on source loop of S-P tuning configuration with a 10 ohm load plotted against frequency.

The MathCAD S-P model of the current on the source loop was calculated as:

$$I_{150} = 6.952$$

The ADS simulation circuit model gave a magnitude of 6.940 Amperes.

For the resonant current in the receiver loop we can see an agreement of the ADS circuit simulation, as shown in figure 16, and the MathCAD model. It is shown that the narrow band resonant response characteristic is depicted as expected.

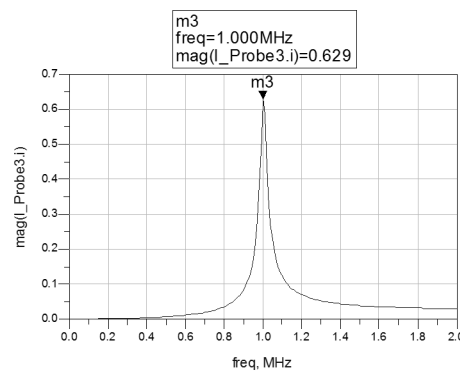


Figure 16. Current on receiver loop of S-P tuning configuration with a 10 ohm load plotted against frequency.

The MathCAD S-P model of the current on the receiver loop was calculated as:

$$I_{250} = 2.717 \times 10^{-9} + 0.63i$$

The ADS simulation circuit model gave a magnitude of 0.629 Amperes.

For the resonant voltage in the receiver loop we can see an agreement of the ADS circuit simulation, as noted in figure 17 below, and the MathCAD model. It is shown that the narrow band resonant response characteristic is depicted as expected.

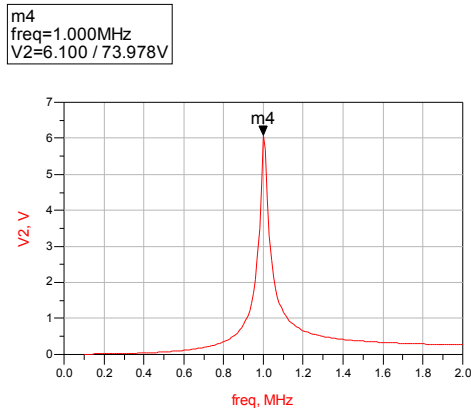


Figure 17. Voltage on receiver loop of S-P tuning configuration with a 10 ohm load plotted against frequency.

The MathCAD S-P model of the voltage on the receiver loop battery load was calculated as:

$$V_{2_{50}} = 2.63 \times 10^{-8} + 6.102i$$

The ADS simulation circuit model gave a magnitude of 6.1 Volts.

For the resonant real power the source loop we can see an agreement of the ADS circuit simulation, as seen in figure 18 below, and the MathCAD model. It is shown that the narrow band resonant response characteristic is depicted as expected.

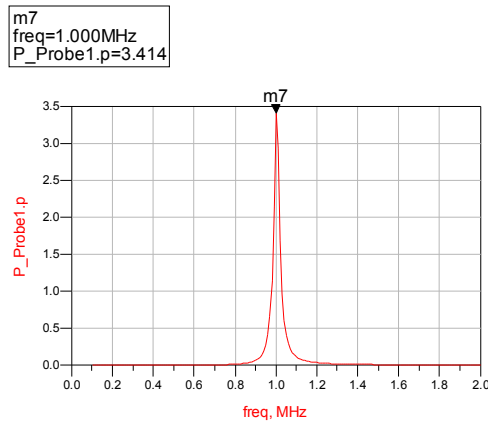


Figure 18. Real power on source loop of S-P tuning configuration with a 10 ohm load plotted against frequency.

The MathCAD S-P model of the real power on the source loop is calculated as:

$$Ptr_{50} = 6.952$$

The ADS simulation circuit model gave a magnitude of 3.414Watts. When multiplied by two to recover the one-half gives 6.828 Watts.

For the resonant real power in the receiver loop we can see an agreement of the ADS circuit simulation, as seen in figure 19 below, and the MathCAD model. It is shown that the narrow band resonant response characteristic is depicted as expected.

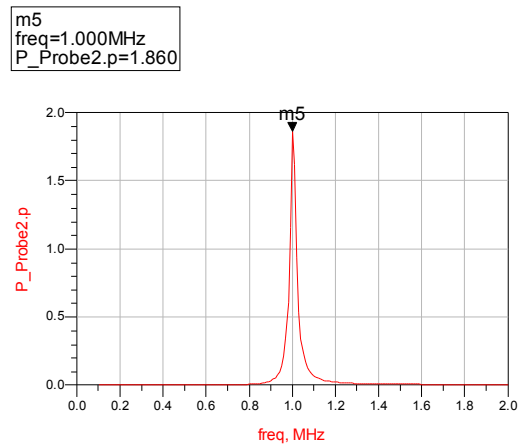


Figure 19. Real power on receiver loop of S-P tuning configuration with a 10 ohm load plotted against frequency.

The MathCAD S-P model of the real power on the receiver loop battery load was calculated as:

$$P_{batt_{50}} = 3.973$$

The ADS simulation circuit model gave a magnitude of 1.86 Watts. When multiplied by two to recover the one-half gives 3.72 Watts.

Next, the source loop is changed from a series tuned circuit to a parallel tuned circuit and the receiver loop was changed back to a series tuned circuit. The initial P-S simulation circuit is shown in figure 20 below.



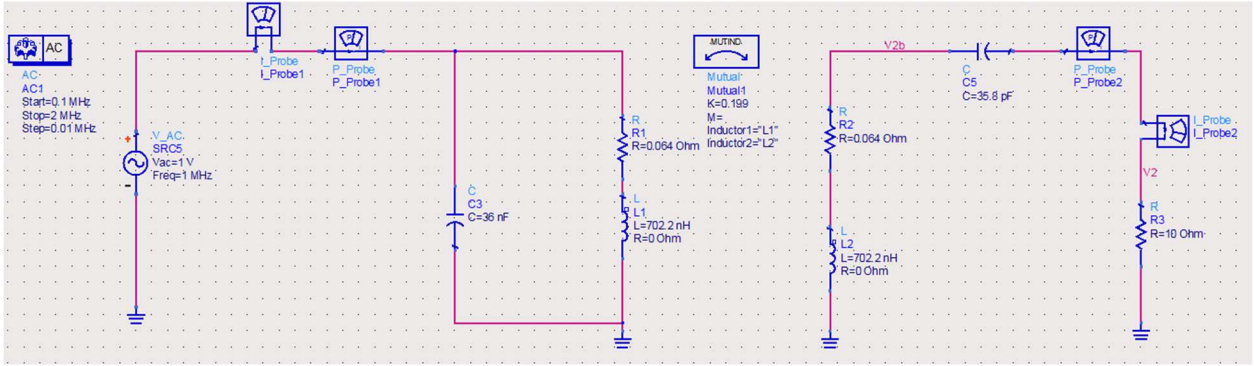


Figure 20. P-S equivalent tuning circuit for power transfer of the source loop to the receiver loop as designed in ADS.

The simulation results for P-S AC simulation are as follows: For the resonant current in the source loop it can be shown there is an agreement with the ADS circuit simulation, as shown in figure 21, and the MathCAD model. It is shown that the narrow band theoretical resonant response characteristic does not have the sharp characteristic response as expected.

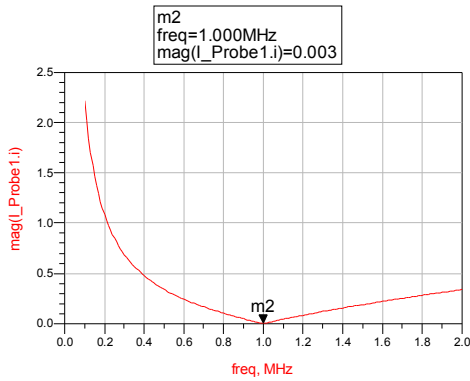


Figure 21. Current on source loop of P-S tuning configuration with a 10 ohm load plotted against frequency.

The MathCAD P-S model of the current on the source loop was calculated as:

$$I_{150} = 3.3 \times 10^{-3} + 3.592i \times 10^{-15}$$

The ADS simulation circuit model gave a magnitude of 0.003 Amperes.

For the resonant current in the receiver loop it shows an agreement of the ADS circuit simulation, as shown in figure 22 below, and the MathCAD model. It is shown that the narrow band theoretical resonant response characteristic does not have the sharp characteristic response as expected.

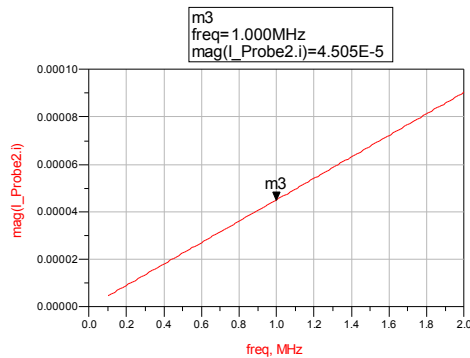


Figure 22. Current on receiver loop of P-S tuning configuration with a 10 ohm load plotted against frequency.

Where the MathCAD P-S model of the current on the receiver loop was calculated as:

$$I_{250} = -1.24 \times 10^{-12} - 2.878i \times 10^{-4}$$

The ADS simulation circuit model gave a magnitude of  $4.505 \times 10^{-5}$  Amperes.

For the resonant voltage in the receiver loop it shows an agreement of the ADS circuit simulation, as shown in figure 23 below, and the MathCAD model. It is shown that the narrow band theoretical resonant response characteristic does not have the sharp characteristic response as expected.

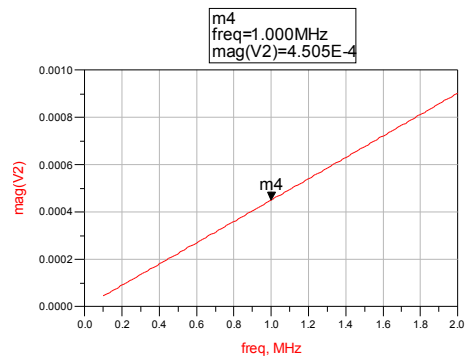


Figure 23. Voltage on receiver loop of P-S tuning configuration with a 10 ohm load plotted against frequency.

The MathCAD P-S model of the voltage on the receiver loop battery load is calculated as:

$$V_{2_{50}} = 1.248 \times 10^{-11} + 2.896i \times 10^{-3}$$

The ADS simulation circuit model gave a magnitude of  $4.505 \times 10^{-4}$  Volts.

For the resonant real power in the source loop it shows an agreement of the ADS circuit simulation, as shown in figure 24 below, and the MathCAD model. It is shown that the narrow band theoretical resonant response characteristic does not have the sharp characteristic response as expected.

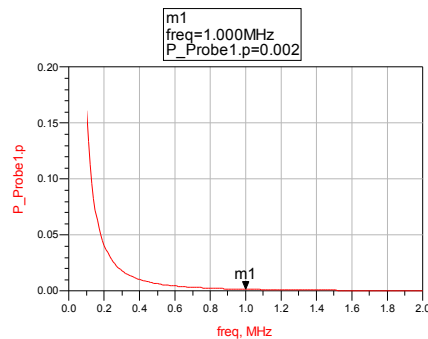


Figure 24 .Real power on source loop of P-S tuning configuration with a 10 ohm load plotted against frequency.

The MathCAD P-S model of the real power on the source loop is calculated as:

$$Ptr_{50} = 3.3 \times 10^{-3}$$

The ADS simulation circuit model gave a magnitude of 0.002 Watts. When multiplied by two to recover the one-half gives 0.004 Watts.

For the resonant real power in the receiver loop it shows an agreement of the ADS circuit simulation, as shown in figure 25 below, and the MathCAD model. It is shown that the narrow band theoretical resonant response characteristic does not have the sharp characteristic response as expected.

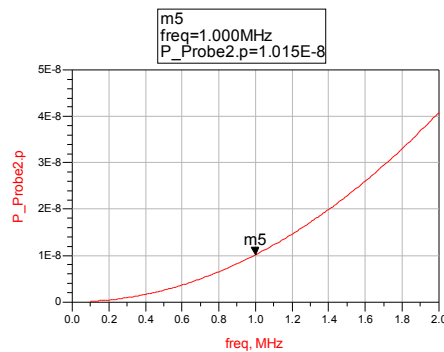


Figure 25. Real power on receiver loop of P-S tuning configuration with a 10 ohm load plotted against frequency.

The MathCAD P-S model of the real power on the receiver loop battery load was calculated as:

$$Pbatt_{50} = 8.281 \times 10^{-7}$$

The ADS simulation circuit model gave a magnitude that was very small in magnitude and on the order of micro watts.

Finally, the source loop is a parallel tuned circuit and the receiver loop was changed to a parallel tuned circuit and the initial P-P simulation circuit is shown in figure 26 below

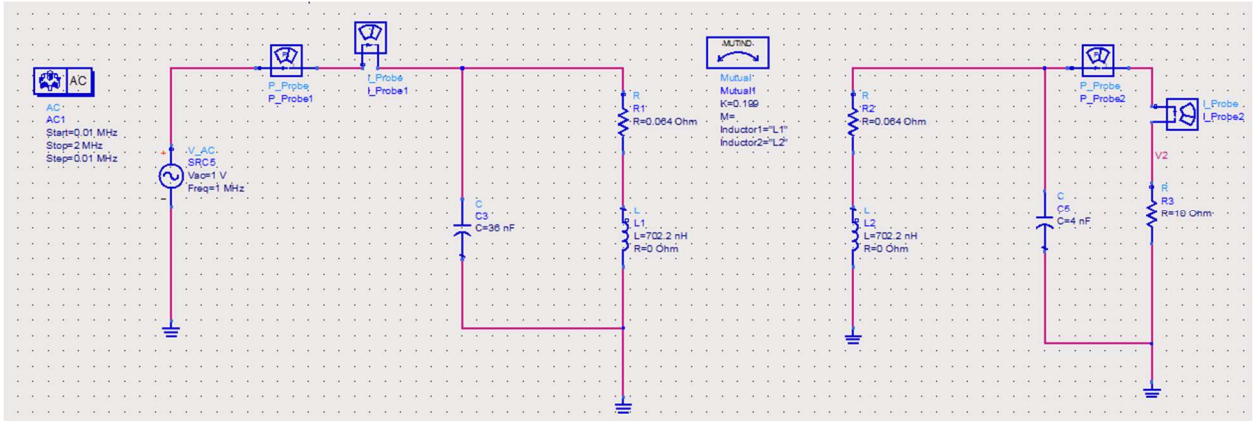


Figure 26. P-P equivalent tuning circuit for power transfer of the source loop to the receiver loop as viewed in ADS.

The simulation results for P-P AC simulation are now reviewed. For the resonant current in the source loop it can be shown there is an agreement of the ADS circuit simulation, as shown in figure 27, and the MathCAD model. It is shown that the narrow band theoretical resonant response characteristic does not have the sharp characteristic response as expected.

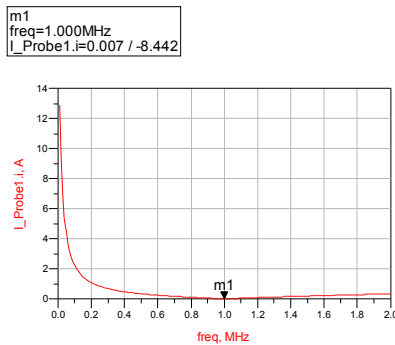


Figure 27. Current on source loop of P-P tuning configuration with a 10 ohm load plotted against frequency.

The MathCAD P-P model of the current on the source loop was calculated as:

$$I_{150} = 3.299 \times 10^{-3} + 3.735i \times 10^{-15}$$

The ADS simulation circuit model gave a magnitude of 0.007 Amperes.

For the resonant current in the receiver loop it shows an agreement of the ADS circuit simulation, as shown in figure 28 below, and the MathCAD model. It is shown that the narrow band theoretical resonant response characteristic does not have the sharp characteristic response as expected.

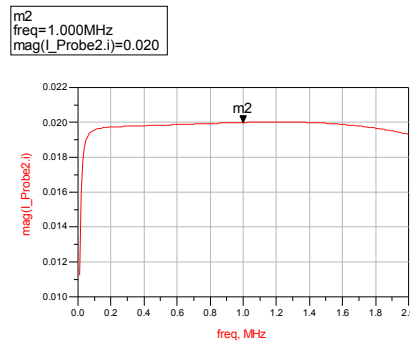


Figure 28. Current on receiver loop of P-P tuning configuration with a 10 ohm load plotted against frequency.

Where the MathCAD P-P model of the current on the receiver loop was calculated as:

$$I_{250} = -1.289 \times 10^{-12} - 2.992i \times 10^{-4}$$

For the resonant voltage in the receiver loop it shows an agreement of the ADS circuit simulation, as shown in figure 29 below, and the MathCAD model. It is shown that the

narrow band theoretical resonant response characteristic does not have the sharp characteristic response as expected.

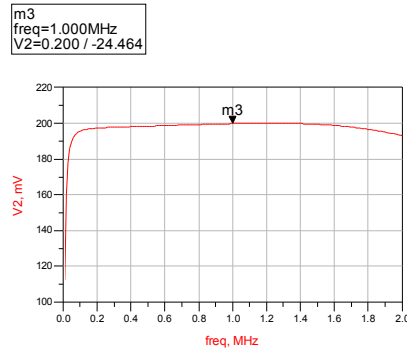


Figure 29. Voltage on receiver loop of P-P tuning configuration with a 10 ohm load.

The MathCAD P-P model of the voltage on the receiver loop battery load was calculated as:

$$V2_{50} = 1.248 \times 10^{-11} + 2.896i \times 10^{-3}$$

For the resonant real power in the source loop it shows an agreement of the ADS circuit simulation, as shown in 30 below, and the MathCAD model. It is shown that the narrow band theoretical resonant response characteristic does not have the sharp characteristic response as expected.

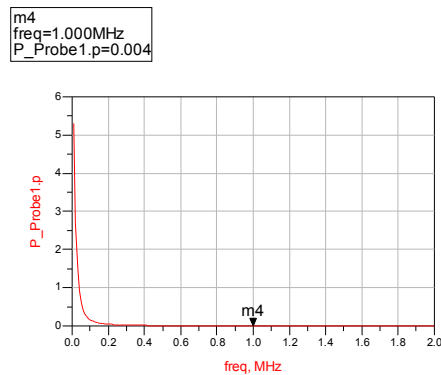


Figure 30. Real power on source loop of P-P tuning configuration with a 10 ohm load plotted against frequency.

The MathCAD P-P model of the real power on the source loop is calculated as:

$$Ptr_{50} = 3.299 \times 10^{-3}$$

For the resonant real power in the receiver loop it shows an agreement of the ADS circuit simulation, as shown in figure 31 below, and the MathCAD model. It is shown that the narrow band theoretical resonant response characteristic does not have the sharp characteristic response as expected.

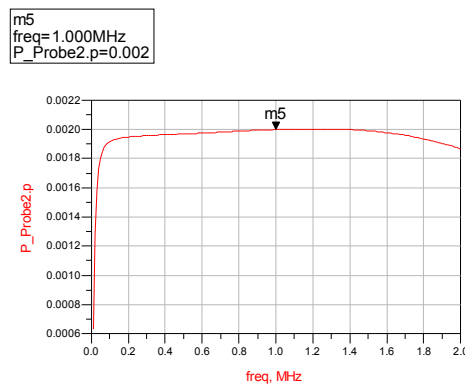


Figure 31. Real power on receiver loop of P-P tuning configuration with a 10 ohm load plotted against frequency.

The MathCAD P-P model of the real power on the receiver loop battery load was calculated as:

$$Pbatt_{50} = 8.951 \times 10^{-7}$$

Please refer to Table 1 below, which summarizes the MathCAD and ADS results for the four different coupling circuits: series-series, series-parallel, parallel-parallel, and



parallel-series. For comparisons of both MathCAD model results and ADS results, the magnitude was realized for generating a table that readily compares and contrasts the current, voltage and power of the two loop system.

Table 1. MathCAD simulations compared to respective ADS simulations

<b>Circuit</b>	<b>Model</b>	<b>I1</b>	<b>I2</b>	<b>V2</b>	<b>Power 1</b>	<b>Power to Load</b>
(Tuning)	(Tool)	(Amp)	(Amp)	(Volts)	(Watts)	(Watts)
Series-Series	MathCAD	7.101	0.619	6.233	7.101	3.836
	ADS	7.084	0.620	6.202	7.804	3.846
Series-Parallel	MathCAD	6.952	0.630	6.102	6.952	3.973
	ADS	6.940	0.629	6.100	6.828	3.72
Parallel-Series	MathCAD	3.0 m	290 μ	3.0 m	3.3 m	828 n
	ADS	3.0 m	45μ	450 μ	4.0 m	20 n
Parallel-Parallel	MathCAD	3.3 m	3.0 m	3.0 m	3.3 m	895 n
	ADS	7.0 m	20.0 m	200 m	4.0 m	4.0 m

Table 2 below lists the relative error/difference between MathCAD and ADS. Where the error can be expressed as  $\%Error = \frac{|ADS - MathCAD|}{|ADS|} \cdot 100$  and the results tabulated below.

Table 2. Percent error between MathCAD and ADS results

<b>Circuit Model</b>	<b>I1</b>	<b>I2</b>	<b>V2</b>	<b>Power 1</b>	<b>Power to Load</b>
(Tuning)	(% Error)	(% Error)	(% Error)	(% Error)	(% Error)
Series – Series	0.3	0.2	0.5	9.1	0.3

Series – Parallel	0.2	0.2	0.1	1.8	6.4
-------------------	-----	-----	-----	-----	-----

It is good to note that the MathCAD model accounts for radiation loss, however I do not think ADS will recognize the loss due to radiation nor is it modeled/considered in the circuit simulated.

Finally, Table 3 below lists the power transfer efficiency.

Table 3. Power transfer efficiency for each tuning circuit

0.05 meter distance	S – S	S – P	P – S	P – P
% Efficiency	54	57	0.02	0.02

### 3.3.5.1 Efficiency Comparisons of Loop Tuning Strategies with a 10-Ohm Battery Load

The four tuning configurations were setup in MathCAD for evaluating the Efficiency versus separation distance of the two loops. The Efficiency is defined as the real power delivered to the battery load, divided by the incident real power derived from the transmission line source, multiplied by 100 to state it as a percentage. It is expressed as follows:

$$Eff_Z := \left( \frac{P_{battZ}}{P_{incZ}} \right) \cdot 100 \quad (49)$$

The initial investigation assumed a 10 ohm load for simplicity. It was realized that efficiency is directly impacted by the Ohmic loading of the added load. Initial assumptions reduced the efficiency to a very low value and results were nearly incomparable. Hence, for finding a reasonable base line that made evaluation of the tuning easier, it was decided to begin by assuming a 10 ohm load. The efficiency is plotted for each tuning configuration. Four efficiency plots are shown in which two show significant advance in terms of percentage efficiency and both are of the same order.

Additionally, the efficiency in MathCAD vector format is shown for a quantitative comparison. Notably the S-S and S-P configurations of the MathCAD model and the ADS model performed very similar, within approximately three percent the 10 ohm load investigation. Both the P-S and the P-P performance are poor when compared to S-S and S-P configurations. Note that for a 10 ohm load the efficiency is only slightly better for the S-P than the S-S tuning configuration. Figures 32 – 35 show the efficiency plotted against the spacing for the respective circuit configurations in MathCAD

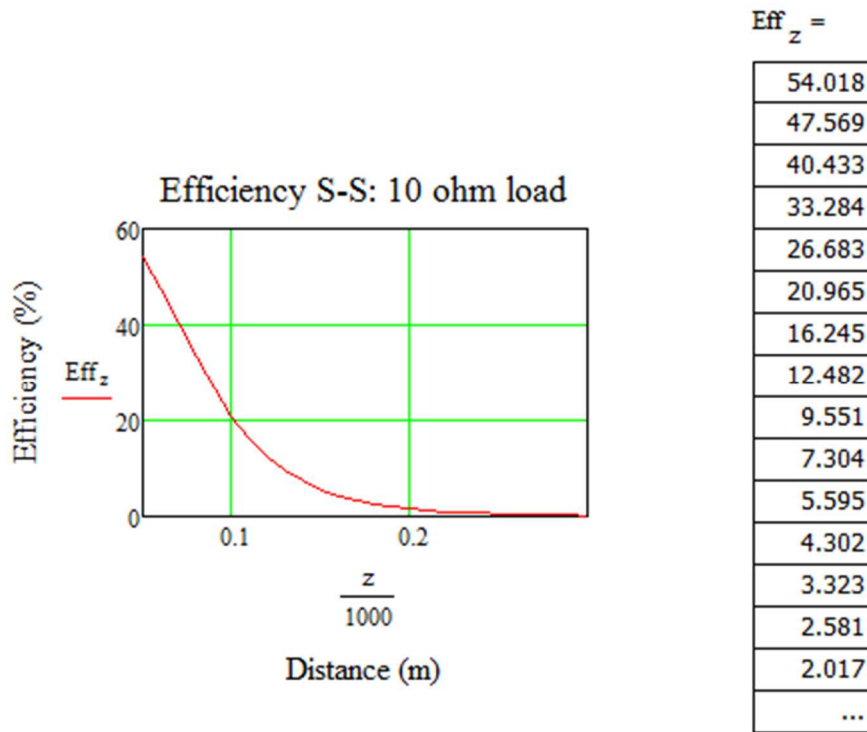


Figure 32. S-S tuning configuration with a 10 ohm load in graphical and vector format.

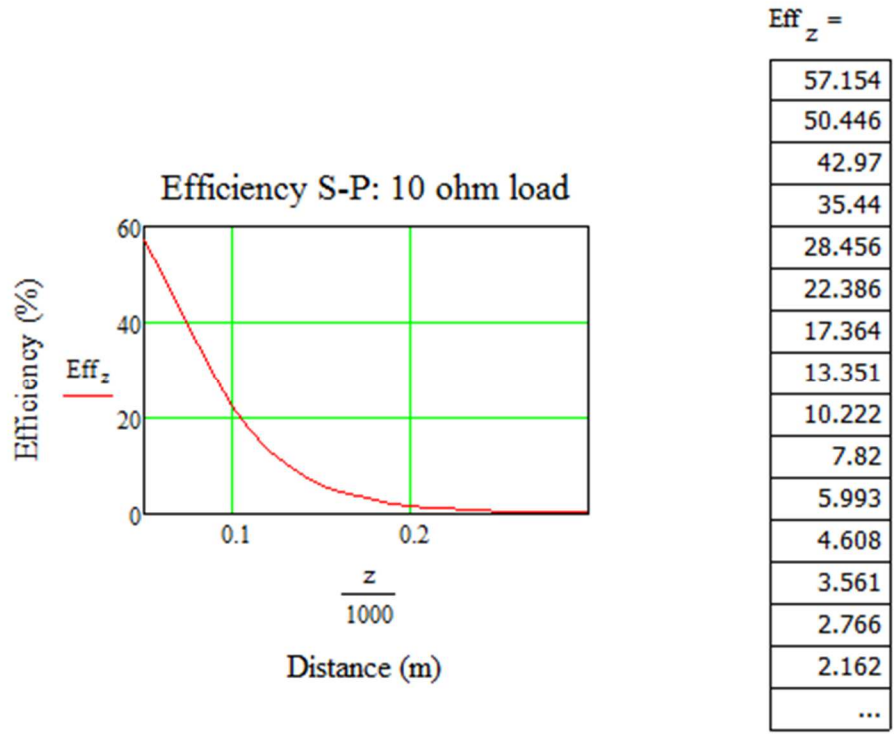


Figure 33. S-P tuning configuration with a 10 ohm load in graphical and vector format.

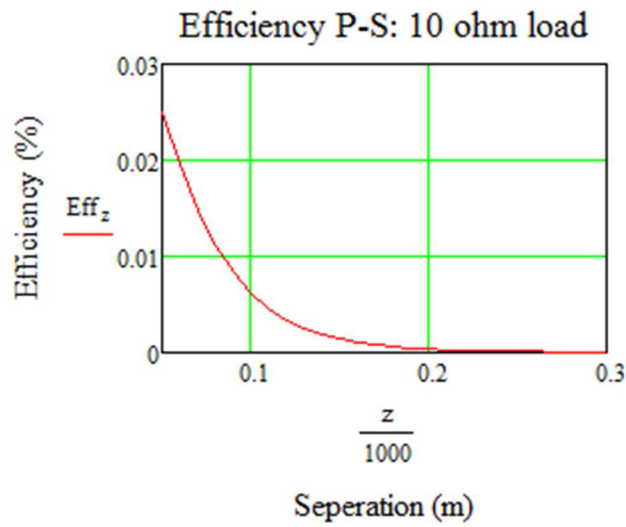


Figure 34. P-S tuning configuration with a 10 ohm load in graphical representation.

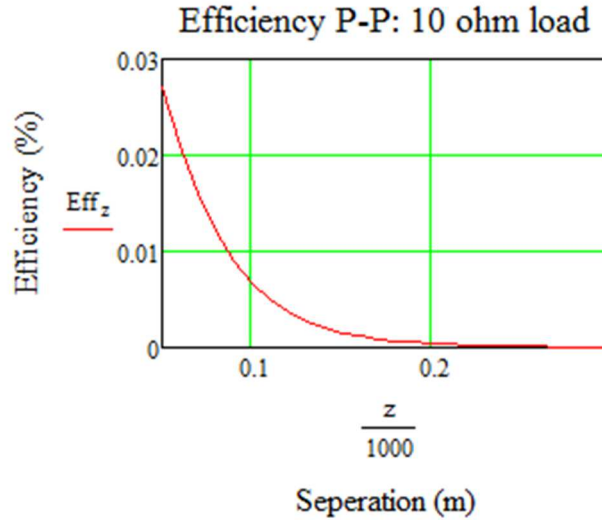


Figure 35. P-P tuning configuration with a 10 ohm load in graphical representation.

### 3.3.5.2 Efficiency Comparisons of Loop Tuning Strategies with a 300-Ohm Battery Load

Four tuning configurations were setup in MathCAD for evaluating the Efficiency versus a given half radius separation distance of the two loops. A surrogate 300 ohm load is used in place of the initial 10 ohm load. The 300 ohm load holds merit as a realistic pacemaker battery resistance [8]. The same analysis was repeated for plotting efficiency for each tuning configuration. It is shown that configurations S-S and S-P are similar in magnitude. Additionally, the MathCAD efficiency vector is shown for quantitative clarity of the efficiency percentage. It is shown below that the P-S and P-P configurations exhibit less than 1% efficiency. The P-S and P-P configurations are also noted as relatively poor performers when compared to S-S and S-P configuration, which are greater than 10% at 0.5 radius distances for a 0.1m radius and a 1MHz source. Figures 36 – 39 plot the respective Efficiency versus separation distance using the 300 ohm load.

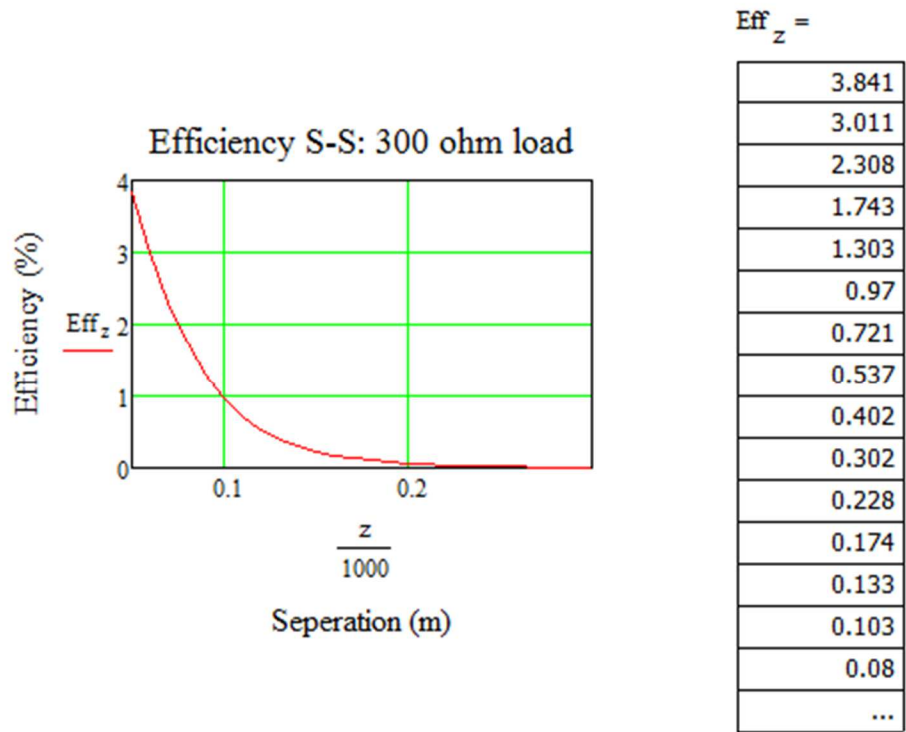


Figure 36. S-S tuning configuration with a 300 ohm load in graphical and vector format.

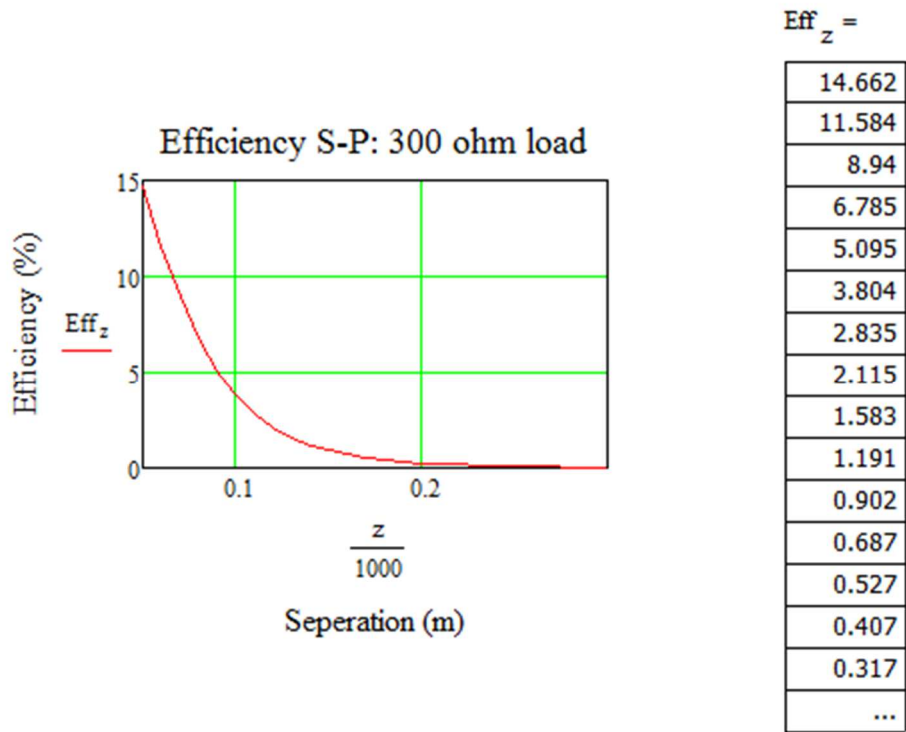


Figure 37. S-P tuning configuration with a 300 ohm load in graphical and vector format.

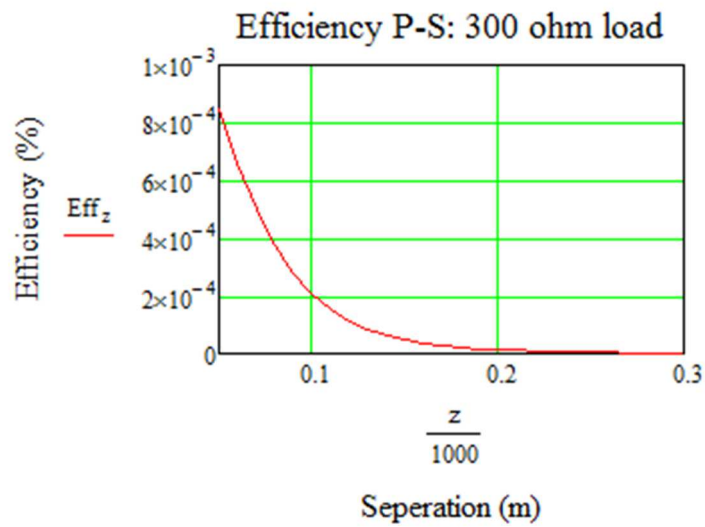


Figure 38. P-S tuning configuration with a 300 ohm load in graphical representation.

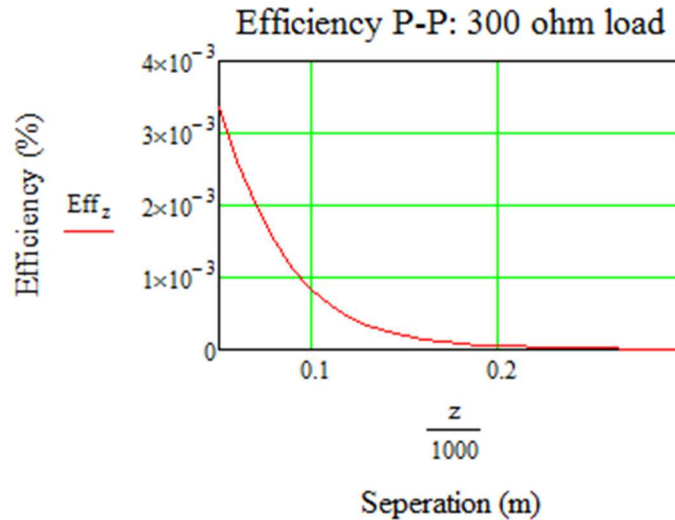


Figure 39. P-P tuning configuration with a 300 ohm load in graphical representation.

### 3.3.5.3 Efficiency Comparisons Discussion

A total of eight efficiency graphs representing the respective parallel or series tuning methods are shown. The first four graphs assume a 10 ohm load added to the receiver loop. The last four graphs assume a common battery load of 300 ohms representing the typical medical pacemakers [citation].

As noted by the efficiency graphs above, the S-P configuration is the most efficient method for tuning a loop in wireless power transfer for transferring power from the transmitter to the receiver load.

There are many papers and investigations that suggest S-P is the best method for tuning a two circuit system to maximize efficiency, yet the reasoning behind the attained efficiency is not discussed. Investigation into the explanation of the phenomenon has not been identified.

The reasoning behind the most efficient tuning method S-P can be explained in terms of the quality factor Q. The quality factor Q is a measure of the loss of a resonant circuit



[3]. Hence, lower loss implies higher Q. The efficiency study carried out above shows that the loss of the circuit, or efficiency, varies with different tuning configurations. The Q for a series resonant circuit is defined as:

$$Q_s = \frac{(\omega_0 L)}{(R)} \quad (50)$$

Where

$\omega_0$  is the angular frequency defined as  $2\pi f$

$L$  is the inductance of the copper wire loop in Henries per meter and

$R$  is the Ohmic resistance of the copper wire loop.

For the series resonant loop, Q gets smaller with added resistance.

For the Q of a parallel resonant circuit, the definition is expressed as:

$$Q_p = \frac{(R)}{(\omega_0 L)} \quad (51)$$

For the parallel resonant loop, Q becomes larger with added resistance.

Furthermore, it is known that the Series Resonator stores magnetic and electric energy as a function of current, while the Parallel Resonator stores magnetic and electric energy as a function of voltage [3]. With regards to wireless power transfer via near field inductive coupling of the magnetic energy, the focus will remain on the magnetic energy stored.

The stored magnetic energy of the series resonator can be expressed as:

$$W_m = \frac{1}{4} |I|^2 L \quad (52)$$

Where

$I$  is the current supplied to the loop circuit and

$L$  is the inductance of the copper wire loop in Henries per meter.

The stored magnetic energy of the parallel resonator can be expressed as:

$$W_m = \frac{1}{4} |V|^2 \frac{1}{\omega_0^2 L} \quad (53)$$

Where

$V$  is the voltage supplied to the loop circuit and

$L$  is the inductance of the copper wire loop in Henries per meter and

$\omega_0$  is the angular frequency defined as  $2\pi f$ , with  $f$  being the frequency in Hertz of the source generator.

The stored magnetic energy is realized by considering the interaction of the two loops.

The transmitting loop generates magnetic flux which passed through the inside perimeter of the second loop. As the second loop captures the magnetic flux due to the first loop and it drives current. The resistance then increases and directly impacts  $Q$  as shown in equations 50 and 51. For the primary loop, known as the transmitter loop, its series capacitor tuning is better for the simple reason that if the primary is connected to a source with parallel tuning, significant amounts of current will tend to shunt to ground through the parallel capacitor.

### 3.4 Discussion

In this chapter a two loop wireless power transfer physics model was developed in MathCAD with the equivalent circuit for the two loop wireless power transfer is built and simulated in ADS. The current, voltage and power values on the transmitter and receiver loop from the ADS simulations were then compared to the physics model developed in MathCAD.

Next, the series tuning and parallel tuning combinations of the two loop wireless system were investigated to determine the maximum efficiency in wireless power transfer to the load on the receiver loop. It is shown that the series resonant tuning configuration on the

transmitter loop and a parallel resonant tuning configuration on the receiver loop is the best approach, with respect to an Ohmic load on the receiver loop, to maximize the power transfer of the wireless power transfer system.

Finally, it is expressed that the reasoning for series resonant tuning on the transmitter loop and parallel resonant tuning on the receiver loop is explained in terms of the quality factor  $Q$ . The quality factor  $Q$  confirms the series-parallel configuration is the most efficient option based on the mathematical physics model assumption of a closed form solution which is developed in MathCAD for investigating wireless power transfer.

## CHAPTER 4

### SHIELDED LOOP POWER TRANSFER PROPERTIES OF THE TWO LOOP SYSTEM

#### 4.1 Introduction background for Shielded Loops

Shielded loops and their characteristics, and comparisons with the wireless power transfer model will be investigated. The shielded loop has performance advantages over a single turn wire loop [14]. Consider a 50- $\Omega$  RG-58 copper shielded loop of 0.1 meter radius. The loop is assumed to be sourced by a neck feed that has a smooth transition from the feed to the loop itself, with the neck feed also being composed of copper RG-58 transmission line conductor. An RG-58 shielded loop of 0.1 meter radius is shown in figure 40 below.

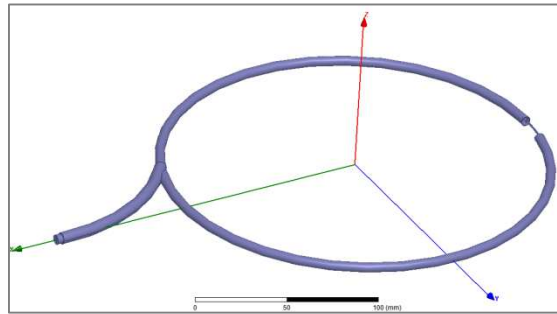


Figure 40. A single 50- $\Omega$  copper shielded loop of 0.1m radius.

The construction of the loop itself consists of the first-half of the loop made of RG-58 coaxial transmission line as shown in Figure 41.

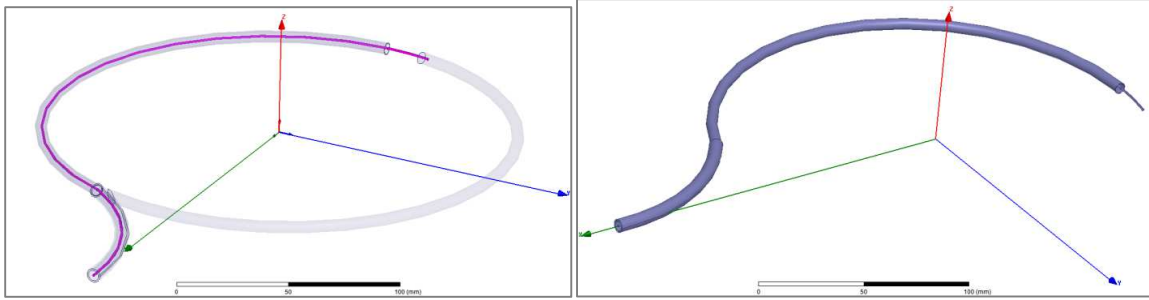


Figure 41. A single 50-Ω copper shielded loop of 0.1m radius depicting the first half and neck as RG-58 coaxial cable.

At approximately half of a turn (180 degrees from neck feed) the RG-58 coaxial construction of the outer shield is terminated while the inner conductor continues for approximately 1/10<sup>th</sup> a turn (36 degrees). The center conductor is then physically attached, typically using a weld, to a solid copper conductor with a radius equal to the outer diameter of the RG-58 coaxial transmission line, as shown in Figure 42.

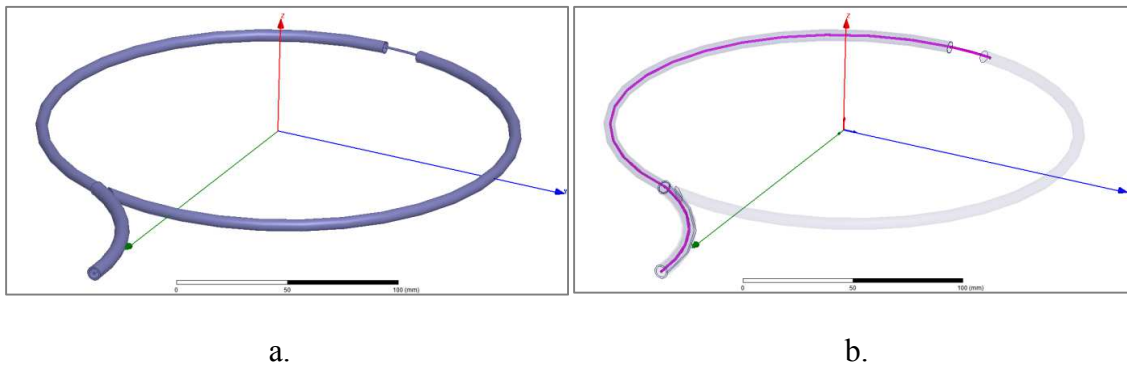


Figure 42. A single 50-Ω copper shielded loop of 0.1m radius depicting center conductor united with a solid object of RG-58 coaxial cable dimensions, with *a* the general outside figure appearance, while *b* shows the outside coaxial cable being transparent to highlight the inner conductor.

The solid copper conductor then continues to construct the loop until it reaches the feed/neck, where it makes electrical contact with the outer conductor/shielding of the RF-58 coaxial loop as shown in Figure 43

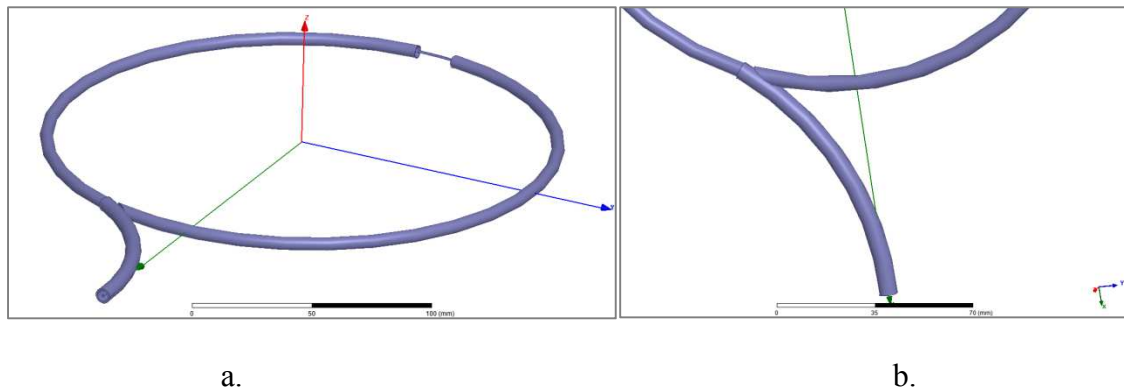


Figure 43. a) A single 50- $\Omega$  copper shielded loop of 0.1m radius depicting the neck feed composed of RG-58 coaxial cable dimensions, with b) an enlargement of the feed/neck location

#### 4.2 Two Loop Coupling System Methodology

Two shielded loops composed of a transmitter and a receiver are used for validating the MathCAD wireless power transfer model. The initial efforts in simulating wireless power transfer for comparing the MathCAD wireless power transfer physics model begin with both loops of equal dimensions separated by half of the loop's radius distance, with a radius of 0.1 meters. By placing HFSS wave ports at the mouths of the neck feed lines the two loop simulation is modeled as a two port device. Thus, the HFSS simulation for the co-axial loops will readily give the S-matrix values of the two shielded loop system. The HFSS S-matrix results can then be readily compared with the MathCAD model results by calculating the S-matrix from the impedance matrix.

The first simulation will consist of a single shielded loop without any resonance tuning in the simulation setup. The next simulation will consist of two shielded loops, with the neck feeds mirrored to each other and no resonant tuning incorporated into the simulation setups. These simulations shall be labeled as untuned shielded loop simulations, in which neither the receiving and transmitting loops, nor source is impedance matched or tuned.

Due to asymmetry of the E-fields that occurs at the open end of the coaxial cable located approximately 180 degrees from the neck feed; expected results are impacted due to the E-field concentrated from both shielded loops at one end resulting in a dipole behavior. A final simulation configuration of the two untuned shielded loop is setup with the neck feeds drawn at 180 degrees opposed to each other as shown in figure 44.

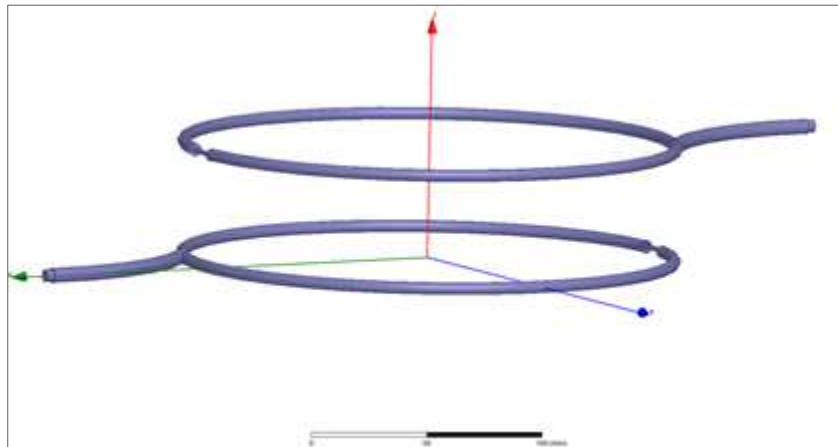


Figure 44. Two shielded loops with neck feeds 180 degrees opposite of each other.

It is proposed that as an additional candidate for investigating the wireless power transfer MathCAD models will be to use the HFSS S-matrix results of resonant tuned shielded loops. This will allow for investigating how much of the power delivered from the source loop to the receiving loop is transferred and quantify the efficiency, as also

performed in chapter 3, for each configuration. For quantitative analysis of wireless power transfer radiation loss, both the HFSS simulation radiation loss and the MathCAD model radiation loss will be compared. Additionally, the Ohmic losses for both models will be used to verify power conservation and model validation. Although relatively small, it is noted that the additional transmission line length of the loop due to the neck feed will add a subtle difference in geometric length which will impact the final impedance result given by HFSS simulation.

Finally, the investigation into power transfer efficiency vs radiation loss will be considered. Power transfer efficiency is a function of frequency and it is proportional to radiation loss into the far field.

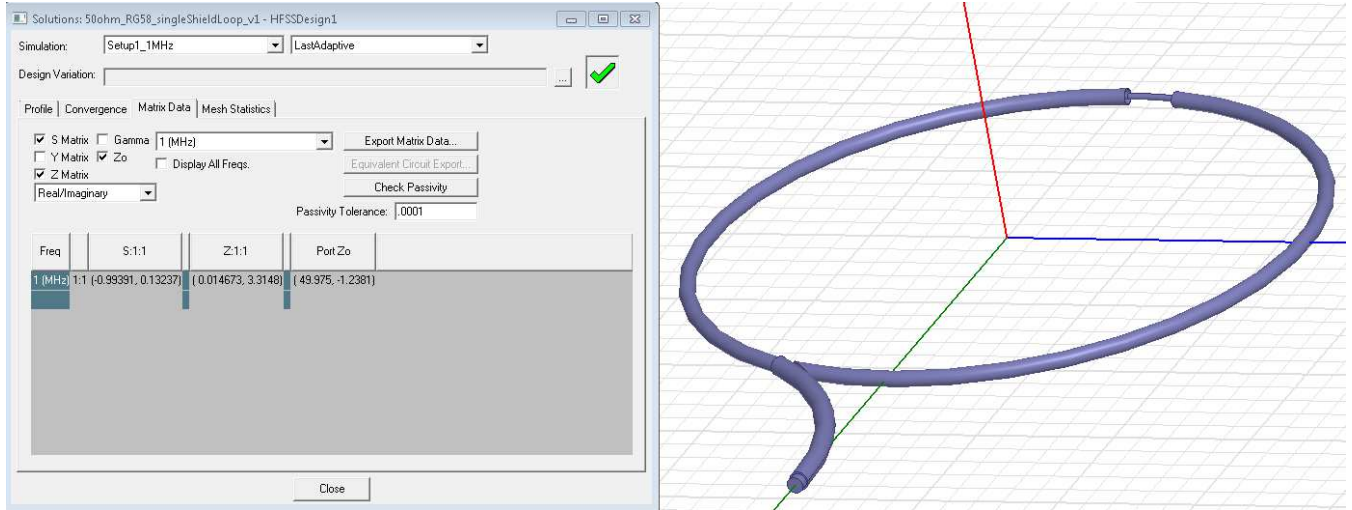
Regarding design analysis considerations, it can be shown that the power transfer efficiency and radiation loss trade-off can be optimized and used as a baseline model of a baseline system. This baseline model will be used for considering an optimal power transfer system with reduced radiation loss as the first iteration for a final design. The baseline model needed will be derived from the shielded loop analysis given in the following pages of this chapter.

#### 4.2.1 HFSS S-Matrix Untuned Shielded Loop Results

A single untuned shielded loop constructed of RG58 dimensions and with a loop radius of 0.1 meters was simulated at 1MHz using HFSS, with the results of the S-parameters, Z-parameters and characteristic impedance equaling  $Z_0 \cong 50\Omega$ . The HFSS



drawing and results are shown in figure 45.

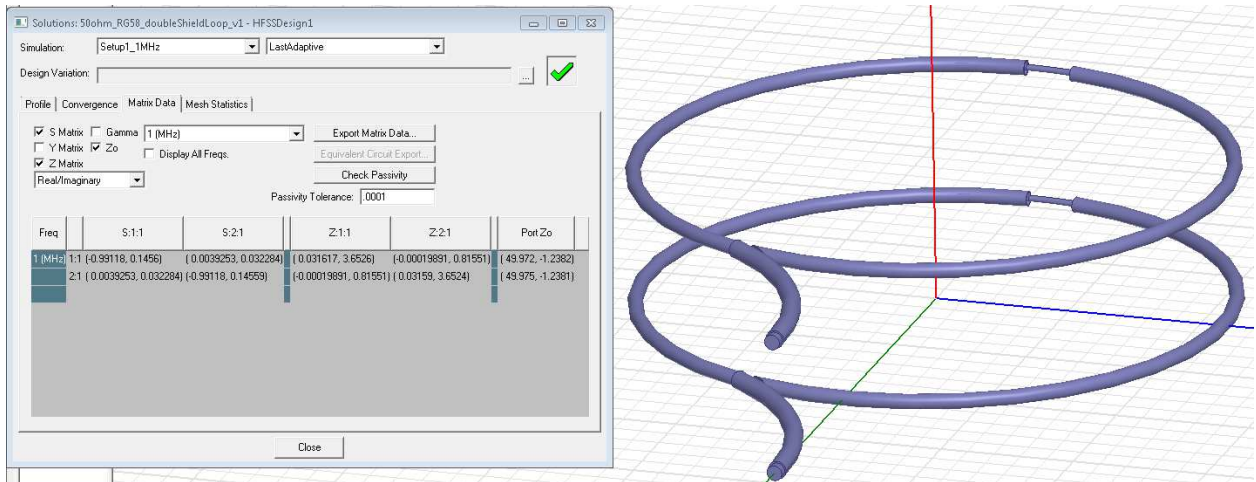


a.

b.

Figure 45. a) Single Shielded loop results and b) its physical configuration.

Next, two untuned shielded loops constructed of RG58 dimensions and with a loop radius of 0.1 meters was simulated at 1MHz using HFSS. The first configuration involved simulating with both neck feeds on the same side, as shown in figure 46 below. Thus, the two shielded loops are configured as mirrors of each other separated by half a loop radius. The shielded loops are simulated in HFSS and the results of the S-parameters, Z-parameters and characteristic impedance was  $Z_0 \cong 50\Omega$ . The HFSS drawing and results are shown in figure 46.



a.

b.

Figure 46. a) Two shielded loop results and b) the physical configuration showing the orientation of the neck feeds.

The last untuned simulation with a half loop radius separation will be drawn as two untuned shielded loops constructed of RG58 dimensions and with a radius of 0.1 meters. The HFSS simulation frequency for this analysis is also 1MHz. The configuration shall begin by simulating both neck feeds 180 degrees apart, as shown in figure 47. In other words, it may be considered that the two shielded loop neck feeds are configured as reciprocals of each other, separated by half a loop radius. The shielded loops are simulated in HFSS with the results of the S-parameter's, Z-parameters and characteristic impedance being  $Z_0 \cong 50\Omega$ . The HFSS drawing and results are shown in figure 47.

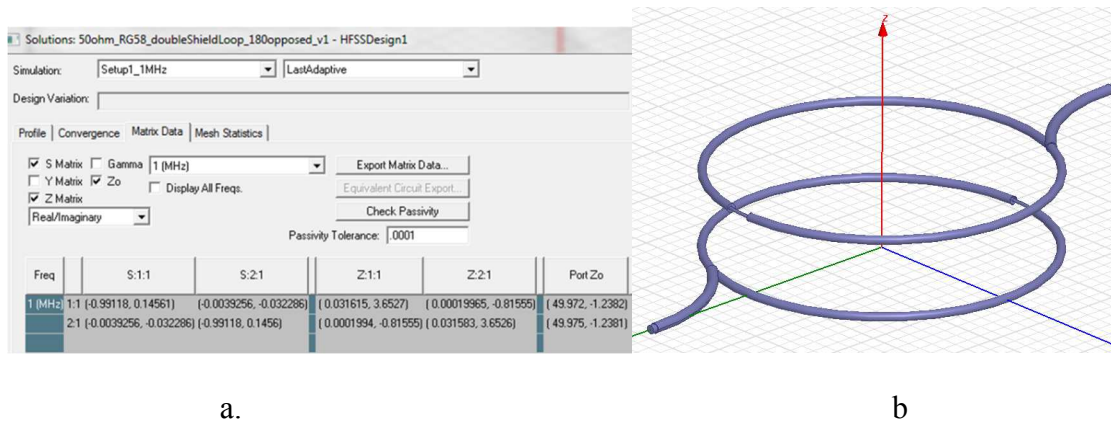


Figure 47. a) The simulation results and b) the physical configuration of the two shielded loops with neck feeds 180 degrees apart.

#### 4.2.2 HFSS MathCAD Wireless Power Transfer models using untuned loops

For additional validation of wireless power transfer model, the HFSS results of the simulation of the configured two shielded loop, with neck feeds 180 degrees apart, will be used as the reference for wireless power transfer model. The wireless power transfer model is altered so that the wire thickness matches the center conductor of the HFSS two shielded loop simulation. Furthermore, the HFSS S-parameter S12 and S21 results will need the phase re-calculated due to the phase shift from the length of the transmission line starting at the neck feed all the way to the solid conductor, which includes half the perimeter of the shielded loop and the neck feed that was added for simulation. The neck feed is needed in the HFSS simulation simply for the case if the shielded loop is physically constructed with actual RG58. Thus, the added length is used to form a physical realizable system that may be used in measurements of S-parameters. The s-parameters realized via HFSS simulation is expressed previously in Figure 47 and is also tabulated below in table 4 for comparison of wireless power transfer model using

MathCAD. The table shows both real and imaginary s-parameters of a two port system at 1MHz, with a radius of 0.1m and separated by half a radius.

Table 4. S-parameters of two shielded loops with neck feeds 180 degrees apart

2 Shielded Loops			S-Parameters							
Seperation	Radius	Freq	HFSS							
Radius	m	MHz	S[1,1]_Real	S[1,1]_Imag	S[1,2]_Real	S[1,2]_Imag	S[2,1]_Real	S[2,1]_Imag	S[2,2]_Real	S[2,2]_Imag
0.5	0.1	1	9.91E-01	1.46E-01	3.93E-03	3.23E-02	3.93E-03	3.23E-02	9.91E-01	1.46E-01

The s-parameter results for an untuned two loop system realized via MathCAD wireless power transfer model is tabulated below in table 5. The table shows both real and imaginary s-parameters of a two port system at 1MHz, with a radius of 0.1m and separated by half a radius.

Table 5. Wireless Power Transfer Model s-parameters of two loops

2 Shielded Loops			S-Parameters							
Seperation	Radius	Freq	Wireless Power Transfer Model							
Radius	m	MHz	S[1,1]_Real	S[1,1]_Imag	S[1,2]_Real	S[1,2]_Imag	S[2,1]_Real	S[2,1]_Imag	S[2,2]_Real	S[2,2]_Imag
0.5	0.1	1	9.99E-01	3.90E-02	5.01E-04	9.28E-03	5.01E-04	9.28E-03	9.99E-01	3.90E-02

The error metric is used to compare the accuracy of the mathematical wireless power transfer (i. e. MathCAD) model in comparison with the HFSS two shielded loops system for untuned loops. The percentage error calculation for comparing s-parameter results for an untuned two loop system realized via MathCAD wireless power transfer model and HFSS two shielded loop system is tabulated below in table 6. The results show reasonable agreement within 5% error and are as low as less than 1% error. This achievement is considered good enough for modeling a wireless power transfer system using two untuned shielded loops at 1MHz.

Table 6. Percent error s-parameter for two methods of two loops

2 Shielded Loops			HFSS vs Wireless Power Transfer Model			
Seperation	Radius	Freq	Percentage Error (%)			
Radius	m	MHz	S11	S12*	S21*	S22
0.5	0.1	1	0.21%	3.36%	3.36%	0.21%
* Phase adjusted for Transmission Line electrical length						

#### 4.3 Post processing of shielded loop HFSS simulation

In the HFSS shielded loop simulations the coaxial line from neck feed to coaxial outer shield termination contributes a phase and therefore post processing is used to correct for the distance traveled. HFSS has a post process operation, however because the HFSS post processing is only capable of one dimensional processing and coaxial cable of the loop run is a two dimensional trace, a mathematical post process in MathCAD is required. Hence, the post processing for the HFSS simulation was required due to the additional RG58 coax that is added at the neck feed. The sources of the two loop system in the MathCAD model assumes a lossless source that is matched anywhere within the loop. The HFSS feed source for the shielded two loop system is composed of additional RG58 line and has a finite length that contributes additional Ohmic loss and reactance. This difference in Ohmic loss and reactance is negligible, however the phase shift added from the neck feed to the end of the coax located at 180 degrees from neck feed, is significant.

#### 4.4 Discussion

Two shielded loops are built, simulated and the results are compared to the MathCAD wireless power transfer model results. The shielded loop results are slightly different than the wireless power transfer model due to physical characteristic variation of the solid copper wire to the RG58 coaxial cable physical dimensions. HFSS simulation results of

the shielded loop power transfer configuration show reasonable agreement with wireless power transfer model.

## CHAPTER 5

### HELIX LOOP INVESTIGATION OF THE TWO LOOP SYSTEM

#### 5.1 Introduction background for Helix Loops

The design intent of a two loop system of conductors is to control the H-Field while reducing or minimizing the near E-Field. Thus, our goal is to minimize all far field radiation, and having a good understanding/control of a designed, shaped near H-Field. The HFSS software package will be used to test the geometry and initial setup design, and conduct the analysis, simulation and plotting for evaluation and iterative design. The initial Helix investigation focuses on double helix loop conductors, that include twisted loops of 4-cycles (4-spirals) along a radial path in a  $2\pi$  sweep in the  $x-y$  plane of an  $x-y-z$  coordinate system. The radius of the conductor will consist of the same geometry as the well-known industry “twin-line” (twin-lead) conductor, composed of copper metal. The initial Helix approach is to design a 10cm radius loop with a conductor radius of 0.406 mm. The distance apart from conductor to conductor is 7.5 mm (edge-to-edge).

#### 5.2 HFSS setup

Investigating the E & H field characteristics will start by first creating a single loop baseline design in order to obtain a benchmark, with the remaining two helix designs evaluated against this bench setup. The geometric design goal is for all loops to be modeled after the dimensions of a twin-line conductor. Three loop geometries will be studied, with the first geometry being a flat single conductor, the second geometry being a single helical shaped 4-cycle conductor, and the last geometry is a double helix loop 4-cycle conductor. Single loops will use a single wave port, whereas the double helix loop

designs will use two wave ports. The simulation solution type in HFSS is set to Driven Modal.

### 5.2.1 HFSS Tetrahedral defaults

HFSS uses tetrahedral mesh elements to determine the electromagnetic solution and for result precision. HFSS simulation algorithms include running initial simulation(s) and developing refined tetrahedral mesh elements by method of tetrahedral refinement. No tetrahedral refinement is executed at this time.

### 5.2.2 HFSS poly-line setup for field plotting

For investigating E & H field characteristics vs distance, poly-lines of 800mm in length are drawn on each axis. These specific poly-lines are used for plotting the magnitude of E and H fields along each individual axis in a rectangular plot format. The plots show each individual field component as a function of distance from center of the loop to a distance of 800mm.

Next, using global planes as a reference, Field Overlay plots are used for contour plots of fields on all three planes ( $XY$ ,  $XZ$ , and  $YZ$ ) of an  $x$ - $y$ - $z$  space. These contour plots show the complex magnitude for both E & H fields along all three planes, starting at the center of the loop and extending to a distance in which the field remains constant or negligible change.

In the E-field planar contours, both spiral designs of the single and the double helix conductors show a strong E-field at the source, however the E-field has a significant drop by the time it reached the opposite side of the loop, 180 degrees away. This phenomenon is due to the loops being electrically small compared to the EM wavelength.



### 5.2.3 Single flat loop

A simulation setup was prepared for a single flat loop conductor. The simulation for this geometry is setup to yield a field overlay of the H-field vectors and is plotted on top of the single loop geometry. The single flat loop and H-field overlay can be seen in Figure 48. Next, H and E fields are plotted using rectangular plots and planar contour plots. The rectangular plots are used for observing characteristics and any field peak shifts when comparing all design simulation results. The rectangular plots represent field magnitude versus distance for both E and H fields separately along all three axes. The plot  $H_z$  is shown in Figure 49.

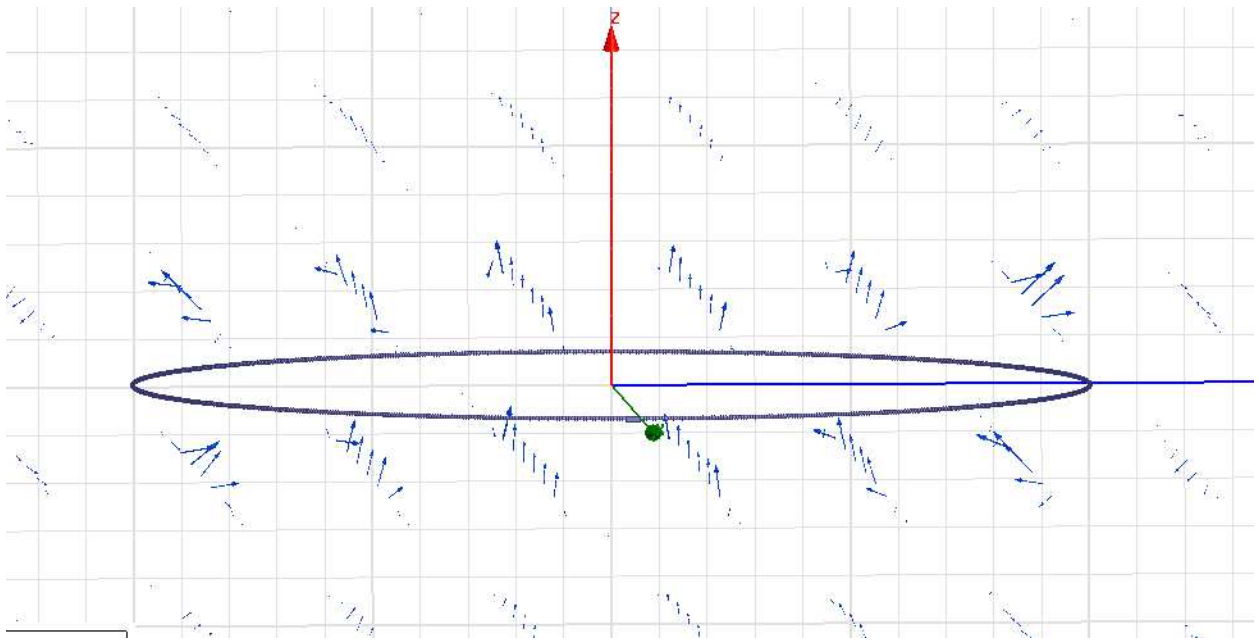


Figure 48. H-field vectors for single loop conductor.

Figure 48 shows a single flat loop conductor with dimensions realized in the intro. The vectors are H-Field vectors. The source is very close to the x-axis and can be seen as a

small rectangle. The current is flowing counter clockwise and by using right hand rule it can be seen the vectors are curling inside the loop from bottom up.

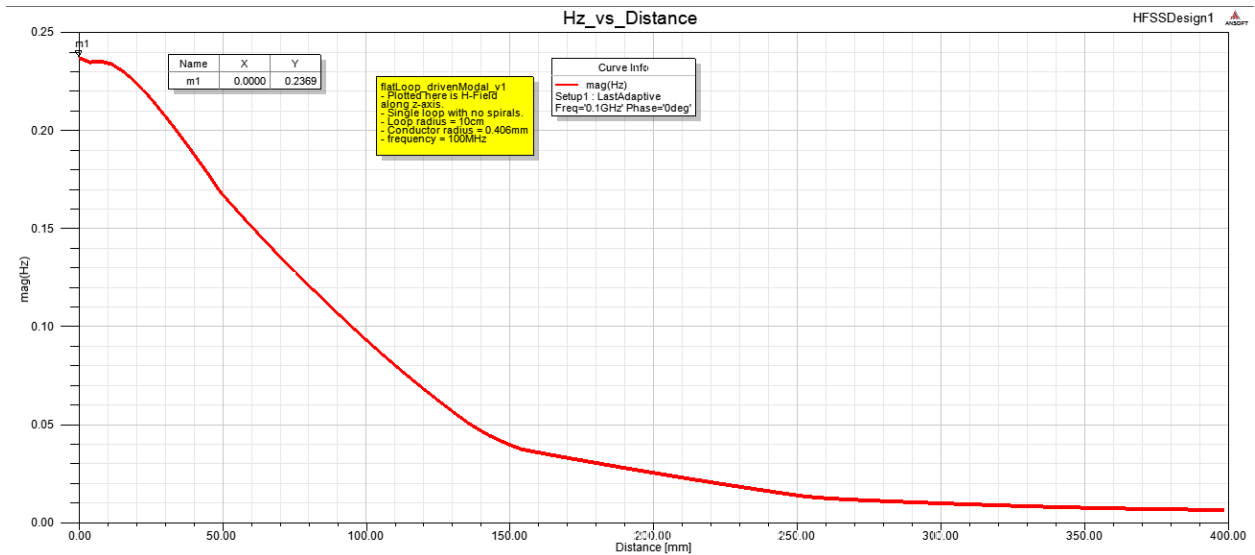


Figure 49. H-field vs distance of single loop along z-axis.

The Figure 49 plot is the H-field along z-axis results for the single loop geometry design in Figure 48. Plotting the H-field along the z-axis from zero out to approximately 400mm, the field decays as expected. As expected the location of the peak magnitude at a distance of zero along the z-axis.

#### 5.2.4 Contour plots overlays of single flat loop by electrically small phenomenon.

H-field field overlays for complex magnitude are shown for the Hxy, Hxz and Hyz planes and are depicted in Figure 50-51-52, respectively. The E-field field overlays for complex magnitude are shown for Exy, Exz and Eyz planes and are depicted in Figure 53-54-55, respectively. The effects of electrically small antennas are expressed here visually through the mentioned planar overlays that are generated by HFSS.

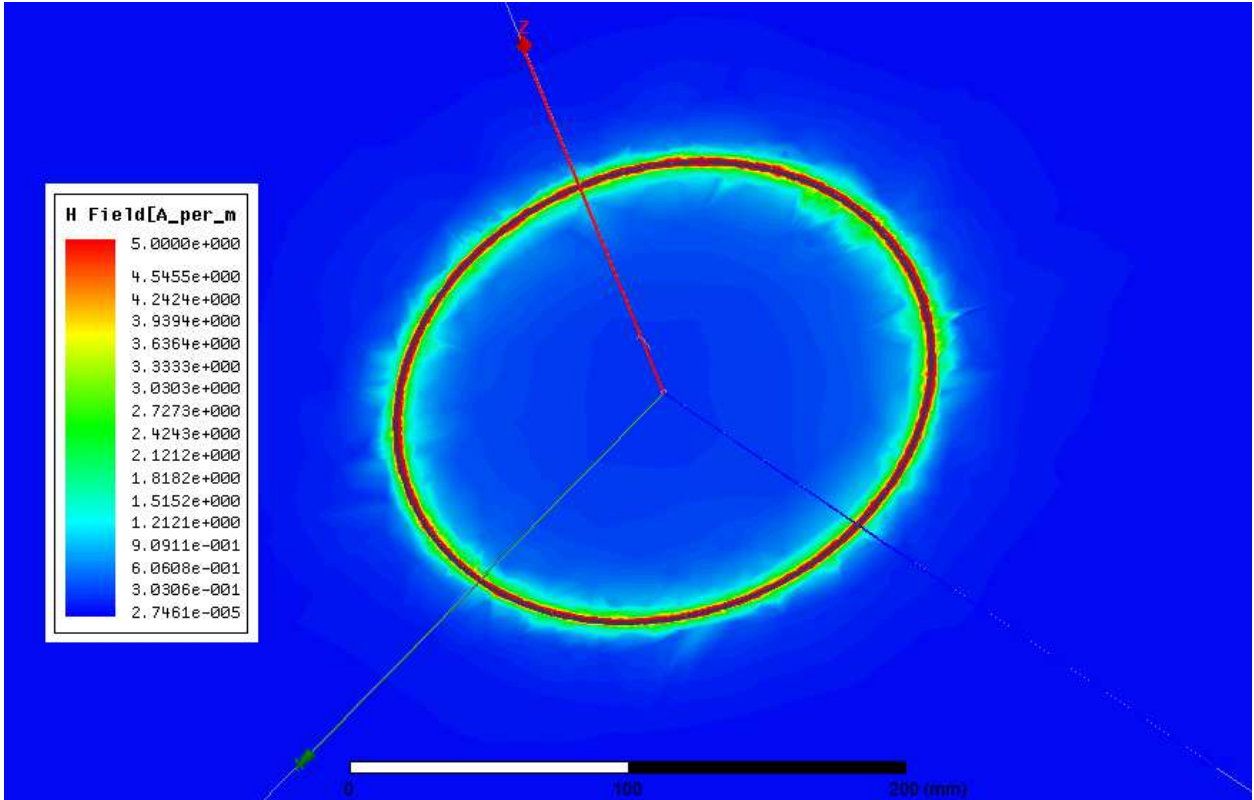


Figure 50. Single flat loop conductor Hxy complex magnitude field overlay for a 1V-100MHz source.

The Figure 50 shows the H-field results for the single loop geometry design of Figure 48 of the xy-plane. The field overlay plot shown here is also biased by a 1v-100MHz source. The H-field appears to be symmetric around the loop as expected for a single flat loop.

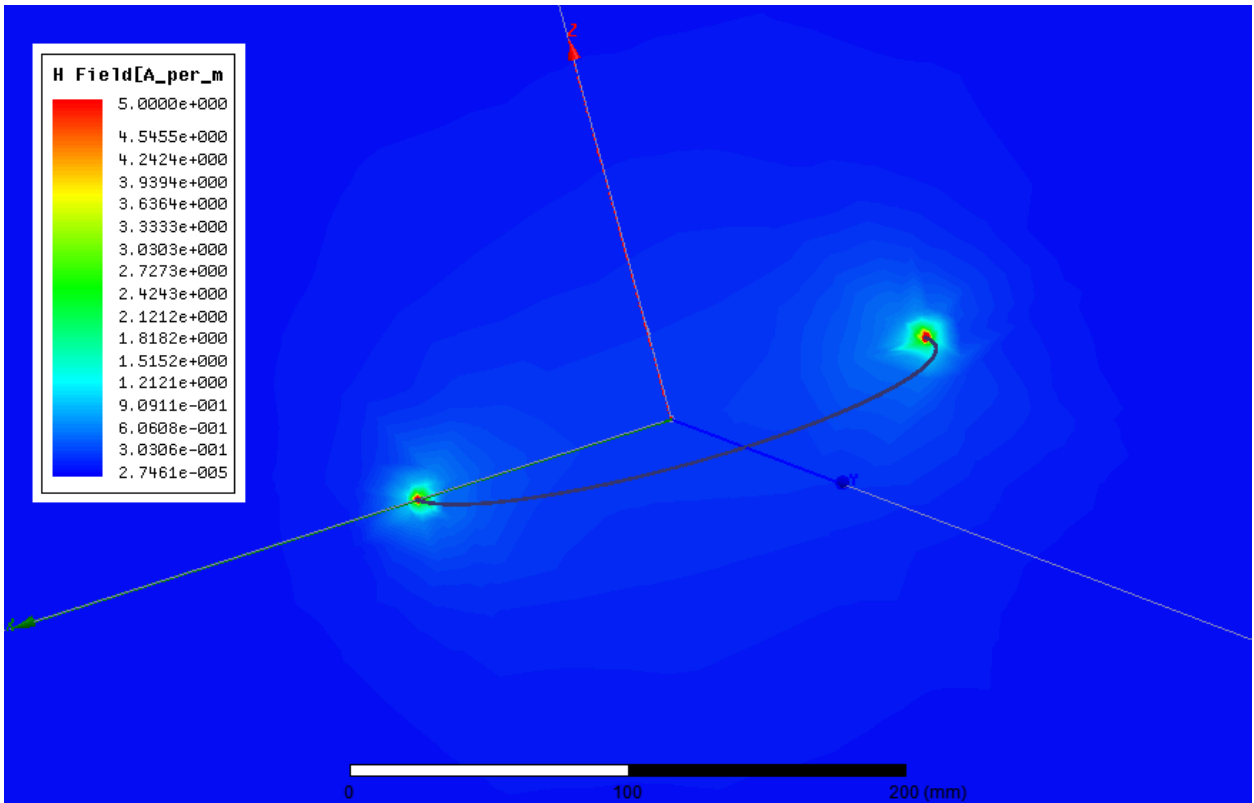


Figure 51. Single flat loop conductor Hxz complex magnitude field overlay for a 1V-100MHz source.

The Figure 51 shows the H-field results for the single flat loop geometry design of Figure 1 of the xz-plane. The field overlay plot is shown here for a 1v-100MHz source. The H-field appears to be symmetric as expected for a single flat loop.

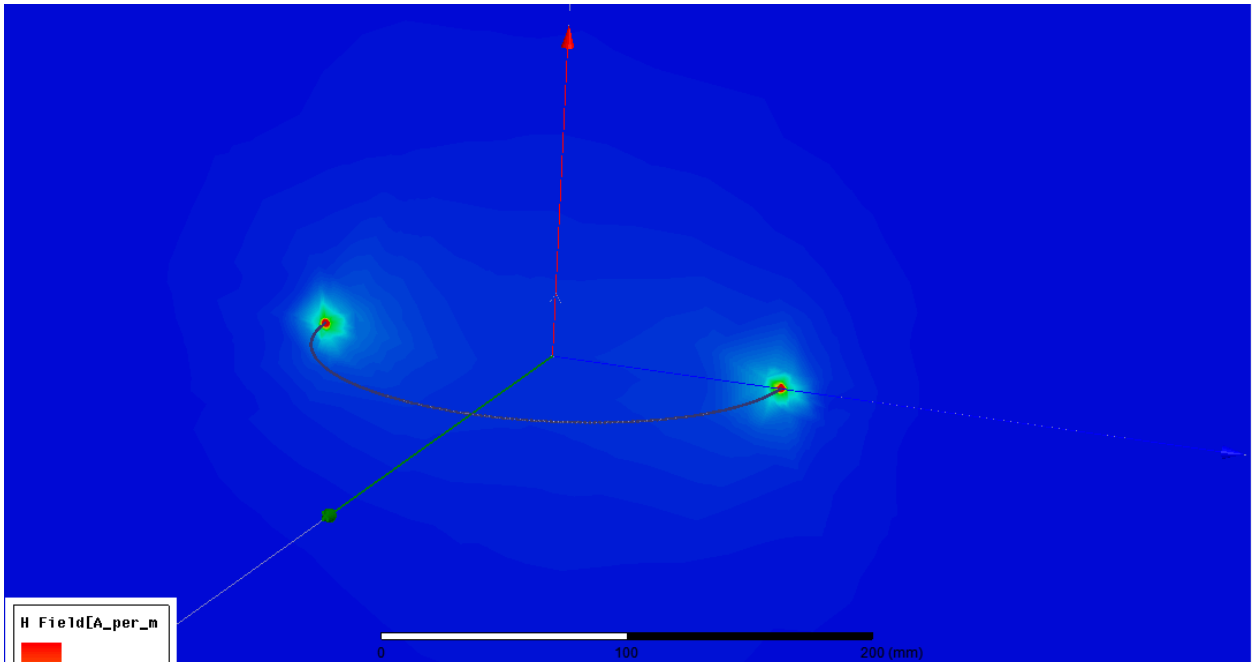


Figure 52. Single flat loop conductor Hyz complex magnitude field overlay.

The Figure 52 shows the H-field results for the single loop geometry design of Figure 1 of the yz-plane. The field overlay plot is shown here for a 1v-100MHz source. The H-field appears to be symmetric as expected for a single flat loop.

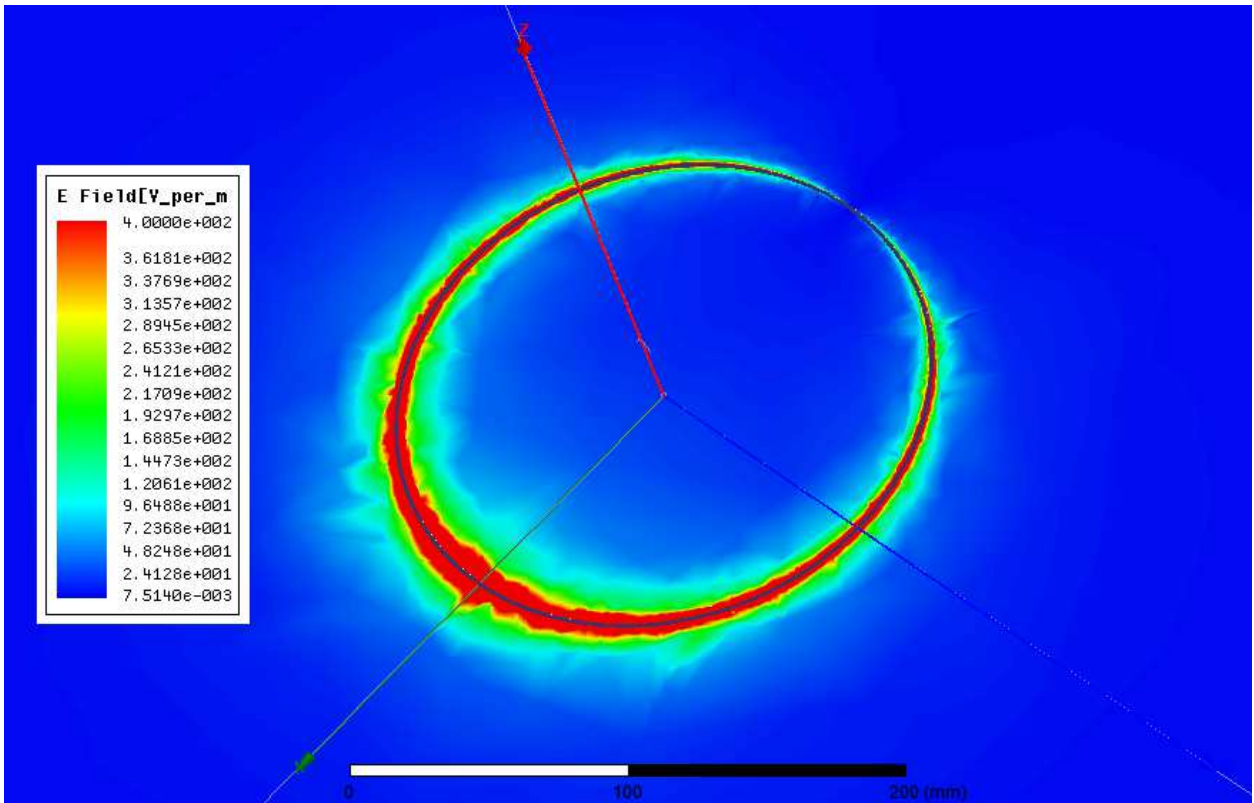


Figure 53. Single flat loop conductor Exy complex magnitude field overlay for a 1V-100MHz source.

The Figure 53 shows the E-field results for the single flat loop geometry design of Figure 1 in the xy-plane. The field overlay plot shown here is for a 1v-100MHz source. Note that the E-field is not symmetric as originally expected. The E-field gradient depicted here is due to the loop appearing electrically small relative to the wavelength. A lower frequency would be required to get away from the non-uniform current effect which appears to be the dominant factor shown here in the non-uniform E-field.

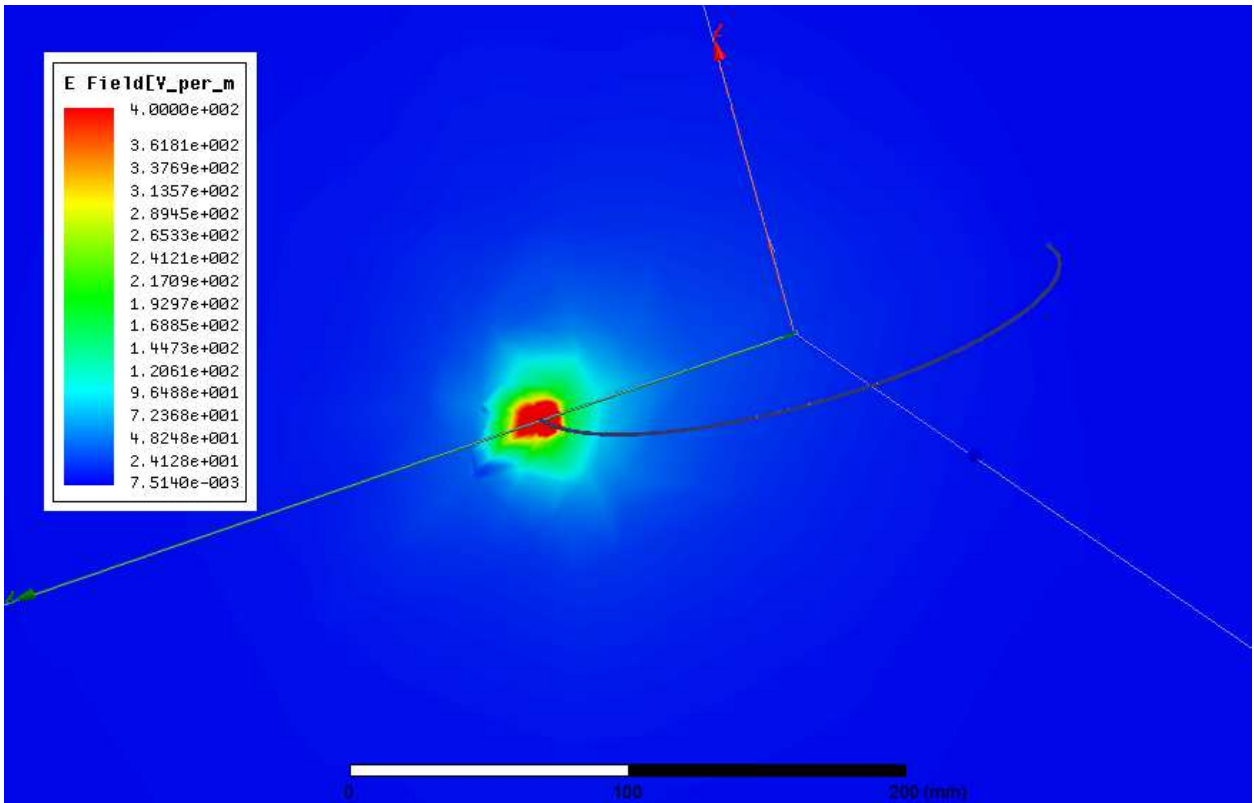


Figure 54. Single flat loop conductor Exz complex magnitude field overlay for a 1V-100MHz source.

The Figure 54 shows the E-field results for the single loop geometry design of Figure 1 of the xz-plane. The field overlay plot is shown here is for a 1v-100MHz source. The E-field is not symmetric and is expressed by the source illuminating well at one end of the loop, whereas the opposite end of the loop is near the low end of the scale.

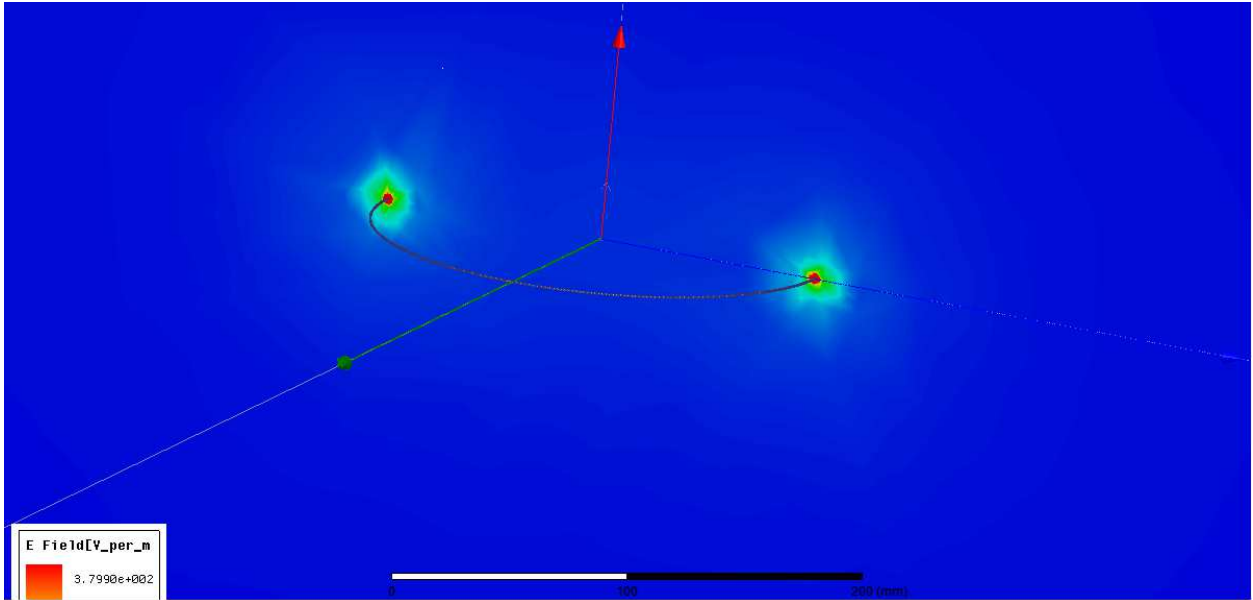


Figure 55. Single flat loop conductor Eyz complex magnitude field overlay.

The Figure 55 shows the E-field results for the single loop geometry design of Figure 1 of the yz-plane. The field overlay plot is shown here for a 1v-100MHz source. The E-field appears to be symmetric as the two points that cross the plane are equal distance from the source of the electrically small loop.

### 5.3 Single loop helix of 4-cycles

Next, a simulation setup was prepared for a single loop 4-cycle helix conductor. The simulation for this geometry is set up to yield a field overlay of H-field vectors and is plotted on top of the single helical shaped loop geometry. The single helical shaped loop and H-field overlay can be seen in Figure 56. Next, all individual  $x$ - $y$ - $z$  field components for H and E fields are plotted using rectangular plots and planar contours plots. The rectangular plots are used for observing characteristics and any field peak shifts when comparing all design simulation results. The rectangular plots contain field magnitude



versus distance for both E and H fields on all three axes. The plot Hz versus distance is shown in Figure 57.

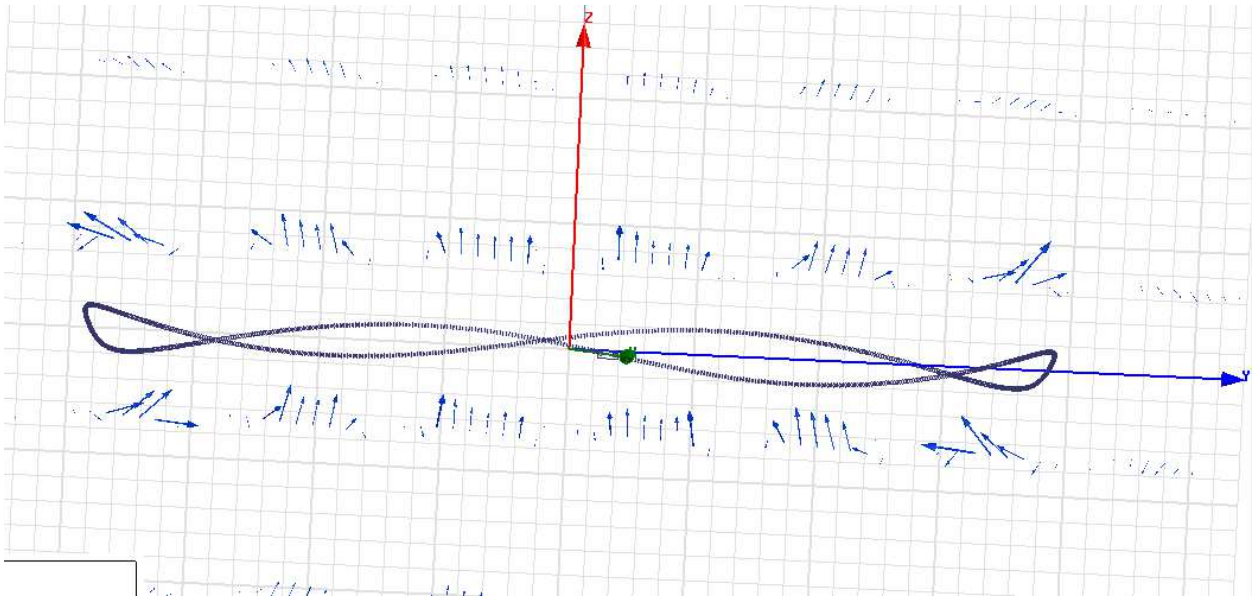


Figure 56. H-field vectors for Single loop 4-cycles conductor.

The figure 56 shows a single helical shaped loop conductor with dimensions mentioned in section 5.2. The vectors shown are the H-Field vectors. The source is very close to the x-axis and can be seen as a small rectangle. The current is flowing counter clockwise and by using right hand rule it can be seen the vectors are curling inside the loop from bottom up.

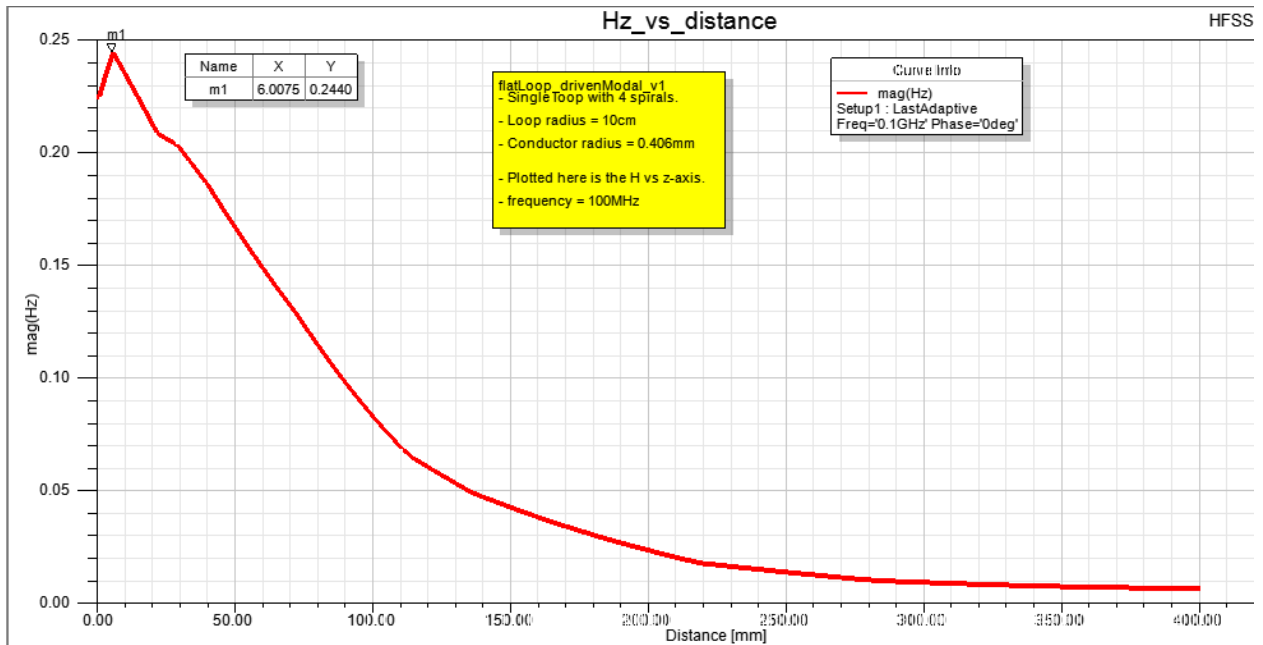


Figure 57. H-field vs distance of single loop helix 4-cycles conductor along the z-axis.

The Figure 57 plot is the H-field along z-axis results for the single loop geometry design in Figure 56. Plotting the H-field along the z-axis from zero out to approximately 400mm, the field decays as expected. Note the location of the peak magnitude has shifted a distance of approximately 10cm from the center of the loop along z-axis.

### 5.3.1 Contour plot overlays of single helical shaped loop by electrically small phenomenon.

H-field field overlays for complex magnitude are shown for the Hxy, Hxz and Hyz planes and are depicted in Figure 58-59-60, respectively. The E-field field overlays for complex magnitude are shown for Exy, Exz and Eyz planes and are depicted in Figure 61-62-63, respectively. The effects of electrically small antennas are expressed here visually through the mentioned planar overlays that are generated by HFSS.

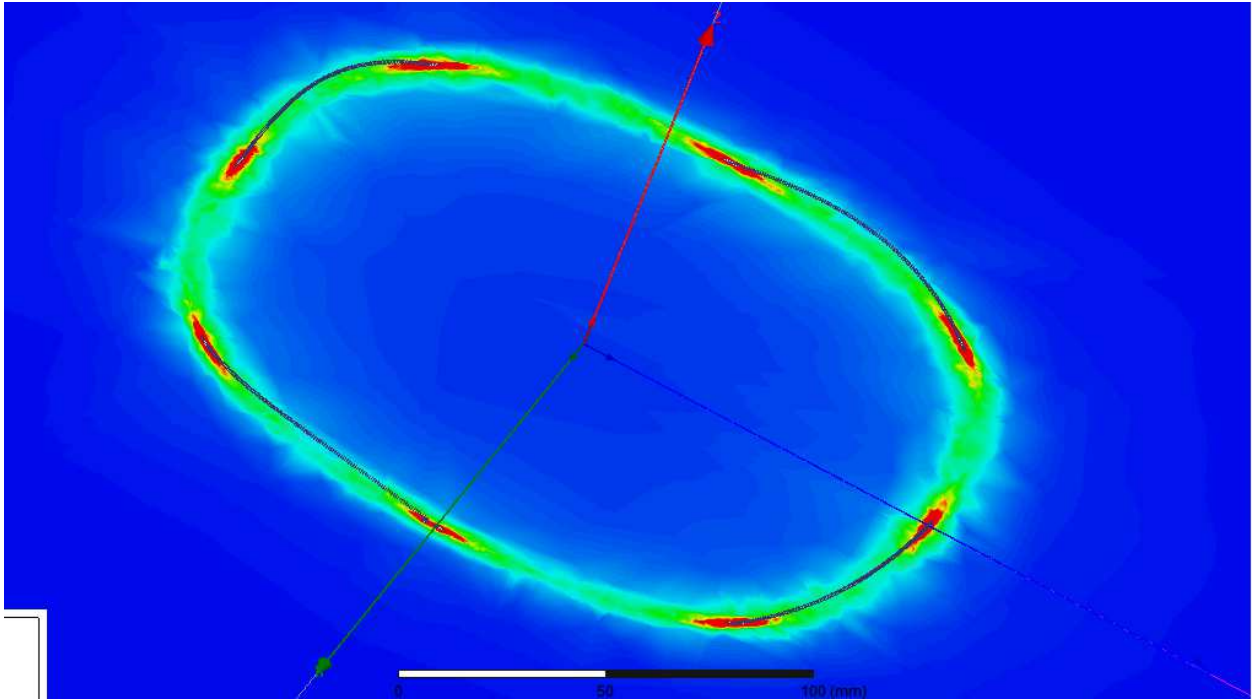


Figure 58. Single loop 4-cycles conductor Hxy complex magnitude field overlay.

The Figure 58 shows the H-field results for the single helical shaped loop of the xy-plane. The field overlay plot shown here is also biased by a 1v-100MHz source. The H-field appears to be symmetric around the loop as expected for a single flat loop. Note the loop is not flat and the plane cut shown here cannot evenly slice through the conductor as in the flat loop.

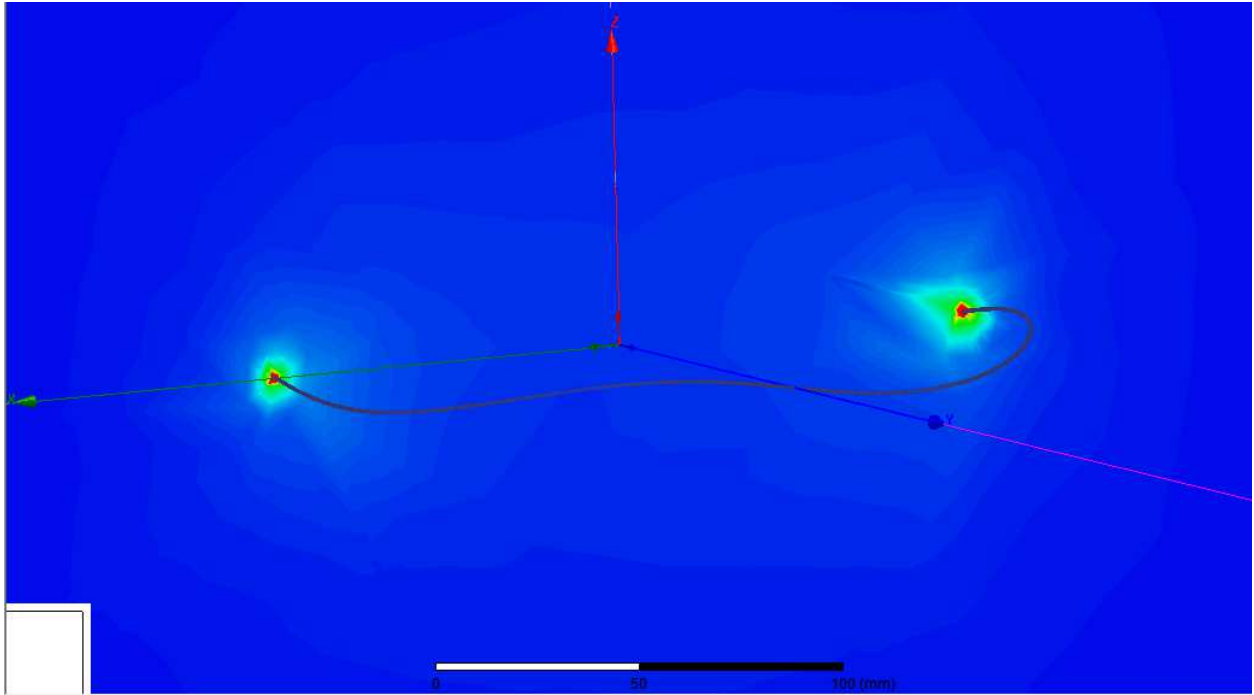


Figure 59. Single loop 4-cycles conductor Hxz complex magnitude field overlay.

The Figure 59 shows the H-field results for the single helical shaped loop of the xz-plane. The field overlay plot is shown here for a 1v-100MHz source. The H-field appears to be symmetric in magnitude as expected for a single flat loop.

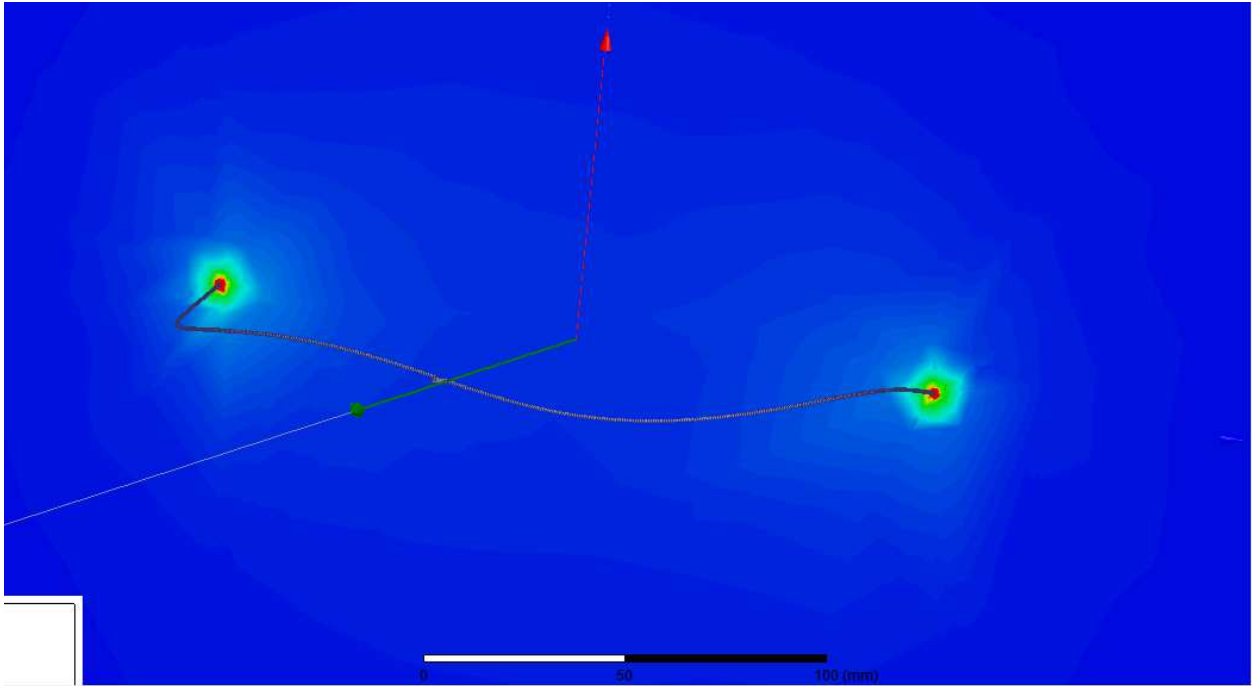


Figure 60. Single loop 4-cycles conductor Hyz complex magnitude field overlay.

The Figure 60 shows the H-field results for the single helical shaped loop of the yz-plane. The field overlay plot is shown here for a 1v-100MHz source. The H-field appears to be symmetric as expected for a single helical shaped loop.

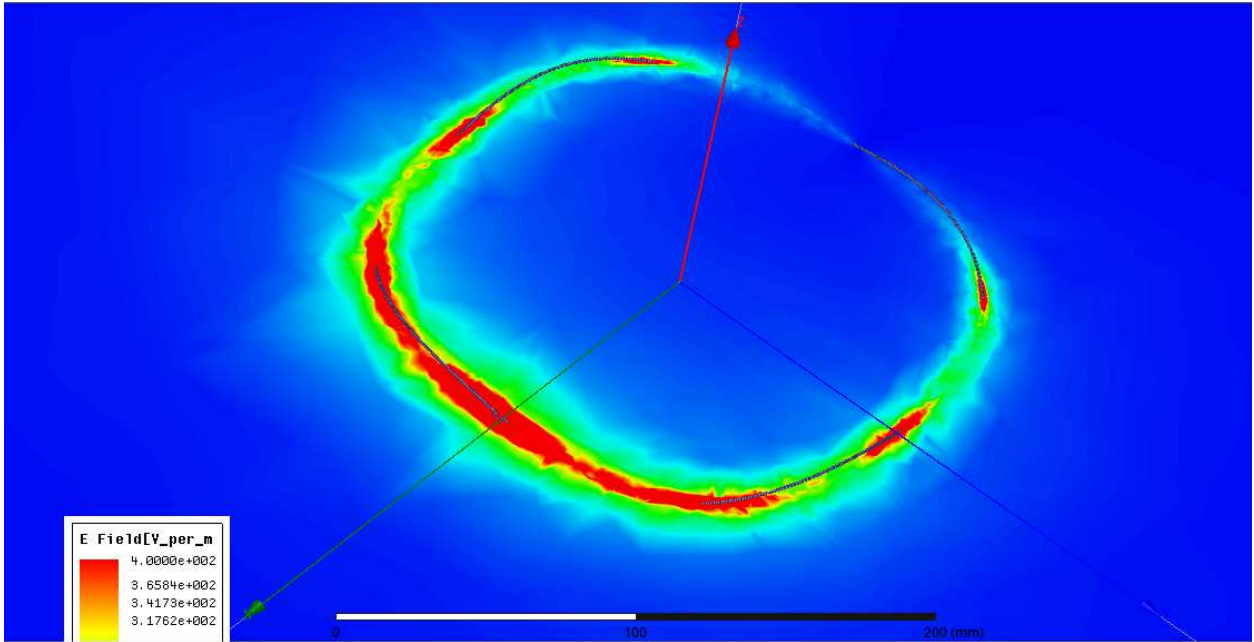


Figure 61. Single loop 4-cycles conductor Exy complex magnitude field overlay.

The Figure 61 shows the E-field results for the single helical shaped loop of the xy-plane. The field overlay plots the non-uniform E-field depicted here is due to the loop appearing electrically small relative to the wavelength. A lower frequency would be required to get away from the non-uniform current effect which appears to be the dominant factor shown here in the non-uniform E-field.

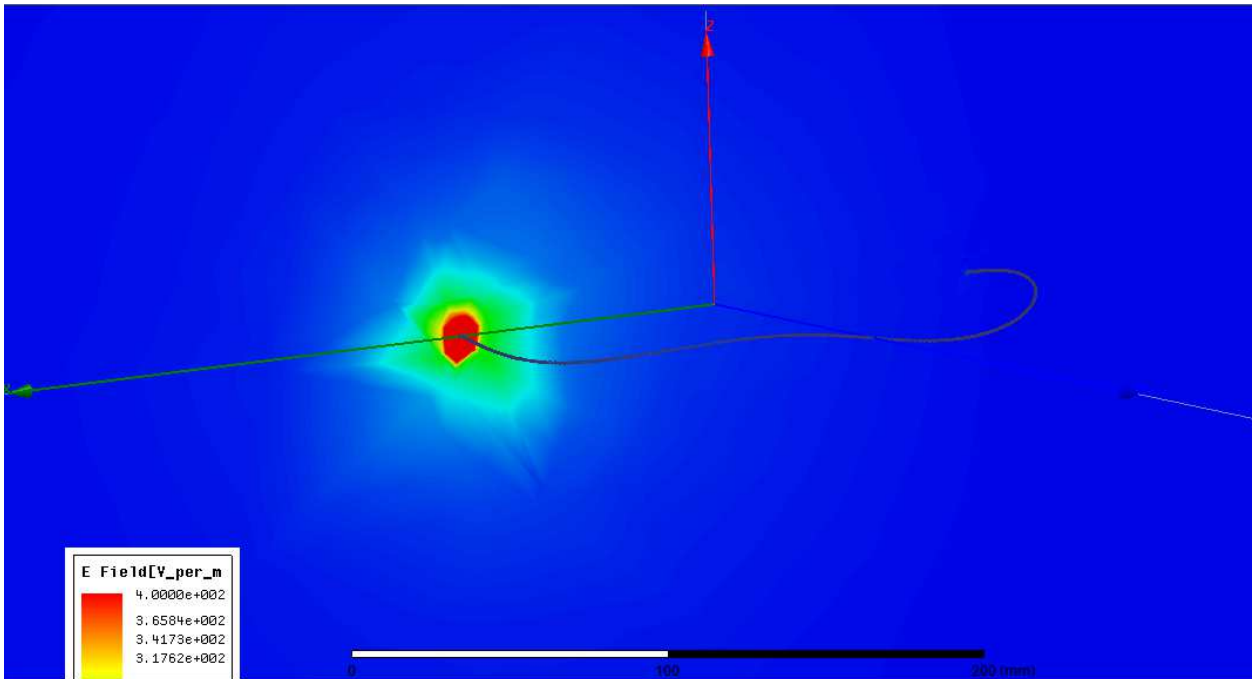


Figure 62. Single loop 4-cycles conductor Exz complex magnitude field overlay.

The Figure 62 shows the E-field results for the single helical shaped loop of the xz-plane. The field overlay plot is shown here for a 1v-100MHz source. Note that the E-field is not symmetric as initially expected. Note in Figure 62 the source illuminates well, whereas the opposite end of the loop is near the low end of the scale.

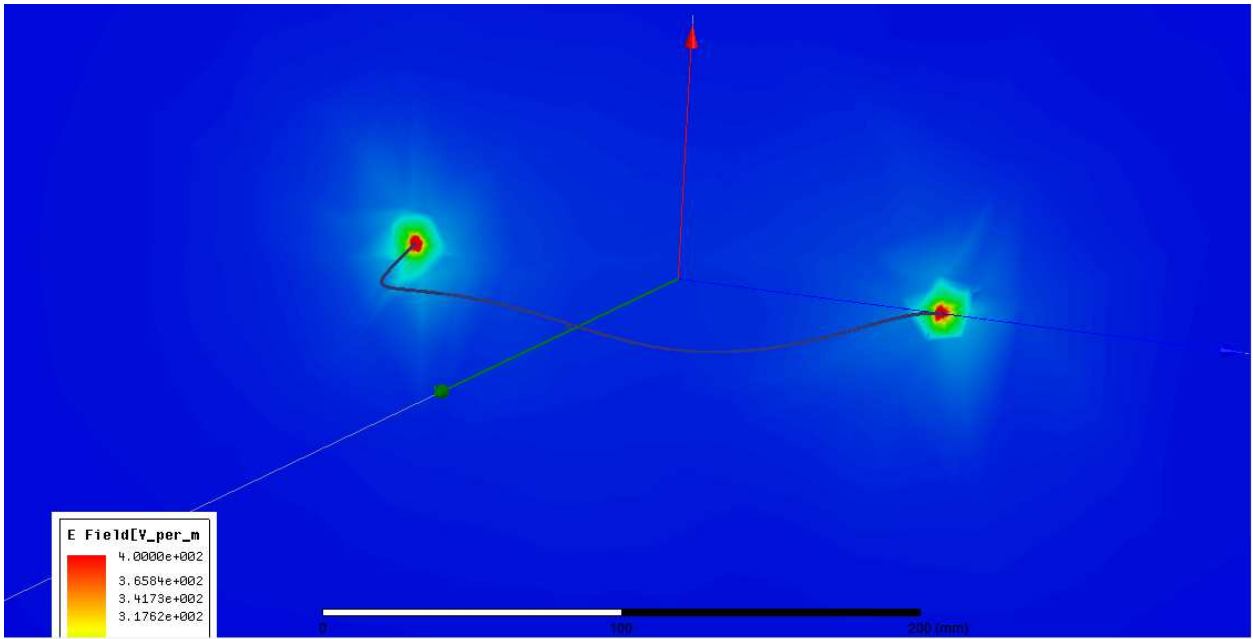


Figure 63. Single loop 4-cycles conductor Eyz complex magnitude field overlay.

The Figure 63 shows the E-field results for the single helical shaped loop of the yz-plane. The field overlay plot is shown here for a 1v-100MHz source. The E-field appears to be symmetric as expected for a single helical shaped loop.

#### 5.4 Helix loop of 4-cycles

A simulation setup was prepared for a helix loop of 4-cycles conductor. The simulation for this geometry is setup to yield a field overlay of H-field vectors and is plotted on top of the two loop geometry. The helix loop of 4-cycles and H-field overlay can be seen in Figure 64. Next, all individual x-y-z field components for H and E fields are plotted using rectangular plots and planar contours plots. The rectangular plots are used for observing characteristics and any field peak shifts when comparing all design simulation results. Plot Hz is shown in Figure 65.



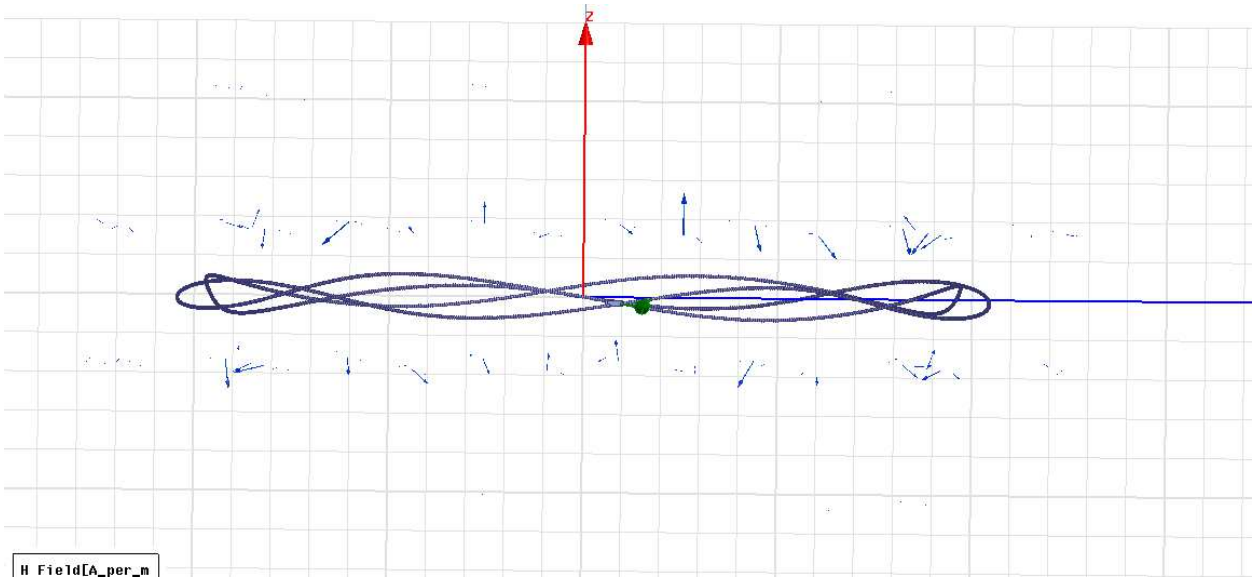


Figure 64. H-field vectors for helix loop of 4-cycles conductor.

This Figure is a helix loop of 4-cycles with two sources opposite of each other. The vectors here are H-Field vectors. In figure 5.9, it appears the H-field vectors are much smaller than the flat loop and single helical shaped loop, however this is a qualitative Figure and no quantitative value is expressed.

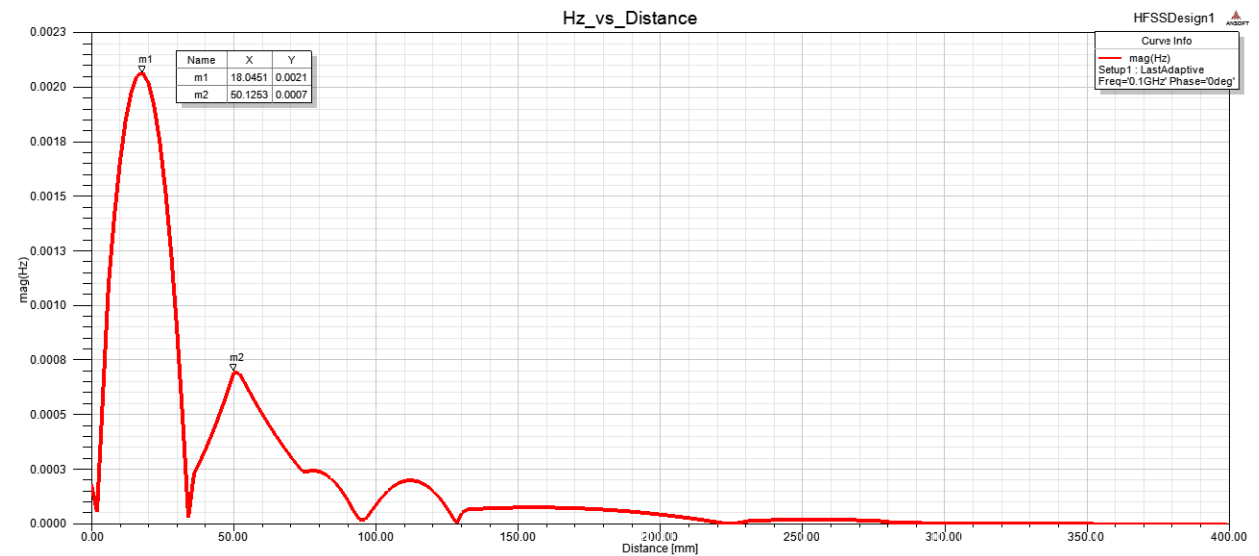


Figure 65. H-field vs distance helix loop of 4-cycles conductor along the z-axis.

The Figure 65 rectangular plot shows the H-field along the z-axis from zero out to approximately 400mm. The location of the peak magnitude is at distance of approximately 18cm from center of loop. Note that the accuracy of the location is dependent on the tetrahedral computed, such that simulation setups and results need tetrahedral refinements. However, a visible shift in the H-field is shown.

#### 5.4.1 Contour plot overlays of a helix loop by electrically small phenomenon.

H-field field overlays for complex magnitude are shown for the Hxy, Hxz and Hyz planes and are depicted in Figure 66-67-68, respectively. The E-field field overlays for complex magnitude are shown for Exy, Exz and Eyz planes and are depicted in Figure 69-70-71, respectively. The effects of electrically small antennas are expressed here visually through the mentioned planar overlays that are generated by HFSS.

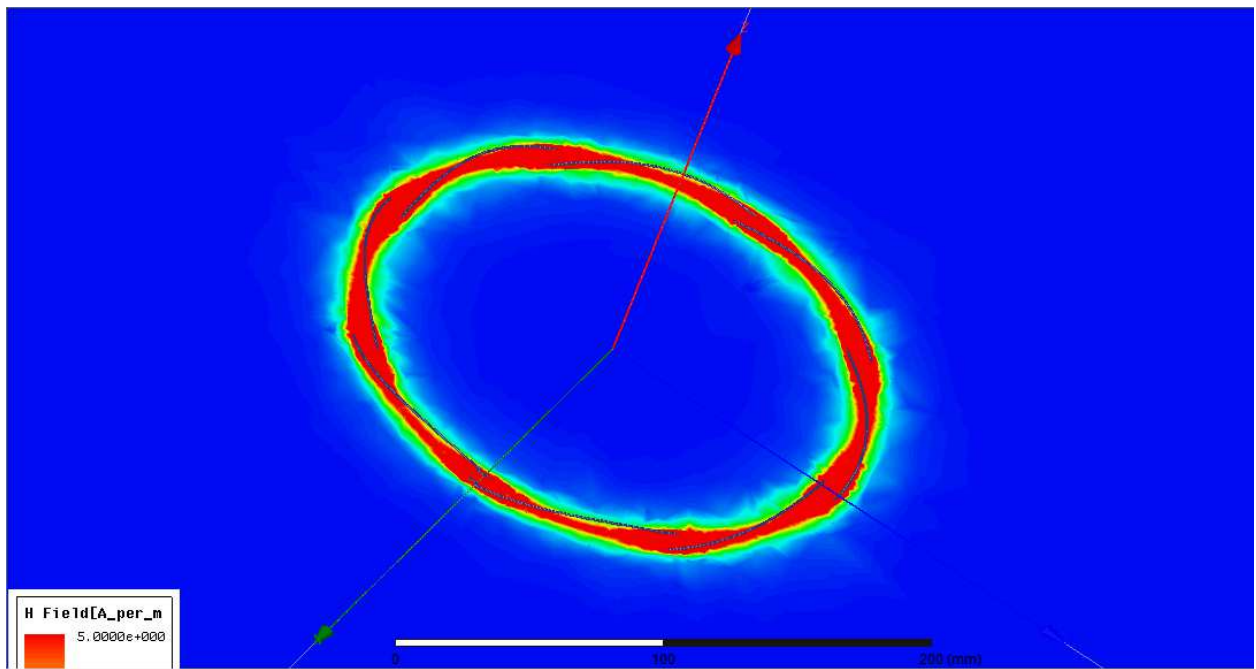


Figure 66. Helix loop of 4-cycles conductor Hxy complex magnitude field overlay.

The Figure 66 shows the H-field results for the single helical shaped loop of the xy-plane. The field overlay plot shown here is also biased by a 1v-100MHz source. The H-field appears to be symmetric around the loop as expected for a helix loop. Note the helix loop is not flat and the plane cut shown here cannot evenly slice through the conductor as in the flat loop.

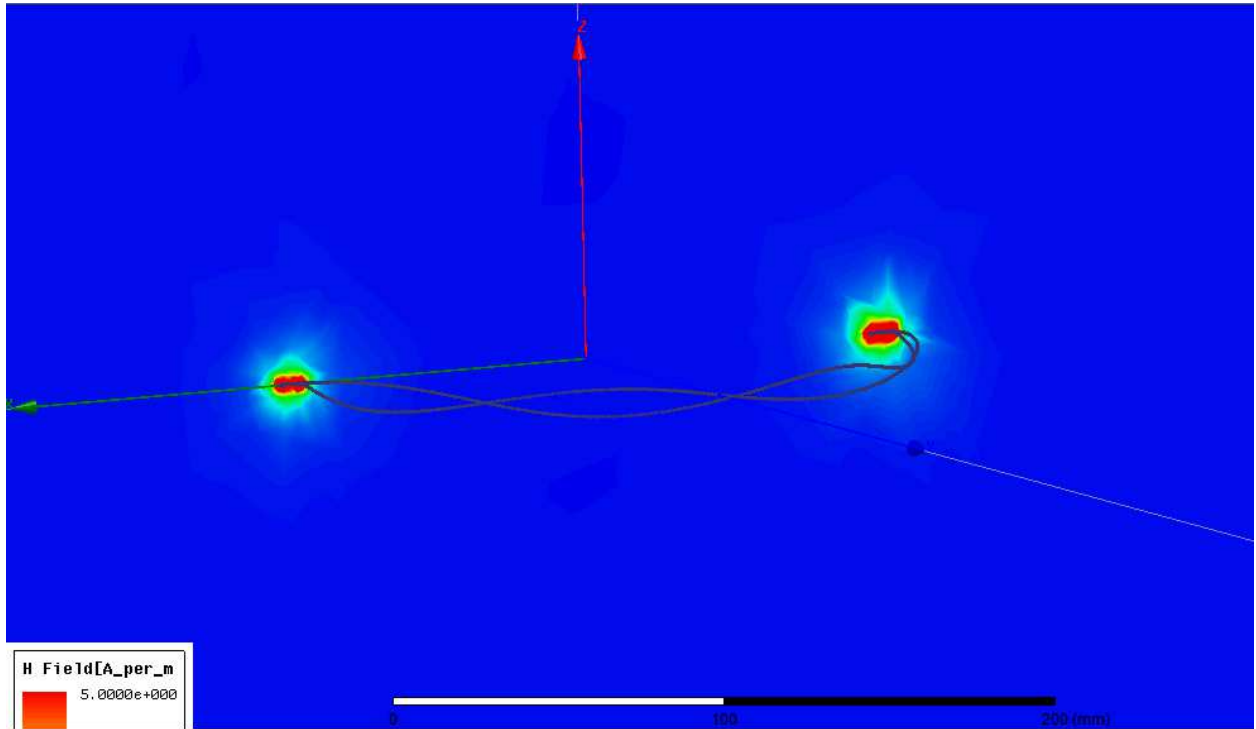


Figure 67. Helix loop of 4-cycles conductor Hxz complex magnitude field overlay.

The Figure 67 shows the H-field results for the single flat loop geometry of the xz-plane. The field overlay plot is shown here for a 1v-100MHz source. The H-field appears to be symmetric as expected for helix loop.

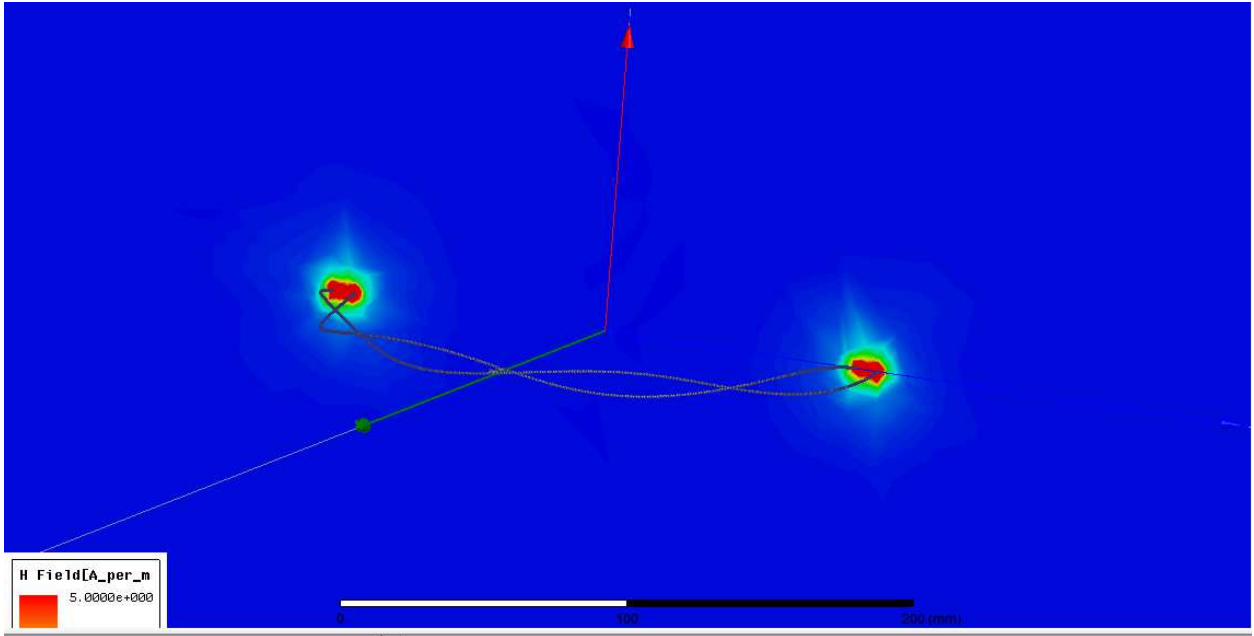


Figure 68. Helix loop of 4-cycles conductor Hyz complex magnitude field overlay.

The Figure 68 shows the H-field results for the single helical shaped loop of the yz-plane.

The field overlay plot is shown here for a 1v-100MHz source. The H-field appears to be symmetric as expected for a helix loop.

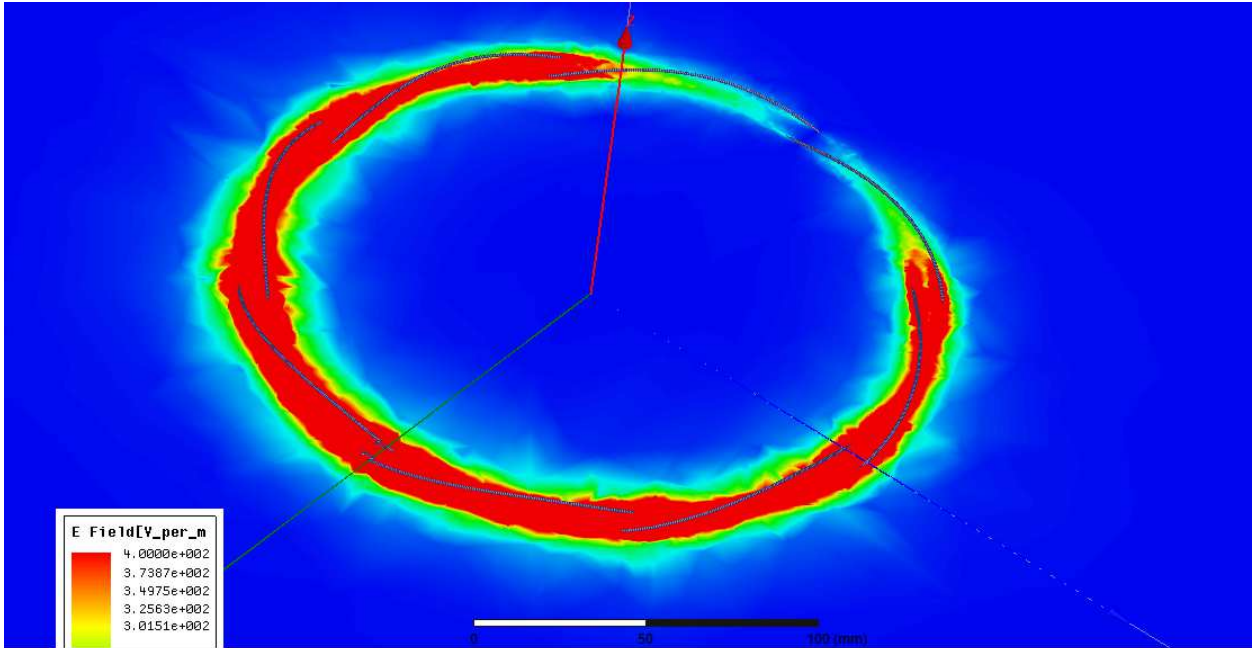


Figure 69. Helix loop of 4-cycles conductor Exy complex magnitude field overlay.

The Figure 69 shows the E-field results for the single helical shaped loop of the xy-plane.

The field overlay plot. The non-uniform E-field depicted here is due to the loop appearing electrically small relative to the wavelength. A lower frequency would be required to get away from the non-uniform current effect which appears to be the dominant factor shown here in the non-uniform E-field.

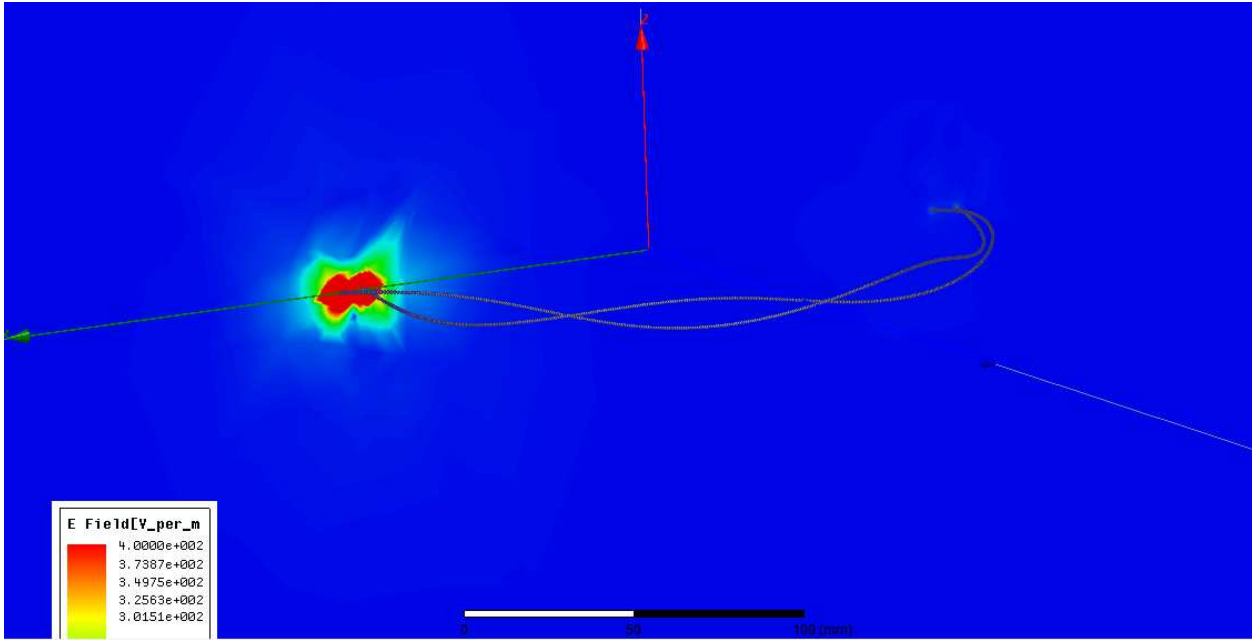


Figure 70. Helix loop of 4-cycles conductor Exz complex magnitude field overlay.

The Figure 70 shows the E-field results for the single helical shaped loop of the xz-plane. The field overlay plot is shown here for a 1v-100MHz source. It is noted that the E-field is not symmetric as initially expected. The source illuminates well, whereas the opposite end of the loop is near the low end of the scale.

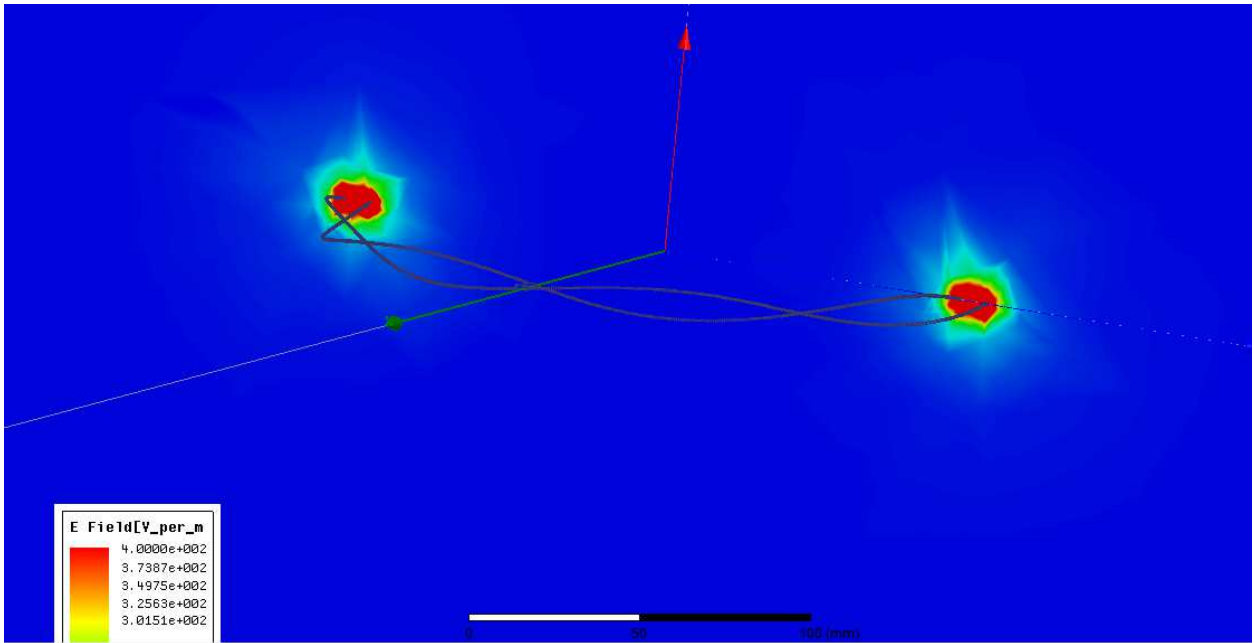


Figure 71. Helix loop of 4-cycles conductor Eyz complex magnitude field overlay.

The Figure 71 shows the E-field results for the single helical shaped loop of the yz-plane. The field overlay plot is shown here for a 1v-100MHz source. The E-field appears to be symmetric as expected for a single helical shaped loop.

### 5.5 Discussion

This initial investigation into two spirals began with a basic bench setup of a single flat loop. All three configurations have the same radius of 10cm and the same source of 1v-100MHz. Several rectangular plots as a function of z-axis were investigated for behavior in both Hz and Ez fields. Contour plots of an individual field for all three planes are used to gain an understanding of the characteristics qualitatively.

In the E-field planar contours, it is noted that both spiral designs of the single and the double conductors show a strong E-field at the source, however the E-field has a significant drop by the time it reached the opposite side of the loop, that is 180 degrees or  $\pi$  radians away. This characteristic is due to the loops being electrically small. The loop

must be electrically small to get away from the non-uniform current distributions which appear to be the dominant factor shown in the non-uniform E-field characteristics.

Further investigation leads to changing the frequency from 100MHz down to 1MHz and it was observed that the helix solutions yielded a Magneto-Static frequency response that will satisfy the Magneto solution of the H-field at the center of the loop. This was achieved by using the wireless power transfer models.



## CHAPTER 6

### PERFORMANCE CHARACTERISTICS FOR A TWO LOOP SYSTEM

#### 6.1 Introduction of Loop Comparison

Two loops within the Near Field distances of each other have power transfer capabilities via magnetic induction while also radiating away power into the far field [4, 10].

Reducing the radiating power into the far field, while studying the shielded loop and the helix loop architecture with respect to the power transfer characteristics are the primary goals. All other spacial alignments are held constant so that the two loops are parallel to each other. All loop systems are excited by a 1 watt power source with a frequency of 1 MHz.

The hypothesis stated in the introduction proposes using higher order poles from the helical loop to reduce radiation. The helix cycles contain the higher order poles by completing a 360 degree turn. The two wires of the cyclic path are also terminated in a moebius configuration enabling the two parallel wires to carry currents traveling in opposite directions. The moebius configuration of opposing currents is shown to more effectively cancel the E field in the far field than conventional loop currents. Each integer cycle twist increases the order of magnetic poles. The downside of each additional cycle is that its near field is also greatly reduced. Therefore, the investigation of the helix design focuses on identifying the optimal cycle for canceling the E-field in order to reduce the power radiation loss. Since the helix loop architecture radiates less power than the shielded loop architecture, the helix loop architecture is superior in this aspect, to all conventional and shielded loop architectures.

The shielded loop power transfer characteristics at a given distance of 5.0 mm separation distance between the respective loops will first be analyzed, and then be evaluated for its power radiated. The 4 cycle helical loop configuration is evaluated for its power radiated and power transferred. The 0 cycle helical loop configuration architecture will then be evaluated for its power radiated and power transferred. For equivalent comparison between these respective systems, a new Figure of Merit (FOM) is defined as the power transferred divided by the power radiated.

$$FOM = \frac{P_{tr}}{P_{rad}} \quad (54)$$

Where,

$P_{tr}$  is power transferred from loop 1 to loop 2 in milli-watts.

$P_{rad}$  is total power radiated in milli-watts from both loops.

The greater the FOM translates to a better performing wireless power transfer system. All loops shall be coaxially separated by 5.0 millimeters from the edge to edge of the conductor, therefore equalizing the space between each system.

## 6.2 Shielded Loop Power transfer

The two shielded loops of the two shielded loop system as defined using HFSS are aligned axially and are shown in figures 72 and figure 73 below.

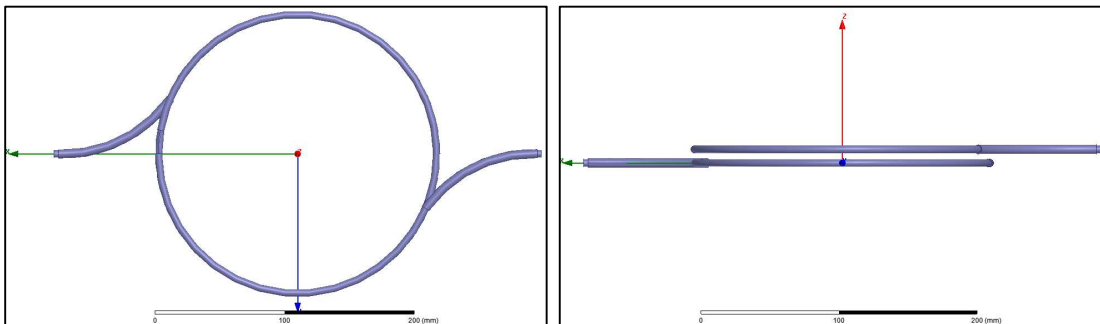


Figure 72. HFSS setup for two shielded loops. Loop 1 is the lower shielded loop and loop 2 is the upper shielded loop.

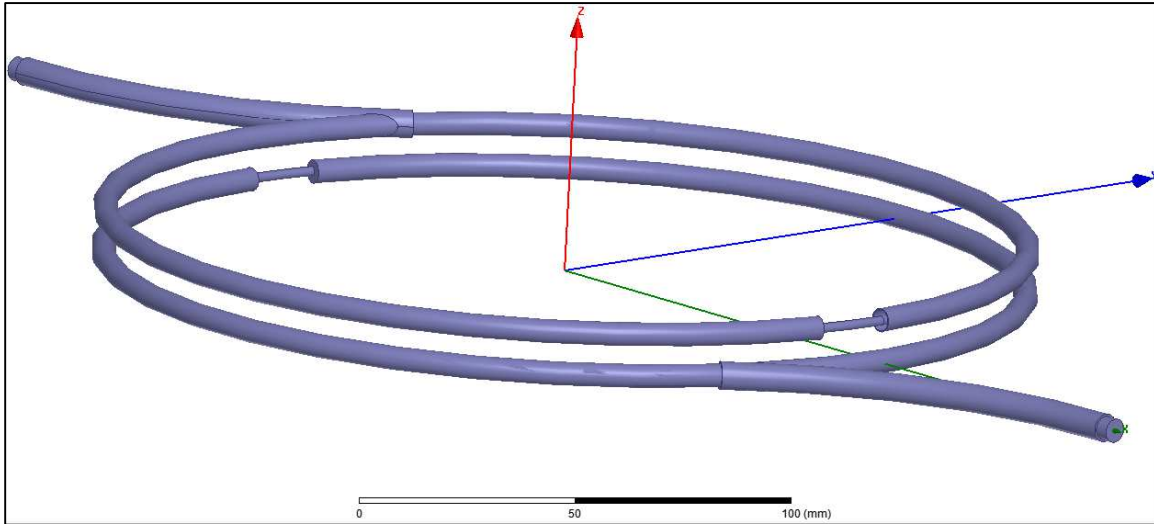


Figure 73. HFSS setup of shielded loops.

The first loop is excited via wave port and is simulated at a 5.0 millimeter separation distance. The S21 for the two shielded loop power transfer is 8.52 dBm.

### 6.3 Shielded loop power radiation

The system power loss due to radiation can be shown as power radiated and is evaluated with a power source at 1MHz and was calculated by the total amount of power crossing the radiation boundary in HFSS. The total power radiated at 5.0 millimeter separation is -46.1 dBm.

### 6.4 Four cycle helix loop power transfer

A two, four cycle helical loop system was investigated using HFSS. The two four cycle helical loops are aligned axially and each loop is shorted 180 degrees away from source terminations and shown in figure 74, figure 75 and figure 76 below.

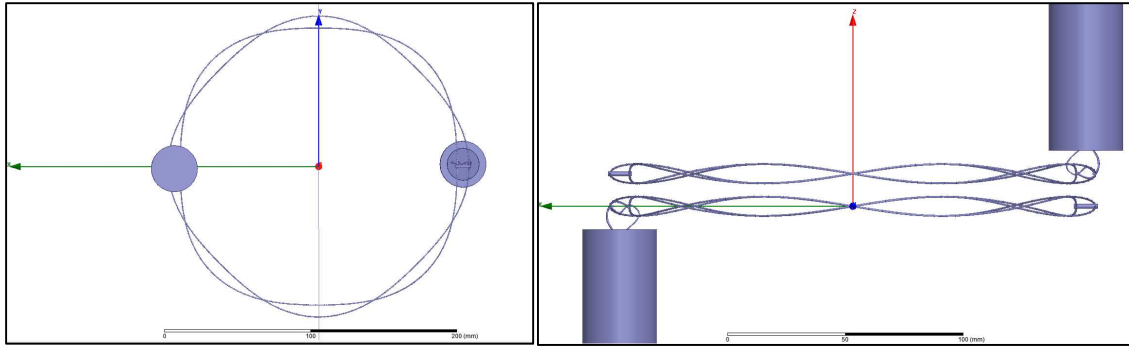


Figure 74. HFSS setup for two four cycle helical loops. Loop 1 is the lower four cycle helical loop and loop 2 is the upper four cycle helical loop.

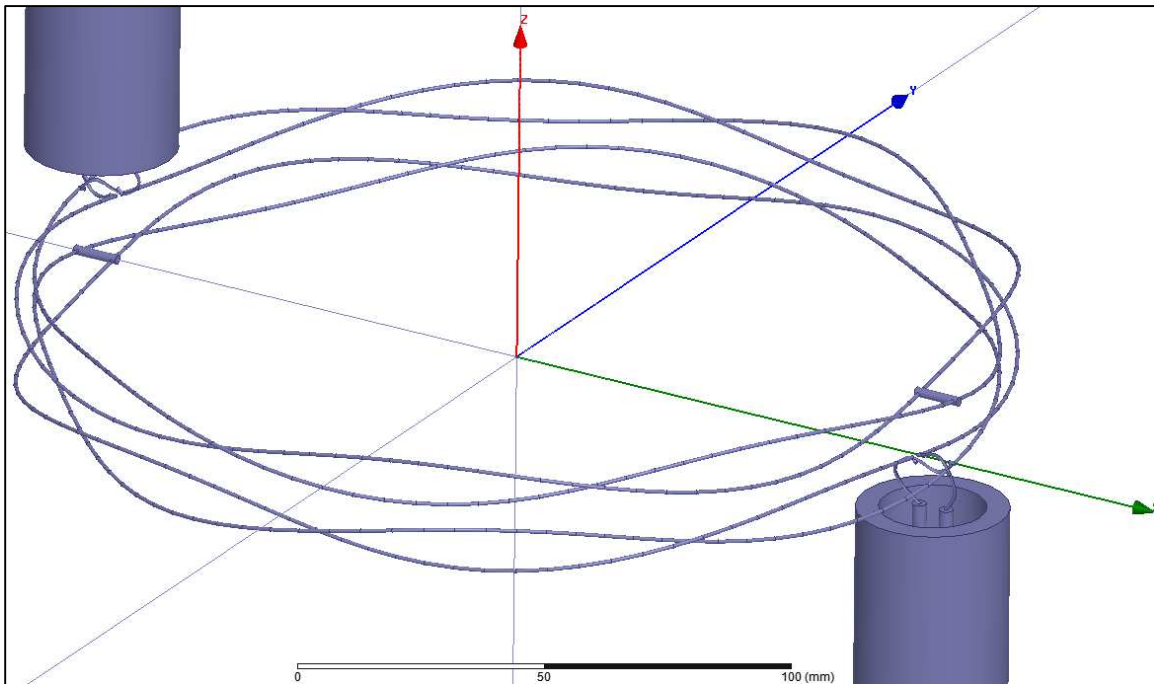


Figure 75. Four cycle helical loops connected to twinax sources in a moebius termination.

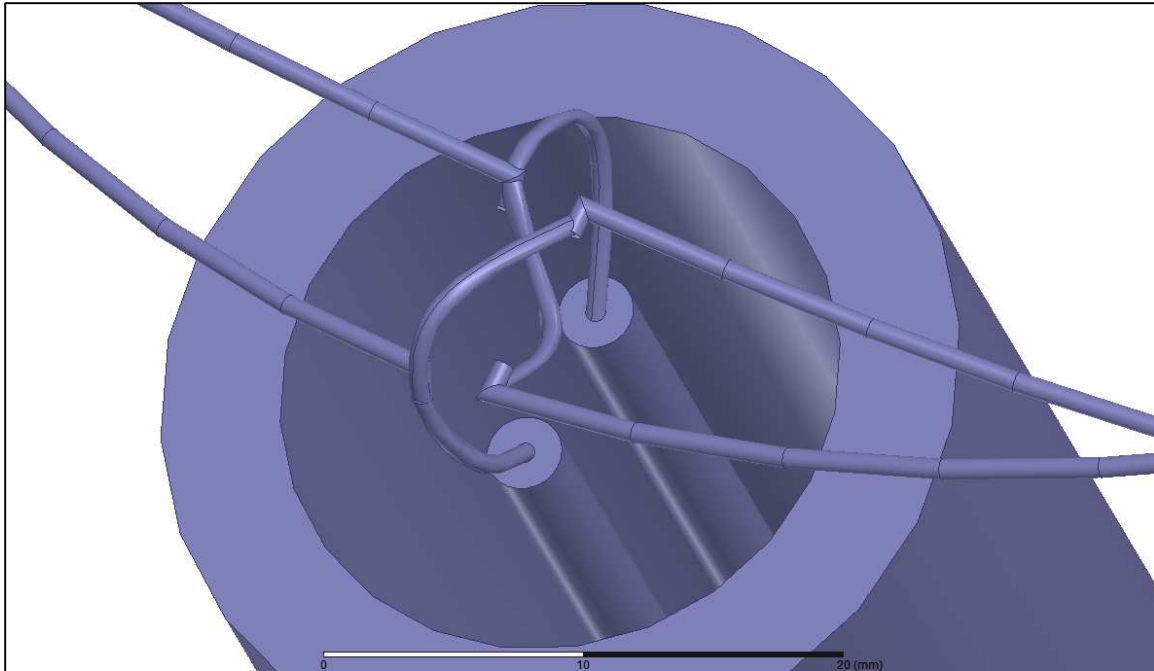


Figure 76. Four cycle helical loop with moebius termination to a twinax source.

The first four cycle helical loop is excited via wave port at the end of a twinax line and is simulated at a 5.0 millimeter separation distance. The S21 parameter for the two four cycle helical loop power transfer is -61.21 dBm.

#### 6.5 Four cycle helix loop power radiation

The system power loss due to power radiated is evaluated at 1MHz, with the total power radiated for a two of the four cycle helical loops at 5.0 millimeter separation equal to -109.83 dBm.

#### 6.6 Zero cycle helix loop power transfer

A two, zero cycle helical loop system, which is the lowest order version of the helices, is simulated in HFSS with the two zero cycle helical loops being aligned axially and each

loop being shorted 180 degrees away from source terminations. The zero cycle helical loops are shown in figure 77 and figure 78 below.

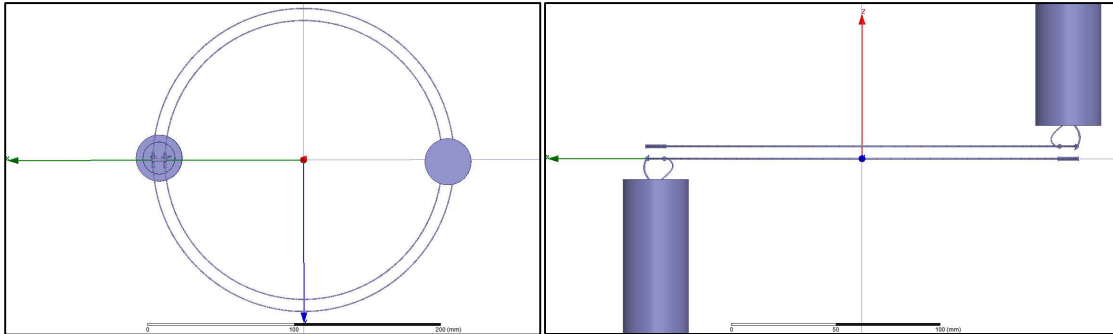


Figure 77. Zero cycle helical loops terminated to twinax sources.

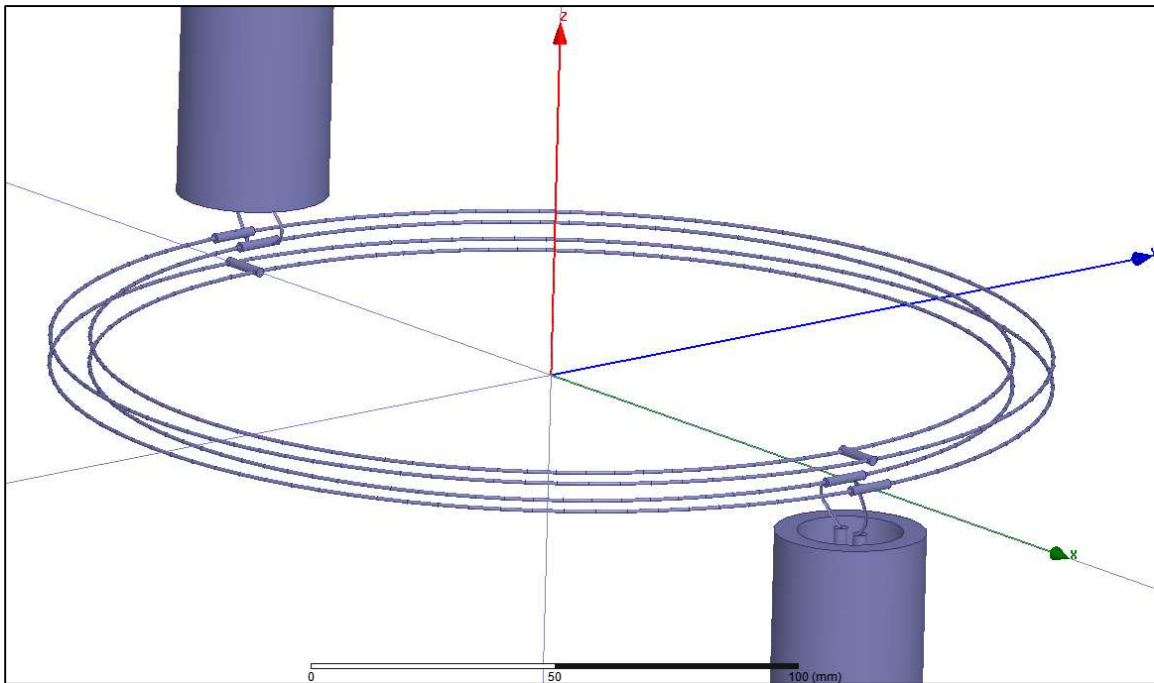


Figure 78. Zero cycle helical loops terminated to twinax sources.

The first zero cycle helical loop is excited via wave port at the end of a twinax line and is simulated at a 5.0 millimeter separation distance, giving an S21 power transfer of -21.57 dBm

### 6.7 Zero cycle helix loop power radiation

The system power loss due to radiation is evaluated at 1MHz, and is calculated to be -98.72 dBm.

### 6.8 Discussion of wireless power transfer systems

The two shielded loops system are simulated as a wireless power transfer alternative to the conventional single one turn wire loop architecture. The performance of the shielded loop system is used as a baseline to evaluate the performance of the respective two loop systems reviewed above. As noted above, the shielded loops' power transfer characteristics are expressed as the S21 parameter with a value of 8.52 dBm, with total power radiated of -46.1dBm. Reducing the radiation power loss requires the development of a novel architecture and thus the helix loop system was developed. The four cycle helical loops simulations produced the power transfer characteristic expressed as S21, of -61.21dBm with total power radiated equal to -109.83dBm. The process is then repeated for the zero cycle helical loops system, producing an S21 of -21.57dBm with total power radiated equal to -98.72dBm. Finally, a FOM is calculated for each system by dividing the power transferred by the power radiated with the highest FOM value being designated as the best performing system. Although the four cycle helix loop reduces the radiation power the greatest, it is out performed by the conventional shielded loop with respect to the FOM. An alternative lowest order pole was considered and investigated. Therefore, the recorded results show the zero cycle helical loops as the best performing architecture with respect to the defined FOM.

The performance comparison for power transfer with a 5.0 millimeter conductor

to conductor separation distance and power radiation mitigation is summarized in table 7 below.

Table 7. Performance summary of wireless power transfer characteristics.

1 Watt (30dBm) source - 5.0 mm conductor to conductor separation.					
Configuration	S21	Power Radiated	S21	Power Radiated	Figure Of Merit
(HFSS)	(dBm)	(dBm)	(mW)	(mW)	(FOM)
Shielded Loop	8.52	-46.1	7.11E+00	2.46E-05	2.90E+05
4 Cycle Helical Loop	-61.21	-109.83	7.57E-07	1.04E-11	7.28E+04
0 Cycle Helical Loop	-21.57	-98.72	6.97E-03	1.343E-10	5.19E+07



## CHAPTER 7

### WIRELESS POWER TRANSFER CONCLUSION

#### 7.1 INTRODUCTION CHAPTER SUMMARY

Two loops within the Near Field distances of each other have power transfer capabilities via magnetic induction while also radiating away power into the far field [4, 10]. The power transfer capabilities for military applications holds value in respect to modern technological advanced soldiers. Soldier wireless charging stealth technology allows the operator to recharge necessary modern warfare electronics covertly. It is proposed to investigate a wireless recharging system by using a loop antenna configuration that is electrically quiet and using the magnetic field for coupling to a second loop. A helical loop with a moebius termination to the source is proposed as a platform for stealthy wireless power transfer that will mitigate power radiation into the far field by the canceling of the E-field. Therefore, this project seeks to answer the question “Can we reduce radiation and preserve coupling by going to a higher order “pole” version of the standard current loop?”

#### 7.2 BASELINE PROPERTIES OF POWER TRANSFER SYSTEM SUMMARY

Mutual impedance and mutual inductance were investigated for a two loop system. The mutual impedance of a two loop system was determined by calculating the flux of the magnetic field from one loop, through the area of the second loop and calculating the mutual inductance using four different methods: a magneto-statics approach for calculating mutual inductance, an approach using elliptical functions for two identical sized loops, the magnetic dipole approach for calculating the mutual inductance and an

approach using electrodynamic fields using a rastering method. The electrodynamic method results were then compared to the flux results from magneto-statics calculation. The results showed the electrodynamic approach to be within 0.5 % error of the magneto-statics solution. The mutual inductance of the transducer was then used to calculate the coupling coefficient. In conclusion, the electrodynamic approach allows for a broad range of frequencies that can be used to calculate the mutual inductance and coupling coefficient of a system and was validated by comparing three additional different approaches.

### 7.3 POWER TRANSFER PROPERTIES OF TWO LOOPS SUMMARY

Transducer theory for modeling a two loop system is used to calculate the system properties. A loop antenna admittance equivalent circuit is used to model radiation conductance and loop properties over the conventional loop antenna impedance equivalent circuit. Next, an ohmic load connected to the receiver, loop 2, and real power transferred to the load of the system is calculated in MathCAD. The equivalent circuit of a two loop power transfer system is then represented by ADS and the simulations of this method are compared to the calculated results. All loop calculations are performed with a loop radius of 0.1 meter at a frequency of 1MHz. The results of the two methods were compared and percent error for power to the load was under 0.3% for a series-series tuned circuit. The efficiency for a four combinations of tuning; series-series (s-s), series-parallel (s-p), parallel-series (p-s), parallel-parallel (p-p) was then evaluated to determine the most efficient configuration using a 10 ohm load, and then re-evaluated for a 300 ohm load. The series-parallel tuning circuit shows to be the best configuration using a 300 ohm load. The series-parallel configuration performs over 3 times more efficiently than

the next best performer, series-series. The series-parallel tuning circuit outperforms all other combinations due to the Q of the parallel resonant circuit of the secondary loop. The quality factor Q confirms the series-parallel configuration is the most efficient option based on the mathematical physics model assumption of a closed form solution which is developed in MathCAD for investigating wireless power transfer. In conclusion, the four physics models developed in MathCAD are shown to be verified by ADS equivalent circuit simulations. We are now ready to simulate in HFSS a shielded loop system.

#### 7.4 SHIELDED LOOP POWER TRANSFER PROPERTIES SUMMARY

Shielded loops are antenna composed of coaxial line, where the outer conductor is ended half-way around the loop and the center conductor is continued along a loop path until it is shorted to the outer conductor. Thus, shielded loops are constructed and simulated in HFSS as a two port device and thus will act as our baseline. S-parameter matrices parameters of the HFSS simulations are then compared to the MathCAD physics models for a loop radius of 0.1 meter and a frequency of 1MHz. These simulation and calculated results agree to within 4% error. The shielded loop results are slightly different than the wireless power transfer model due to physical characteristic between the solid copper wire and the RG58 coaxial cable physical dimensions. Two shielded loops are built, simulated and the results then are compared to the MathCAD wireless power transfer model results. HFSS simulation results of the shielded loop power transfer configuration show less than 4% error agreement with wireless power transfer model. Now we have verified HFSS simulation results of shielded loop with MathCAD physical model results of the shielded loop, we are now ready to develop the helical loop pair system.

#### 7.5 HELIX LOOP INVESTIGATION SUMMARY

A helical loop pair configuration was constructed in HFSS for characteristic investigation. The single helical loop of four cycles is investigated, followed by a double helical loop of four cycles. Poly-lines were used for investigating the characteristics of the E & H fields along all three axes of all loops. Frequencies of 100MHz are used and uneven current distributions were observed due to the loops not being electrically small at 100MHz. Further investigation led to changing the frequency from 100MHz to 1MHz and it was observed that the helix solutions yielded a Magneto-Static frequency response that satisfied the Magneto-static solution of the H-field at the center of the loop. This was achieved by comparing the wireless power transfer models of a loop. Finally, we are set to compare the different two loop system models: the Shielded Loop, the 4 Cycle Helix Loop, and optimizing the Helical model – the 0 Cycle Helix Loop system.

## 7.6 CONCLUSION A TWO LOOP SYSTEM

Based on what we set out to do, we have successfully designed a two loop system architecture which greatly improves the power transfer characteristic in the near field while reducing the power radiated in the far field with respect to the shielded loop configuration. A new Figure of Merit has been introduced as a method to equivalently evaluate the overall performance of the baseline, shielded, two loop architecture with that of the helix based two loop architectures developed. The best performing configuration was the zero cycle helical loop system, with an S21 value of -21.57 dBm and power radiated value of -98.72 dBm, resulting in the highest FOM of  $5.19 \times 10^7$ . The zero cycle helical loop FOM performance was compared to the shielded loop FOM, which is  $2.9 \times 10^5$ .

In previous chapters it is shown that the best configuration for maximizing power transfer to an ohmic load is to resonate the primary loop with a series capacitor by canceling the imaginary inductive reactance with the proper calculated capacitance. The secondary loop, which is known to contain a battery or ohmic load, is tuned by adding it in parallel to the load tuning capacitor. Therefore, using S-P as a performance optimization technique is recommended over using the S-S, P-S or the P-S resonance techniques. Future studies may benefit from tuning the loops respective to loads and the separation distances simultaneously. Additionally, it is recommended that multi-turn helix loops be investigated for system efficiencies. In conclusion, the zero turn helical loops system is a novel design that tremendously improves on reducing the far field radiation while providing efficient wireless power transfer.

## REFERENCES

1. Constantine A. Balanis, *Antenna Theory Analysis and Design*, 3<sup>rd</sup> Edition, John Wiley & Sons, 2005. Print.
2. C. F. M. Carobbi, L. M. Millanta, L. Chiosi, “The High-Frequency of the Shield in the Magnetic-Field Probes”, *IEEE* (2000): 0-7803-5677-2/00.
3. David M. Pozar, *Microwave Engineering*, 3<sup>rd</sup> Edition John Wiley & Sons, Inc. 2005. Print.
4. David K. Cheng, *Field and Wave Electromagnetics*, 2<sup>nd</sup> Edition, Pearson Education, Inc, 1989. Print.
5. E. C. Jordan, *Electromagnetic Waves and Radiating Systems*, Prentice-Hall, Inc. Englewood Cliffs, New Jersey, Prentice-Hall Electrical Engineering Series, 1950. Print.
6. Frank M. Greene, “The Near-Zone Magnetic Field of a Small Circular-Loop Antenna”, *Journal of Research of National Bureau of Standards*, Vol. 71C, No. 4, (1967): 319-326. Print.
7. James T. Aberle and Robert Loespringer-Romak, *Antennas with Non-Foster Matching Networks*, Morgan & Claypool, 2007. Print.
8. Pedro Arzuaga, “Cardiac Pacemakers: Past, Present and Future”, *IEEE Instrumentation & Measurement Magazine*, (2014): 1094-6969/14. Print.
9. Sergei A. Schelkunoff, *Advanced Antenna Theory*, New York. John Wiley & Sons, Inc. London. Chapman & Hall, Limited, 1952. Print.
10. Sergei A. Schelkunoff and Harald T. Friis, *Antennas: Theory and Practice – a thorough treatment of the principles necessary for understanding antenna behavior and design*, New York. John Wiley & Sons, Inc. London. Chapman & Hall, Limited, 1952. Print.
11. Simon Ramo and John R. Whinnery and Theodore Van Duzer, *Fields and Waves in Communication Electronics*, 2<sup>nd</sup> Edition, John Wiley & Sons, New York, Chichester, Brisbane, Toronto, Singapore, 1965, 1984. Print.
12. W. L. Weeks, *Electromagnetic Theory for Engineering Applications*, John Wiley & Sons, Inc. New York. London. Sydney, 1964. Print.

## APPENDIX A

WIRELESS POWER TRANSFER MODELS TUNED THROUGH SERIES-SERIES,  
SERIES-PARALLEL, PARALLEL-SERIES AND PARALLEL-PARALLEL  
CONFIGURATIONS.

## Wireless Power Transfer Model: Series-Series

A wireless power transfer model for a two loops system was built. The tuning configuration consists of the first loop tuned in series for canceling reactance and the second loop tuned in series for canceling its reactance. Both loop reactance cancelation was performed assuming each loop was alone in free space.



By Duality and reference of RamoWhinnery, and Van Duzer (p.586) we can write the Magnetic field components of a magnetic dipole for Hr and Hθ , and express them here with the Magnetic Dipole Moment seen as ρ m.

$$\rho_m := I \cdot \pi \cdot a^2 \quad I := j \cdot \omega \cdot q \quad f := 1 \cdot 10^6 \quad \epsilon_r := 1 \quad \mu_0 := 4\pi \cdot 10^{-7} \quad \epsilon_0 := 8.85 \cdot 10^{-12}$$

Series - Series Program

$$\eta := \sqrt{\frac{\mu_0}{\epsilon_0 \cdot \epsilon_r}} \quad k_0 := \omega \cdot \sqrt{\mu_0 \cdot \epsilon_0 \cdot \epsilon_r} \quad k_0 = 0.021$$

Position of source as the center of the coordinate system (Cartesian):

$$x_{src} := 0 \quad y_{src} := 0 \quad z_{src} := 0$$

Radius of larger loop:  $a := 0.1$

Radius of equivalent loop:  $b := 0.1$

Unit Area dimensions:  
drop into equations after everything  
is  
working.

$$dx := \frac{a}{20} \quad dy := \frac{a}{20} \quad dz := 0$$

$$dx = 5 \times 10^{-3} \quad dy = 5 \times 10^{-3} \quad dz = 0$$

Position coordinates of  
loop observer (Large Loop).

$$x_{c\_obs} := 0$$

$$y_{c\_obs} := 0$$

$$z_{c\_obs} := 0$$

Planar from  $b+2*a$  to  $N*b$ :  $N := 200$   $(b + 2a) = 0.3$   $N \cdot b = 200$

$$z := 50, 60.. 300$$

$$h_z := \frac{z}{1000}$$

Build a Raster Function :

$$p := 0.. 1590$$

Row:

$$m_p := \text{floor}\left(\frac{p}{40}\right)$$

Column:

$$n_p := p - (40 \cdot m_p)$$

$$X_{\text{obs}_p} := \left( xc_{\text{obs}} - a + \frac{m_p}{199} + \frac{a}{80} \right)$$

Define the X and Y positions as observers for an square mesh of loop.

$$Y_{\text{obs}_p} := \left( yc_{\text{obs}} + a - \frac{n_p}{199} - \frac{a}{80} \right)$$

$$Z_{\text{obs}_z} := -(h_z + zc_{\text{obs}})$$

R - distance from source to center of Observer loop:

$$R_{p,z} := \sqrt{(x_{\text{src}} - X_{\text{obs}_p})^2 + (y_{\text{src}} - Y_{\text{obs}_p})^2 + (z_{\text{src}} - Z_{\text{obs}_z})^2}$$

This is an A-matrix for storing the positions of Unit Areas:

$$A_{p,z} := \sqrt{(X_{\text{obs}_p} - xc_{\text{obs}})^2 + (Y_{\text{obs}_p} - yc_{\text{obs}})^2}$$

Member of circle Matrix: Use the Heavyside step function to keep all Unit Area squares that compose the area of the Loop observer for a matrix that shapes the loop observer:

$$\text{Member}_{p,z} := \Phi(a - A_p)$$

$$\rho_m := \mathbf{I}_1 \cdot \pi \cdot b^2$$

$$B_{\theta_{p,z}} := \frac{j \cdot \omega \cdot \mu_0^2 \cdot l \cdot b^2}{4} \cdot e^{-j \cdot k_0 \cdot R_{p,z}} \cdot \left[ \frac{j \cdot \omega \cdot \epsilon_0 \cdot \epsilon_r}{R_{p,z}} + \frac{1}{\eta \cdot (R_{p,z})^2} + \frac{1}{j \cdot \omega \cdot \mu_0 \cdot (R_{p,z})^3} \right] \cdot \sqrt{1 - \left[ \frac{(z_{\text{src}} - Z_{\text{obs}_z})}{R_{p,z}} \right]^2}$$

$$B_{r_{p,z}} := \frac{j \cdot \omega \cdot \mu_0^2 \cdot l \cdot b^2}{2} \cdot e^{-j \cdot k_0 \cdot R_{p,z}} \cdot \left[ \frac{1}{\eta \cdot (R_{p,z})^2} + \frac{1}{j \cdot \omega \cdot \mu_0 \cdot (R_{p,z})^3} \right] \cdot \frac{(z_{\text{src}} - Z_{\text{obs}_z})}{R_{p,z}}$$

Unit Area defined:

$$dx = 5 \times 10^{-3} \quad dy = 5 \times 10^{-3} \quad dz = 0$$

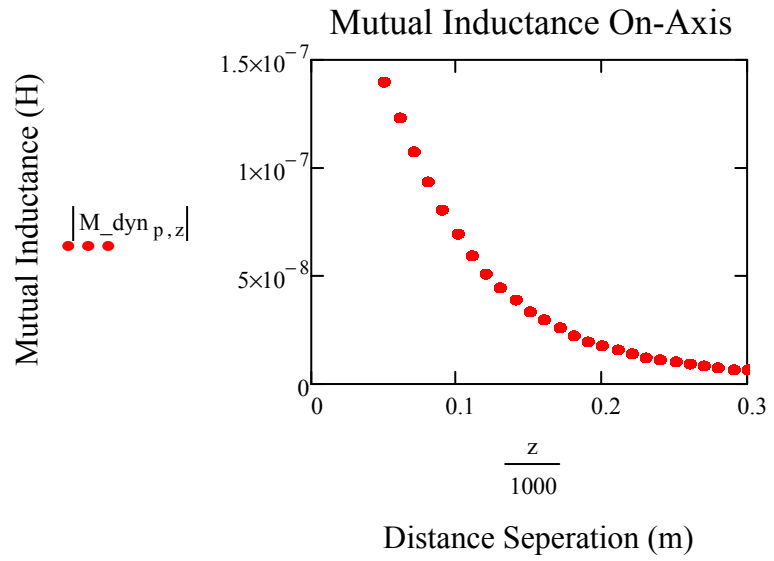
$$dS_z := dx \cdot dy$$

$$dS_{-r_{p,z}} := dS_z \cdot \frac{(z_{\text{src}} - Z_{\text{obs}_z})}{R_{p,z}} \quad dS_{-\theta_{p,z}} := - \left[ dS_z \cdot \sqrt{1 - \left[ \frac{(z_{\text{src}} - Z_{\text{obs}_z})}{R_{p,z}} \right]^2} \right]$$

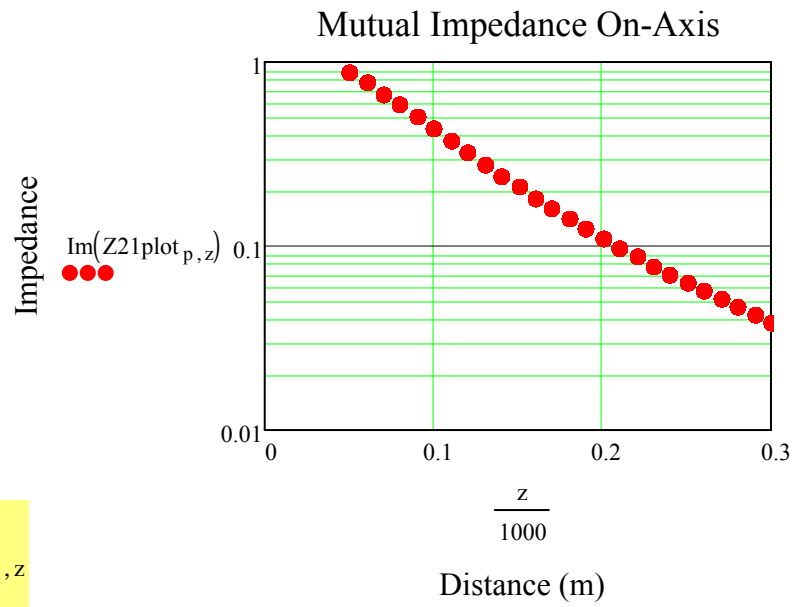
Flux: B-field components dotted with Unit Area components; All in spherical coordinates.

$$\Psi_{21_{p,z}} := (B_{r_{p,z}} \cdot dS_{-r_{p,z}} + B_{\theta_{p,z}} \cdot dS_{-\theta_{p,z}}) \cdot (\text{Member}_{p,z}) \quad \mathbf{I}_1 = \blacksquare$$

$$M_{\text{dyn}_{p,z}} := \frac{\left( \sum_{p=0}^{1599} \Psi_{21_{p,z}} \right)}{1}$$



$$Z_{21\text{plot}_{p,z}} := j \cdot \omega \cdot M_{\text{dyn}_{p,z}}$$



$$Z_{21_z} := j \cdot \omega \cdot \frac{\sum_{p=0}^{1599} \Psi_{21_{p,z}}}{1}$$

Assume wire is copper Twin-Lead line (20 gauge): Diameter=0.812mm, Dist\_apart=7.5mm

$$\sigma := 5.8 \cdot 10^7 \quad \rho_{\text{cu}} := 1.724 \cdot 10^{-8}$$

Temperature coefficient per 1deg Celsius (Human temp ~ 37C):

$$\alpha := 4.29 \cdot 10^{-3} \quad \alpha_{37} := \alpha \cdot 37 \quad dR / R_s = \alpha \cdot dT, \quad dR = \text{change in resistance (ohm)}, R_s = \text{standard resistance according to reference tables (ohm)}, \alpha = \text{temperature coefficient of resistance}, dT = \text{change in temperature (K)}$$

$$dR_{37} := \alpha \cdot dT \cdot R_s \quad dR_{37} := \alpha_{37} \rho_{\text{cu}}$$

$$dR_{37} = 2.737 \times 10^{-9}$$

Large Loop Length:

$$L_{1g} := 2 \cdot \pi \cdot a$$

$$L_{1g} = 0.628$$

Second Loop Length:

$$L_{2nd} := 2 \cdot \pi \cdot b$$

$$L_{2nd} = 0.628$$

Skin Depth (Weeks p372): Surface Resistance (Weeks p373): Schelkunoff (p339)

$$\delta := \sqrt{\frac{2}{(2 \cdot \pi \cdot f) \cdot \mu_0 \cdot \sigma}} \quad R_s := \frac{1}{\sigma \cdot \delta} \quad R_{2s} := \sqrt{\frac{\pi \cdot f \cdot \mu_0}{\sigma}} \quad R_{3s} := 2.61 \cdot 10^{-7} \cdot \sqrt{f}$$

$$R_s = 2.609 \times 10^{-4} \quad R_{2s} = 2.609 \times 10^{-4} \quad R_{3s} = 2.61 \times 10^{-4}$$

Ramo uses Low-Frequency for ratios up to 1 (or lower), High Frequency calcs are > 1. Therefore, High Frequency resistance calculations are needed:

Radius of 20 awg wire:

$$r_{\text{cu20awg}} := 0.000401$$

$$\frac{r_{\text{cu20awg}}}{\delta} = 6.144$$

High Frequency (Ramo p182, Schelkunoff p339):

$$R_{\text{hf}} := \frac{R_s}{2 \cdot \pi \cdot r_{\text{cu20awg}}} \quad R_{\text{hf}} = 0.102 \quad \text{Units are } \Omega / \text{m}$$

$$R_{\text{hf1st}} := R_{\text{hf}} \cdot (L_{1g}) + dR_{37}$$

$$R_{\text{hf1st}} = 0.064$$

$$R_{\text{hf2nd}} := R_{\text{hf}} \cdot (L_{2nd}) + dR_{37}$$

$$R_{\text{hf2nd}} = 0.064$$

$$Z_L := 300$$

$$R_{\text{tot}} := R_{\text{hf2nd}}$$

$$R_{\text{tot}} = 0.064$$

Clearly, the battery load (ZL) has significant impact on efficiency. If assumed 1 ohm, efficiency is very high !!!

The Total Mhos conductance may be found by taking the inverse of the total series resistance.

$$G_{lp1} := \frac{1}{R_{hf1st}} \quad G_{lp1} = 15.562 \quad G_{lp2} := \frac{1}{R_{hf2nd}} \quad G_{lp2} = 15.562$$

Use Schelkunoff Radiation conductance instead of Rad

$$\lambda := \frac{2.99 \cdot 10^8}{f} \quad \lambda = 299$$

----- Magneto-Statics Capacitance of a small loop -----

(Schelkunoff p 321-322)

$$C_{av} := \frac{\pi \cdot \epsilon_0}{\log\left(\frac{b}{a}\right)}$$

Average capacitance between two halves of loop per unit length along the circumference (Voltage distribution across loop).

$$C_{loop} := \frac{1}{3} \cdot C_{av} \cdot b \cdot \pi$$

Loop capacitance:

$$C_{lp1} := \frac{\pi^2 \cdot \epsilon_0 \cdot a}{3 \cdot \ln\left(\frac{a}{r_{cu20awg}}\right)}$$

$$C_{lp1} = 5.287 \times 10^{-13}$$

$$\frac{1}{j \cdot \omega \cdot C_{lp1}} = -3.01i \times 10^5$$

$$C_{lp2} := \frac{\pi^2 \cdot \epsilon_0 \cdot b}{3 \cdot \ln\left(\frac{b}{r_{cu20awg}}\right)}$$

$$C_{lp2} = 5.287 \times 10^{-13}$$

----- Magneto Static Inductance (loop) -----

Internal inductance contribution (Balanis p245):

$$L_{i1} := \frac{a}{\omega \cdot r_{cu20awg}} \cdot \sqrt{\frac{\omega \cdot \mu_0}{2 \cdot \sigma}}$$

$$L_{i2} := \frac{b}{\omega \cdot r_{cu20awg}} \cdot \sqrt{\frac{\omega \cdot \mu_0}{2 \cdot \sigma}}$$

$$L_{i1} = 1.023 \times 10^{-8}$$

$$L_{i2} = 1.023 \times 10^{-8}$$

(Schelkunoff p 321) Small, single turn loop with substantially uniform current (approximate inductance).

$$L_{lp1} := \mu_0 \cdot a \cdot \ln\left(\frac{a}{r_{cu20awg}}\right) + L_{i1}$$

$$L_{lp1} = 7.022 \times 10^{-7}$$

$$j \cdot \omega \cdot L_{lp1} = 4.412i$$

$$L_{lp2} := \mu_0 \cdot b \cdot \ln\left(\frac{b}{r_{cu20awg}}\right) + L_{i2}$$

$$L_{lp2} = 7.022 \times 10^{-7}$$

Conductance - Using Ohmic resistance and the Radiation Resistance::  $\eta = 376.819$

$$G1 := \frac{3 \cdot \pi}{2\eta} \quad G1 = 0.013 \quad G2 := \frac{3 \cdot \pi}{2\eta} \quad G2 = 0.013$$

$$G1 := 320 \pi^4 \cdot \frac{(\pi \cdot a)^2}{\lambda^4} \quad G1 = 0.013 \quad G2 := G1 \quad G2 = 0.013$$

Admittance looking in on equivalent loop circuit, prematching capacitor:

$$Y_{pre1} := \frac{1 + \frac{j \cdot \omega \cdot C_{lp1}}{2} \cdot \left( j \cdot \omega \cdot L_{lp1} + \frac{1}{G_{lp1}} \right)}{j \cdot \omega \cdot L_{lp1} + \frac{1}{G_{lp1}}} + \frac{j \cdot \omega \cdot C_{lp1}}{2 + j \cdot \omega \cdot C_{lp1} \cdot \frac{1}{G1}} \quad Y_{pre1} = 3.3 \times 10^{-3} - 0.227i$$

$$Z_{pre1} := \frac{1}{Y_{pre1}} \quad Z_{pre1} = 0.064 + 4.412i$$

If we know:  $\frac{1}{\omega \cdot L_{eff}} := \omega \cdot C$

Then, the tuning capacitance is:

$$C_{tune} := \frac{1}{\omega^2 \cdot (L_{lp1})}$$

$$C_{tune} = 3.607 \times 10^{-8}$$

$$\frac{1}{i \cdot \omega \cdot C_{tune}} = -4.412i$$

Assume a variable capacitive element that can cancel the complex conjugate:

$$C_{match} := -\text{Im}(Z_{pre1}) \cdot i \quad C_{match} = -4.412i$$

The complex conjugate will add in Series in the Admittance(Impedance) model circuit.

$$Z_{11} := Z_{pre1} + C_{match} \quad Z_{11} = 0.064$$

$$Y_{in1} := \frac{1}{Z_{11}} \quad Y_{in1} = 15.561$$

$$Y_{pre2} := \left[ \frac{1 + \frac{j \cdot \omega \cdot C_{lp2}}{2} \cdot \left( j \cdot \omega \cdot L_{lp2} + \frac{1}{G_{lp2}} \right)}{j \cdot \omega \cdot L_{lp2} + \frac{1}{G_{lp2}}} + \frac{j \cdot \omega \cdot C_{lp2}}{2 + j \cdot \omega \cdot C_{lp2} \cdot \frac{1}{G_2}} \right]$$

$$Y_{pre2} = 3.3 \times 10^{-3} - 0.227i$$

$$Z_{pre2} := \frac{1}{Y_{pre2}}$$

$$Z_{pre2} = 0.064 + 4.412i$$

Assume a variable capacitive element that can cancel the complex conjugate:

$$C_{match2} := -\text{Im}(Z_{pre2}) \cdot i \quad C_{match2} = -4.412i$$

The complex conjugate will add in Series in the Admittance model circuit.

ASSUMPTION: After the Loop has been matched (since battery R changes with charging), then we can add the load to Z22.

$$Z_{22} := (Z_{pre2} + C_{match2}) + Z_L$$

$$Z_{22} = 300.064$$

$$Y_{in2} := \frac{1}{Z_{22}}$$

$$Y_{in2} = 3.333 \times 10^{-3}$$

Now we have the following impedances of the system.

$$Z_{12}_z := Z_{21}_z$$

$$Z_{11} = 0.064$$

Mutual Z at 0.5 Radii  $Z_{21}_{50} = 3.783 \times 10^{-9} + 0.878i$

Mutual Z at 1.0 Radii  $Z_{21}_{100} = 3.783 \times 10^{-9} + 0.435i$

Mutual Z at 2.0 Radii  $Z_{21}_{200} = 3.783 \times 10^{-9} + 0.11i$

In the case of two loops in proximity, such that they can be modeled as a Linear Transducer. Loop1 and Loop2, each with two terminals for pos and neg bias.(Schelkunoff p291)

$$V_1 := Z_{11} \cdot I_1 + Z_{12} \cdot I_2$$

$$V_2 := Z_{21} \cdot I_1 + Z_{22} \cdot I_2$$

In matrix form:

$$\begin{pmatrix} V_1 \\ V_2 \end{pmatrix} := \begin{pmatrix} Z_{11} & Z_{12} \\ Z_{21} & Z_{22} \end{pmatrix} \cdot \begin{pmatrix} I_1 \\ I_2 \end{pmatrix}$$

For Admittance:

- Current at terminals are short circuited
- Y internal calc when all generators are open circuited.

Now, let D be:

$$D := (Z_{11} \cdot Z_{22} - Z_{12} \cdot Z_{21})$$

$$D_z := (Z_{11} \cdot Z_{22} - Z_{12} \cdot Z_{21}_z)$$

Next, we can solve the Matrix and re-write as such:

$$\begin{pmatrix} I_1 \\ I_2 \end{pmatrix} := \begin{pmatrix} \frac{Z_{22}}{D} & \frac{-Z_{12}}{D} \\ \frac{-Z_{21}}{D} & \frac{Z_{11}}{D} \end{pmatrix} \cdot \begin{pmatrix} V_1 \\ V_2 \end{pmatrix}$$

Writing current with respect to admittance gives us:

$$\begin{pmatrix} I_1 \\ I_2 \end{pmatrix} := \begin{pmatrix} Y_{11} & Y_{12} \\ Y_{21} & Y_{22} \end{pmatrix} \cdot \begin{pmatrix} V_1 \\ V_2 \end{pmatrix}$$

$$Y_{11}_z := \frac{Z_{22}}{D_z}$$

$$Y_{12}_z := \frac{-Z_{12}_z}{D_z}$$

$$Y_{21}_z := \frac{-Z_{21}_z}{D_z}$$

$$Y_{22}_z := \frac{Z_{11}}{D_z}$$

verification using Schelkunoff p 407:

$$Y_{12}_z := \frac{-Z_{12}_z}{Z_{11} \cdot Z_{22} - (Z_{12}_z)^2}$$



Now, we have the following:  $I_1 := Y_{11} \cdot V_1 + Y_{12} \cdot V_2$

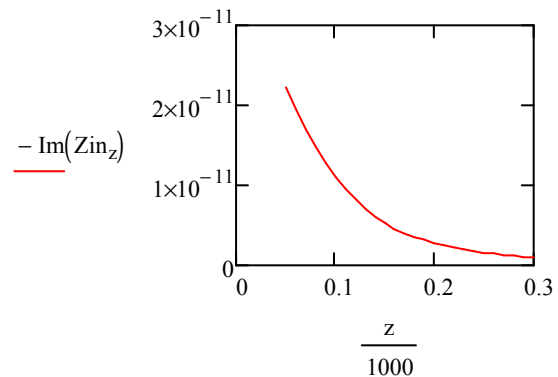
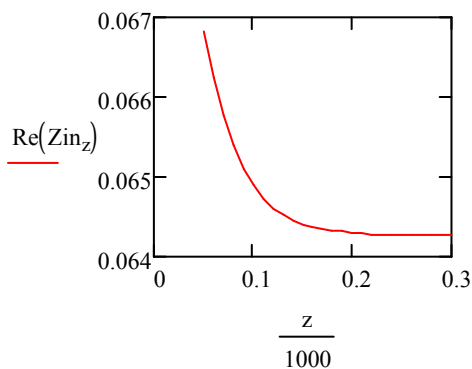
$$I_2 := Y_{21} \cdot V_1 + Y_{22} \cdot V_2$$

We will now assume a transmission line source will be connected to loop1, and then we can solve for I1 and V1

Assuming that loop 2 has a battery load we can solve the impedance matrix by "Collapsing a two-port to a one port network", and use this to calculate the reflection coefficient of the input terminal that the source will see. Then we will know V1 and I1 for power calculations:

ZinBy Schelkunoff:

$$Z_A := Z_{11} - \frac{Z_{12}^2}{Z_{22}} \quad Z_{in_z} := Z_{11} - \frac{(Z_{21_z})^2}{Z_{22}} \quad Z_{in2_z} := Z_{22} - \frac{(Z_{12_z})^2}{Z_{11}}$$



Impedance of the source matched to input of loop1, with loop2 at given distance:

$$Z_0 := [\text{Re}(Z_{in_{50}}) + (-\text{Im}(Z_{in_{50}})i)] \quad Z_0 = 0.067 + 2.213i \times 10^{-11}$$

And the reflection coefficient can now be seen as:

$$\Gamma_{VZ} := \frac{Z_{in_z} - Z_0}{Z_{in_z} + Z_0}$$

If the total voltage and current waves on the line can be written as :

$$V(x) := V_{src} \cdot (e^{-j \cdot \beta \cdot x} + \Gamma \cdot e^{j \cdot \beta \cdot x}) \quad I(x) := \frac{V_{src}}{Z_0} \cdot (e^{-j \cdot \beta \cdot x} - \Gamma \cdot e^{j \cdot \beta \cdot x})$$

Since the distance of transmission line is nearly 0 (negligible), we can express the equations:

$$V_x := V_{\text{src}} \cdot (1 + \Gamma) \quad \text{and} \quad I_x := \frac{V_{\text{src}}}{Z_0} \cdot (1 - \Gamma)$$

Assume a source voltage:

$$V_{\text{src}} := 1$$

$$V1_z := V_{\text{src}} \cdot (1 + \Gamma_z) \quad \text{and, therefore} \quad I1_z := \frac{V_{\text{src}}}{Z_0} \cdot (1 - \Gamma_z)$$

$$V2_z := Z21_z \cdot I1_z$$

$$I2_z := Y21_z \cdot V1_z$$

$$\frac{V_{\text{src}}}{Z_0} = 14.963 - 4.956i \times 10^{-9}$$

Power Radiated (Schelkunoff Antennas p323): NOTE: This is the power radiated by the primary loop antenna. Use Total Complex dipole moment of both antennas.

Power Radiated (Schelkunoff Antennas p323):

Loop 1 with 1amp assumed source:

$$\text{Prad1}_z := \frac{320 \pi^4 \cdot (\pi \cdot a^2)^2 \cdot (I1_z)^2}{\lambda^4 \cdot 2}$$

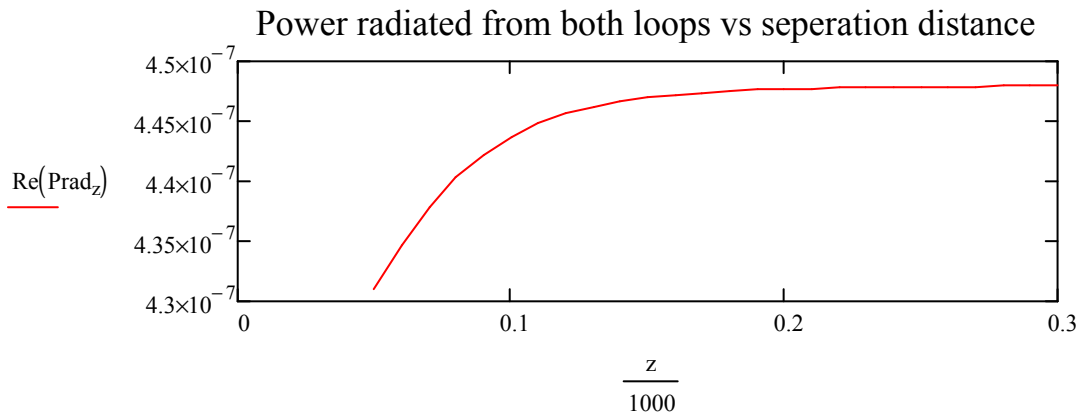
Loop 2 with calculated current (I2) using Linear Transducer Matrix:

$$\text{Prad2}_z := \frac{320 \pi^4 \cdot (\pi \cdot b^2)^2 \cdot (I2_z)^2}{\lambda^4 \cdot 2}$$

Total Complex Dipole Moment (Assuming they are so close and behave as one antenna):

$$I_{\text{tot}_z} := I1_z + I2_z$$

$$\text{Prad}_z := \frac{320 \pi^4 \cdot (\pi \cdot a^2)^2 \cdot (|I_{\text{tot}_z}|)^2}{\lambda^4 \cdot 2}$$



Series-Series Power due to copper at 1MHz:

Incident Power from  
Transmission Line Source

$$P_{inc_z} := \frac{(|V_{src}|)^2}{Re(Z_0)}$$

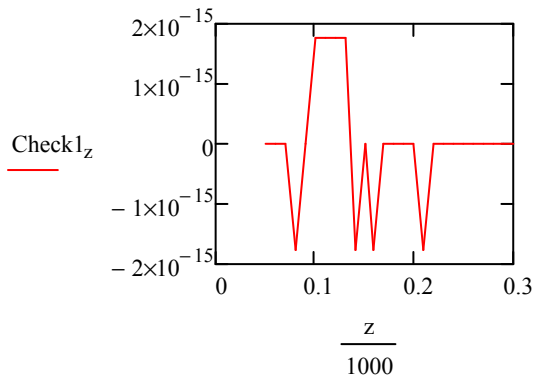
Reflected power to source

$$P_{refl_z} := \frac{(|V_{src}|)^2 \cdot (|\Gamma_z|)^2}{Re(Z_0)}$$

Power after reflection:

$$P_{tr_z} := \frac{(|V_{src}|)^2}{Re(Z_0)} \cdot [1 - (|\Gamma_z|)^2]$$

$$Check1_z := P_{inc_z} - P_{refl_z} - P_{tr_z}$$



## Power Calculations

$$P1ohm_z := \left( |I1_z| \right)^2 \cdot Rhf_{1st}$$

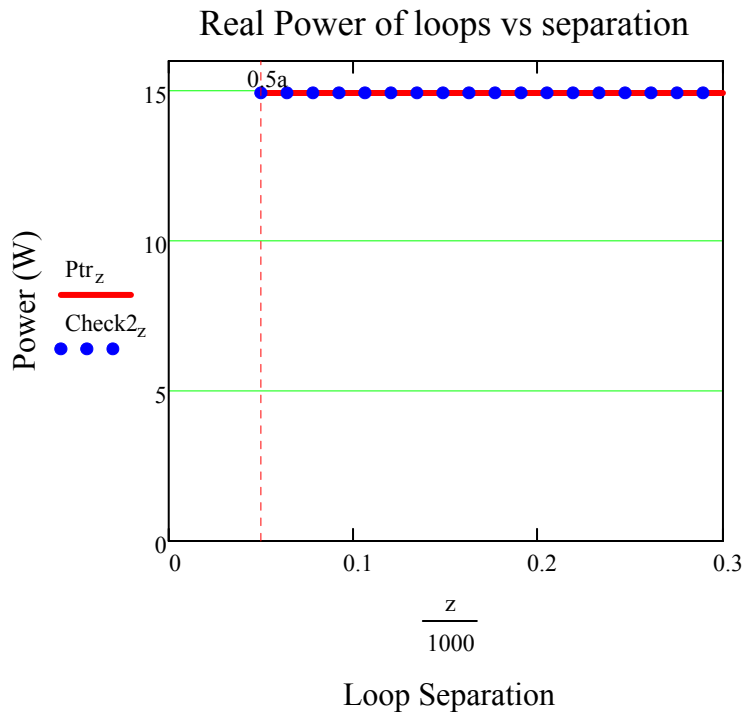
$$P2Rbatt_z := \left( |I2_z| \right)^2 \cdot Z_L$$

$$P2ohm_z := \left( |I2_z| \right)^2 \cdot Rhf_{2nd}$$

Compare power calculations to verify all Real Power is Accounted for in loop system:

$$Ptr_z := \left( |I1_z| \right)^2 \cdot Re(Zin_z) \quad \text{Power sourced to loop1}$$

$$Check2_z := (P1ohm_z) + (P2Rbatt_z) + (P2ohm_z) + (Prad_z)$$



$$Ptr_{50} = 14.963$$

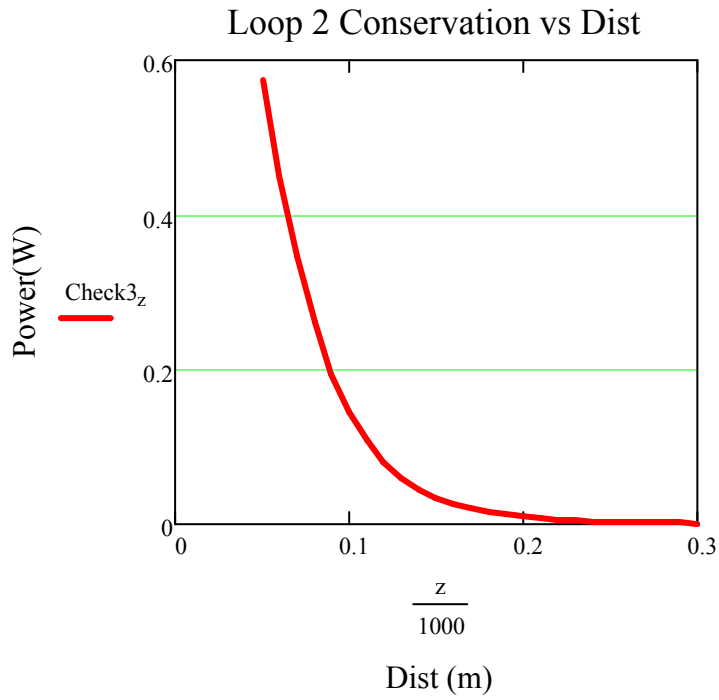
$$P2Rbatt_{50} = 0.575$$

$$P2Rbatt_{100} = 0.145$$

$$P2Rbatt_{200} = 9.411 \times 10^{-3}$$

Compare power calculations to verify all Real Power in Loop2 is Accounted for:

$$\text{Check3}_z := P2R_{\text{batt}_z} + P2\text{ohm}_z$$

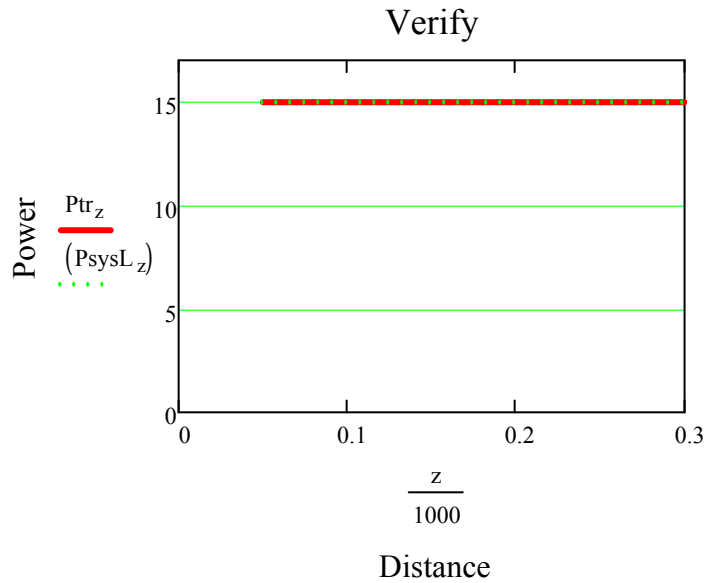


Check3<sub>z</sub> =

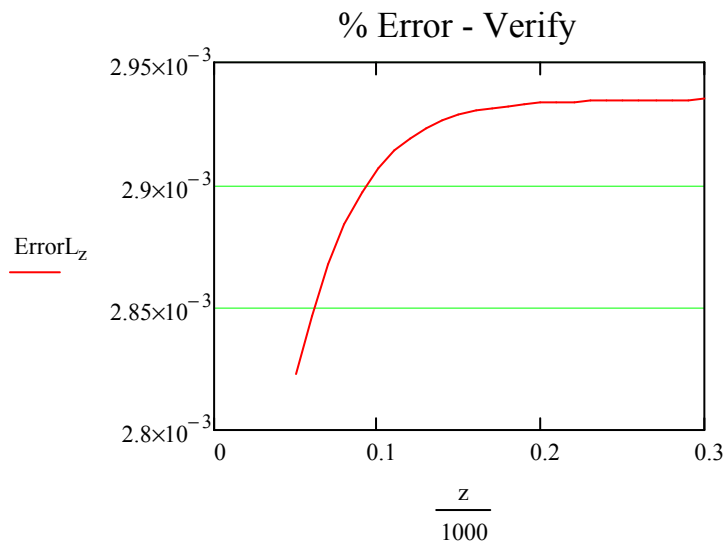
0.575
0.451
0.345
0.261
0.195
0.145
0.108
0.08
0.06
0.045
0.034
0.026
0.02
0.015
0.012
...

Compare power calculations of Matrix quantities and Copper Loss mechanisms to verify all Real Power is Accounted for:

$$P_{\text{sys}L_z} := \left[ \left( P_{1\text{ohm}_z} \right) + \left( P_{2R\text{batt}_z} \right) + \left( P_{2\text{ohm}_z} \right) + \left( P_{\text{rad}_z} \right) \right]$$



$$\text{Error}L_z := \left[ 1 - \frac{\left( P_{\text{sys}L_z} \right)}{\left( P_{\text{tr}_z} \right)} \right] \cdot 100$$



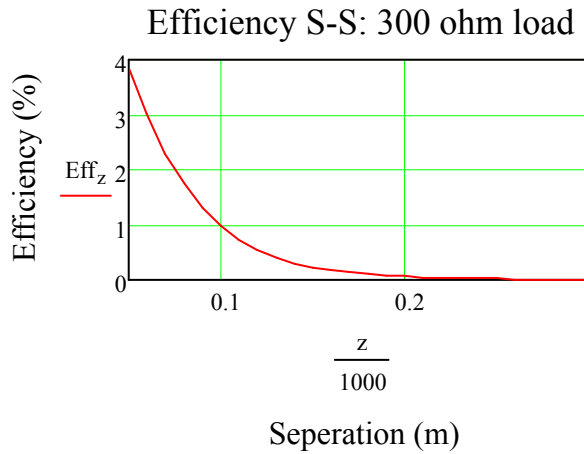
Let's see how much power at the source it requires for power to battery.

$$V_{src} = 1$$

$$\text{Eff}_z := \left( \frac{P_{2R_{batt}_z}}{P_{inc}_z} \right) \cdot 100$$

$$\text{Eff}_z =$$

3.841
3.011
2.308
1.743
1.303
0.97
0.721
0.537
0.402
0.302
0.228
0.174
0.133
0.103
0.08
...

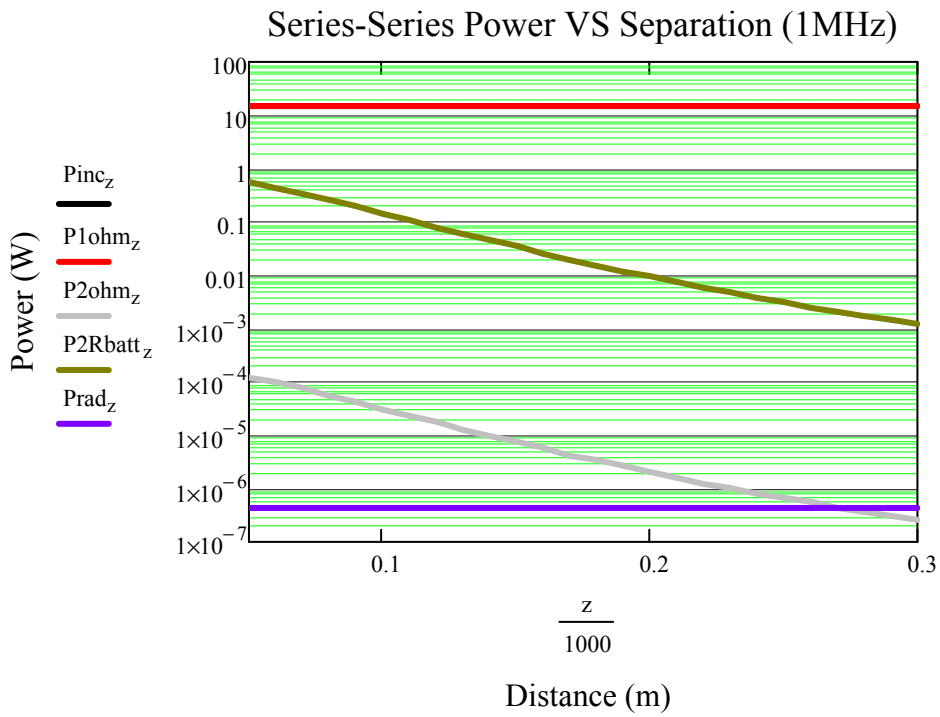
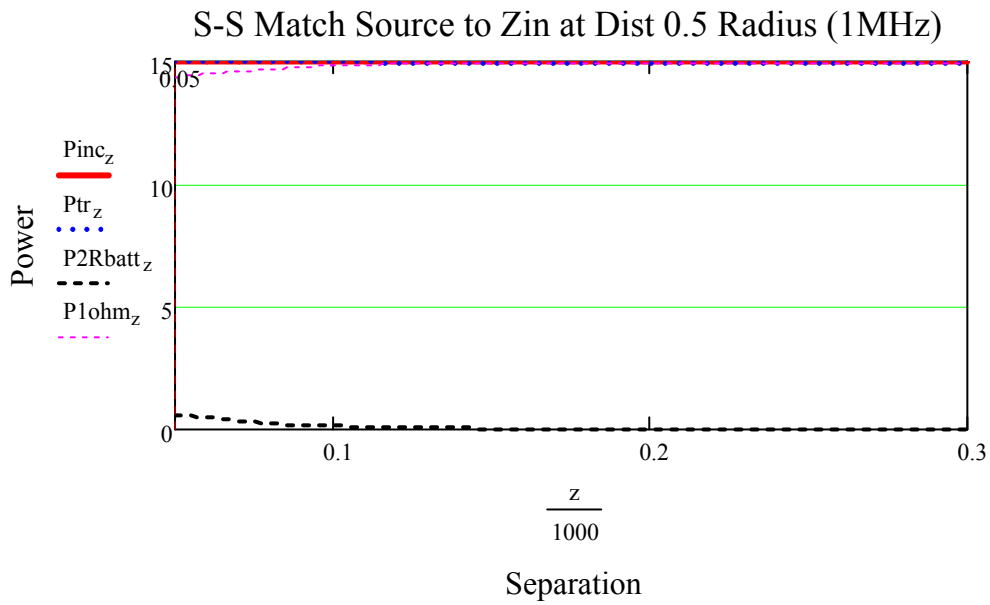


$$\text{Eff}_{50} = 3.841$$

$$\text{Eff}_{100} = 0.97$$

$$\text{Eff}_{200} = 0.063$$

$$\text{Eff}_{300} = 7.877 \times 10^{-3}$$





Coupling coefficient at half a radius (z=50):

For calculating equivalent circuit (NOTE must use Static Mutual and Self Inductances):

$$\text{If we know that: } M := k \cdot \sqrt{L_1 \cdot L_2} \quad M := 1.397 \cdot 10^{-7} \quad L_{p1} = 7.022 \times 10^{-7}$$

$$k := \frac{(M)}{\sqrt{L_{p1} \cdot L_{p2}}} \quad k = 0.199$$

#### Wireless Power Transfer Model: Series-Parallel

A wireless power transfer model for a two loops system was built. The tuning configuration consists of the first loop tuned in series for canceling reactance and the second loop tuned in parallel for canceling its reactance. Both loop reactance cancelation was performed assuming each loop was alone in free space.

By Duality and reference of RamoWhinnery, and Van Duzer (p.586) we can write the Magnetic field components of a magnetic dipole for  $H_r$  and  $H_\theta$ , and express them here with the Magnetic Dipole Moment seen as  $\rho_m$ .

$$\rho_m := I \cdot \pi \cdot a^2 \quad I := j \cdot \omega \cdot q \quad f := 1 \cdot 10^6 \quad \epsilon_r := 1 \quad \mu_0 := 4\pi \cdot 10^{-7} \quad \epsilon_0 := 8.85 \cdot 10^{-12}$$

$$\omega := 2 \cdot \pi \cdot (f)$$

Series - Parallel Program

$$\eta := \sqrt{\frac{\mu_0}{\epsilon_0 \cdot \epsilon_r}} \quad k_0 := \omega \cdot \sqrt{\mu_0 \cdot \epsilon_0 \cdot \epsilon_r} \quad k_0 = 0.021$$

Position of source as the center of the coordinate system (Cartesian):

$$x_{src} := 0 \quad y_{src} := 0 \quad z_{src} := 0$$

Radius of larger loop:

$$a := 0.1$$

Radius of equivalent loop:

$$b := 0.1$$

Unit Area dimensions:  
drop into equations after everything  
is  
working.

$$dx := \frac{a}{20} \quad dy := \frac{a}{20} \quad dz := 0$$

$$dx = 5 \times 10^{-3} \quad dy = 5 \times 10^{-3} \quad dz = 0$$

Position coordinates of  
loop observer (Large Loop).

$$x_{c\_obs} := 0$$

$$y_{c\_obs} := 0$$

$$z_{c\_obs} := 0$$

Planar from  $b+2*a$  to  $N*b$ :

$$N := 2000$$

$$(b + 2a) = 0.3$$

$$N \cdot b = 200$$

$$z := 50, 60.. 300$$

$$h_z := \frac{z}{1000}$$

Build a Raster Function :

$$p := 0.. 1599$$

Row:

Column:

$$m_p := \text{floor}\left(\frac{p}{40}\right)$$

$$n_p := p - (40 \cdot m_p)$$

$$X_{\text{obs}_p} := \left( xc_{\text{obs}} - a + \frac{m_p}{199} + \frac{a}{80} \right)$$

Define the X and Y positions as observers for an square mesh of loop.

$$Y_{\text{obs}_p} := \left( yc_{\text{obs}} + a - \frac{n_p}{199} - \frac{a}{80} \right)$$

$$Z_{\text{obs}_z} := -(h_z + zc_{\text{obs}})$$

R - distance from source to center of Observer loop:

$$R_{p,z} := \sqrt{(x_{\text{src}} - X_{\text{obs}_p})^2 + (y_{\text{src}} - Y_{\text{obs}_p})^2 + (z_{\text{src}} - Z_{\text{obs}_z})^2}$$

This is an A-matrix for storing the positions of Unit Areas:

$$A_{p,z} := \sqrt{(X_{\text{obs}_p} - xc_{\text{obs}})^2 + (Y_{\text{obs}_p} - yc_{\text{obs}})^2}$$

Member of circle Matrix: Use the Heavyside step function to keep all Unit Area squares that compose the area of the Loop observer for a matrix that shapes the loop observer:

$$\text{Member}_{p,z} := \Phi(a - A_p)$$

$$\rho_m := \mathbf{I}_1 \cdot \pi \cdot b^2$$

$$B_{\theta_{p,z}} := \frac{j \cdot \omega \cdot \mu_0^2 \cdot l \cdot b^2}{4} \cdot e^{-j \cdot k_0 \cdot R_{p,z}} \cdot \left[ \frac{j \cdot \omega \cdot \epsilon_0 \cdot \epsilon_r}{R_{p,z}} + \frac{1}{\eta \cdot (R_{p,z})^2} + \frac{1}{j \cdot \omega \cdot \mu_0 \cdot (R_{p,z})^3} \right] \cdot \sqrt{1 - \left[ \frac{(z_{\text{src}} - Z_{\text{obs}_z})^2}{R_{p,z}^2} \right]}$$

$$B_{r_{p,z}} := \frac{j \cdot \omega \cdot \mu_0^2 \cdot l \cdot b^2}{2} \cdot e^{-j \cdot k_0 \cdot R_{p,z}} \cdot \left[ \frac{1}{\eta \cdot (R_{p,z})^2} + \frac{1}{j \cdot \omega \cdot \mu_0 \cdot (R_{p,z})^3} \right] \cdot \frac{(z_{\text{src}} - Z_{\text{obs}_z})}{R_{p,z}}$$

Unit Area defined:

$$dx = 5 \times 10^{-3} \quad dy = 5 \times 10^{-3} \quad dz = 0$$

$$dS_z := dx \cdot dy$$

$$dS_{-r_{p,z}} := dS_z \cdot \frac{(z_{\text{src}} - Z_{\text{obs}_z})}{R_{p,z}}$$

$$dS_{-\theta_{p,z}} := -dS_z \cdot \sqrt{1 - \left[ \frac{(z_{\text{src}} - Z_{\text{obs}_z})^2}{R_{p,z}^2} \right]}$$

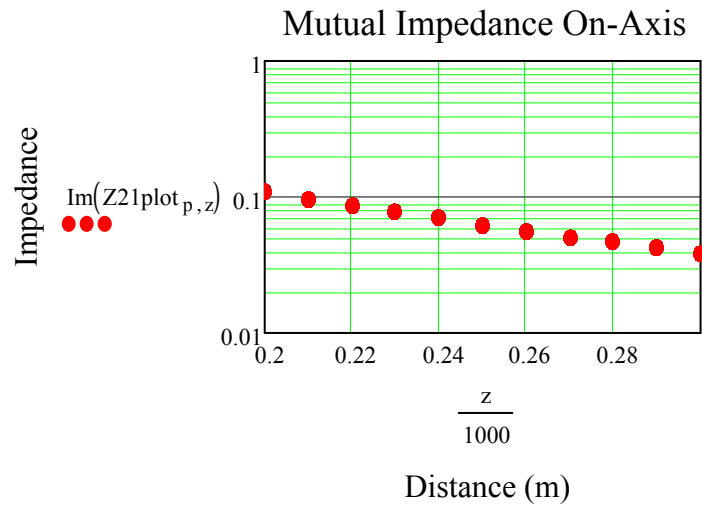
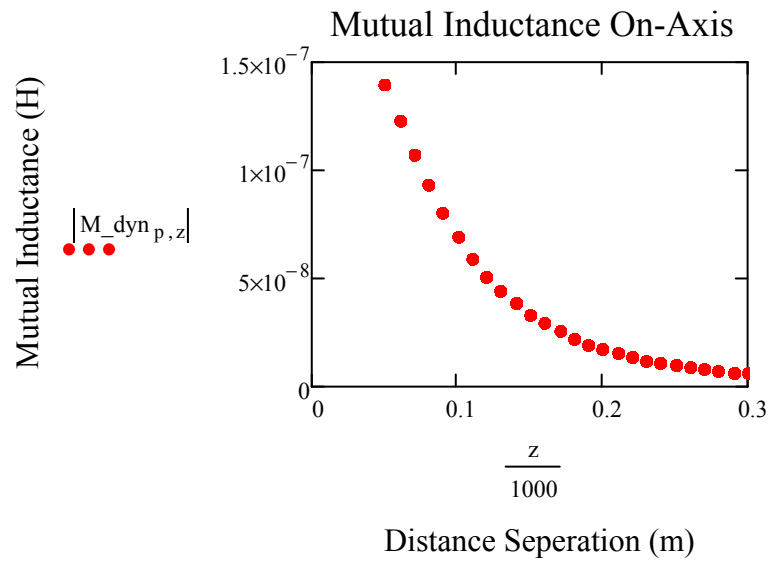
Flux: B-field components dotted with Unit Area components; All in spherical coordinates.

$$\Psi_{21_{p,z}} := (B_{r_{p,z}} \cdot dS_{-r_{p,z}} + B_{\theta_{p,z}} \cdot dS_{-\theta_{p,z}}) \cdot (\text{Member}_{p,z})$$

$$\mathbf{I}_1 = \blacksquare$$

$$M_{\text{dyn}}_{p,z} := \frac{\sum_{p=0}^{1599} \Psi_{21}_{p,z}}{1}$$

$$Z_{21\text{plot}}_{p,z} := j \cdot \omega \cdot M_{\text{dyn}}_{p,z}$$



$$Z_{21_z} := j \cdot \omega \cdot \frac{\sum_{p=0}^{1599} \Psi_{21}_{p,z}}{1}$$

Assume wire is copper Twin-Lead line (20 gauge): Diameter=0.812mm, Dist\_apart=7.5mm

$$\sigma := 5.8 \cdot 10^7 \quad \rho_{\text{cu}} := 1.724 \cdot 10^{-8}$$

Temperature coefficient per 1deg Celsius (Human temp ~ 37C):

$$\alpha := 4.29 \cdot 10^{-3} \quad \alpha_{37} := \alpha \cdot 37 \quad dR / R_s = \alpha \cdot dT, \quad dR = \text{change in resistance (ohm)}, \quad R_s = \text{standard resistance according, reference tables (ohm)}, \quad \alpha = \text{temperature coefficient of resistance, } dT = \text{change in temperature (K)}$$

$$dR_{37} := \alpha \cdot dT \cdot R_s \quad dR_{37} := \alpha_{37} \cdot \rho_{\text{cu}}$$

$$dR_{37} = 2.737 \times 10^{-9}$$

Large Loop Length:

$$L_{1g} := 2 \cdot \pi \cdot a$$

$$L_{1g} = 0.628$$

Second Loop Length:

$$L_{2nd} := 2 \cdot \pi \cdot b$$

$$L_{2nd} = 0.628$$

Skin Depth (Weeks p372): Surface Resistance (Weeks p373): Schelkunoff (p339)

$$\delta := \sqrt{\frac{2}{(2 \cdot \pi \cdot f) \cdot \mu_0 \cdot \sigma}} \quad R_s := \frac{1}{\sigma \cdot \delta} \quad R_{2s} := \sqrt{\frac{\pi \cdot f \cdot \mu_0}{\sigma}} \quad R_{3s} := 2.61 \cdot 10^{-7} \cdot \sqrt{f}$$

$$R_s = 2.609 \times 10^{-4} \quad R_{2s} = 2.609 \times 10^{-4} \quad R_{3s} = 2.61 \times 10^{-4}$$

Ramo uses Low-Frequency for ratios up to 1 (or lower), High Frequency calcs are > 1. Therefore, High Frequency resistance calculations are needed:

Radius of 20 awg wire:

$$r_{\text{cu20awg}} := 0.000406$$

$$\frac{r_{\text{cu20awg}}}{\delta} = 6.144$$

High Frequency (Ramo p182, Schelkunoff p339):

$$R_{\text{hf}} := \frac{R_s}{2 \cdot \pi \cdot r_{\text{cu20awg}}} \quad R_{\text{hf}} = 0.102 \quad \text{Units are } \Omega / \text{m}$$

$$R_{\text{hf}_{1st}} := R_{\text{hf}} \cdot (L_{1g}) + dR_{37}$$

$$R_{\text{hf}_{1st}} = 0.064$$

$$R_{\text{hf}_{2nd}} := R_{\text{hf}} \cdot (L_{2nd}) + dR_{37}$$

$$R_{\text{hf}_{2nd}} = 0.064$$

$$Z_L := 300$$

Clearly, the battery load (ZL) has significant impact on efficiency. If assumed 1 ohm, efficiency is very high !!!

The Total Mhos conductance may be found by taking the inverse of the total series resistance.

$$\sqrt{G_{lp1} := \frac{1}{R_{hf1st}}} \quad G_{lp1} = 15.562 \quad \sqrt{G_{lp2} := \frac{1}{R_{hf2nd}}} \quad G_{lp2} = 15.562$$

Use Schelkunoff Radiation conductance instead of Rrad

$$\lambda := \frac{2.99 \cdot 10^8}{f} \quad \lambda = 299$$

----- Magneto-Statics Capacitance of a small loop -----

(Schelkunoff p 321-322)

$$C_{av} := \frac{\pi \cdot \epsilon_0}{\log\left(\frac{b}{a}\right)} \quad \text{Average capacitance between two halves of loop per unit length along the circumference (Voltage distribution across loop).}$$

$$C_{loop} := \frac{1}{3} \cdot C_{av} \cdot b \cdot \pi \quad \text{Loop capacitance:}$$

$$C_{lp1} := \frac{\pi^2 \cdot \epsilon_0 \cdot a}{3 \cdot \ln\left(\frac{a}{r_{cu20awg}}\right)} \quad C_{lp1} = 5.287 \times 10^{-13} \quad \frac{1}{j \cdot \omega \cdot C_{lp1}} = -3.01i \times 10^5$$

$$C_{lp2} := \frac{\pi^2 \cdot \epsilon_0 \cdot b}{3 \cdot \ln\left(\frac{b}{r_{cu20awg}}\right)} \quad C_{lp2} = 5.287 \times 10^{-13}$$

----- Magneto Static Inductance (loop) -----

Internal inductance contribution (Balanis p245):

$$L_{i1} := \frac{a}{\omega \cdot r_{cu20awg}} \cdot \sqrt{\frac{\omega \cdot \mu_0}{2 \cdot \sigma}} \quad L_{i2} := \frac{b}{\omega \cdot r_{cu20awg}} \cdot \sqrt{\frac{\omega \cdot \mu_0}{2 \cdot \sigma}}$$

$$L_{i1} = 1.023 \times 10^{-8} \quad L_{i2} = 1.023 \times 10^{-8}$$

(Schelkunoff p 321) Small, single turn loop with substantially uniform current (approximate inductance).

$$L_{lp1} := \mu_0 \cdot a \cdot \ln\left(\frac{a}{r_{cu20awg}}\right) + L_{i1} \quad L_{lp1} = 7.022 \times 10^{-7} \quad j \cdot \omega \cdot L_{lp1} = 4.412i$$

$$L_{lp2} := \mu_0 \cdot b \cdot \ln\left(\frac{b}{r_{cu20awg}}\right) + L_{i2} \quad L_{lp2} = 7.022 \times 10^{-7}$$

Conductance - Using Ohmic resistance and the Radiation Resistance::  $\eta = 376.819$

$$G1 := \frac{3 \cdot \pi}{2\eta} \quad G1 = 0.013 \quad G2 := \frac{3 \cdot \pi}{2\eta} \quad G2 = 0.013$$

$$G1 := 320 \cdot \pi^4 \cdot \frac{(\pi \cdot a)^2}{\lambda^4} \quad G1 = 0.013 \quad G2 := G1 \quad G2 = 0.013$$

Admittance looking in on equivalent loop circuit, prematching capacitor:

$$Y_{pre1} := \frac{1 + \frac{j \cdot \omega \cdot C_{lp1}}{2} \cdot \left( j \cdot \omega \cdot L_{lp1} + \frac{1}{G_{lp1}} \right)}{j \cdot \omega \cdot L_{lp1} + \frac{1}{G_{lp1}}} + \frac{j \cdot \omega \cdot C_{lp1}}{2 + j \cdot \omega \cdot C_{lp1} \cdot \frac{1}{G1}} \quad Y_{pre1} = 3.3 \times 10^{-3} - 0.227i$$

$$Z_{pre1} := \frac{1}{Y_{pre1}} \quad Z_{pre1} = 0.064 + 4.412i$$

If we know:  $\frac{1}{\omega \cdot L_{eff}} := \omega \cdot C$

Then, the tuning capacitance is:

$$C_{tune} := \frac{1}{\omega^2 \cdot (L_{lp1})}$$

$$C_{tune} = 3.607 \times 10^{-8}$$

$$\frac{1}{i \cdot \omega \cdot C_{tune}} = -4.412i$$

Assume a variable capacitive element that can cancel the complex conjugate:

$$C_{match} := -\text{Im}(Z_{pre1}) \cdot i \quad C_{match} = -4.412i$$

The complex conjugate will add in Series in the Admittance(Impedance) model circuit.

$$Z_{11} := Z_{pre1} + C_{match} \quad Z_{11} = 0.064$$

$$Y_{in1} := \frac{1}{Z_{11}} \quad Y_{in1} = 15.561$$

Assume a battery Load and re-derive the equation need for modeling the admittance of the second loop. With Battery adding to the loading of the loop2, the Zin equation should change. Power calculation will have to be based on drop across battery loading, not just Ohmic resistance due to wire:

$$Y_{pre2} := \left[ \frac{1 + \frac{j \cdot \omega \cdot C_{lp2}}{2} \cdot \left( j \cdot \omega \cdot L_{lp2} + \frac{1}{G_{lp2}} \right)}{j \cdot \omega \cdot L_{lp2} + \frac{1}{G_{lp2}}} + \frac{j \cdot \omega \cdot C_{lp2}}{2 + j \cdot \omega \cdot C_{lp2} \cdot \frac{1}{G_2}} \right]$$

$$Y_{pre2} = 3.3 \times 10^{-3} - 0.227i$$

$$Z_{pre2} := \frac{1}{Y_{pre2}}$$

$$Z_{pre2} = 0.064 + 4.412i$$

Assume a variable capacitive element that can cancel the complex conjugate:

$$C_{match2} := -\text{Im}(Y_{pre2}) \cdot i \quad C_{match2} = 0.227i$$

$$C := \frac{L}{(R)^2 + \omega^2 \cdot L^2}$$

$$C_{ptune} := \frac{L_{lp2}}{(R_{hf2nd} + Z_L)^2 + \omega^2 \cdot L_{lp2}^2}$$

$$C_{ptune} = 7.797 \times 10^{-12}$$

The complex conjugate will add in Parallel in the Admittance model circuit.

$$Y_{in2} := (Y_{pre2} + C_{match2}) + \frac{1}{Z_L}$$

$$Y_{in2} = 6.634 \times 10^{-3}$$

$$Z_{22} := \frac{1}{Y_{in2}}$$

$$Z_{22} = 150.745$$

Now we have the following impedances of the system.

$$Z_{12_z} := Z_{21_z}$$

$$Z_{11} = 0.064$$

Mutual Z at 0.5 Radii  $Z_{21_{50}} = 3.783 \times 10^{-9} + 0.878i$

Mutual Z at 1.0 Radii  $Z_{21_{100}} = 3.783 \times 10^{-9} + 0.435i$

Mutual Z at 2.0 Radii  $Z_{21_{200}} = 3.783 \times 10^{-9} + 0.11i$



In the case of two loops in proximity, such that they can be modeled as a Linear Transducer. Loop1 and Loop2, each with two terminals for pos and neg bias. (Schelkunoff p291)

$$V_1 := Z_{11} \cdot I_1 + Z_{12} \cdot I_2$$

$$V_2 := Z_{21} \cdot I_1 + Z_{22} \cdot I_2$$

In matrix form:

$$\begin{pmatrix} V_1 \\ V_2 \end{pmatrix} := \begin{pmatrix} Z_{11} & Z_{12} \\ Z_{21} & Z_{22} \end{pmatrix} \cdot \begin{pmatrix} I_1 \\ I_2 \end{pmatrix}$$

For Admittance:

- Current at terminals are short circuited
- Y internal calc when all generators are open circuited.

Now, let D be:

$$D := (Z_{11} \cdot Z_{22} - Z_{12} \cdot Z_{21})$$

$$D_z := (Z_{11} \cdot Z_{22} - Z_{12}_z \cdot Z_{21}_z)$$

Next, we can solve the Matrix and re-write as such:

$$\begin{pmatrix} I_1 \\ I_2 \end{pmatrix} := \begin{pmatrix} \frac{Z_{22}}{D} & \frac{-Z_{12}}{D} \\ \frac{-Z_{21}}{D} & \frac{Z_{11}}{D} \end{pmatrix} \cdot \begin{pmatrix} V_1 \\ V_2 \end{pmatrix}$$

Writing current with respect to admittance gives us:

$$\begin{pmatrix} I_1 \\ I_2 \end{pmatrix} := \begin{pmatrix} Y_{11} & Y_{12} \\ Y_{21} & Y_{22} \end{pmatrix} \cdot \begin{pmatrix} V_1 \\ V_2 \end{pmatrix}$$

$$Y_{11}_z := \frac{Z_{22}}{D_z}$$

$$Y_{12}_z := \frac{-Z_{12}_z}{D_z}$$

$$Y_{21}_z := \frac{-Z_{21}_z}{D_z}$$

$$Y_{22}_z := \frac{Z_{11}}{D_z}$$

verification using Schelkunoff p 407:

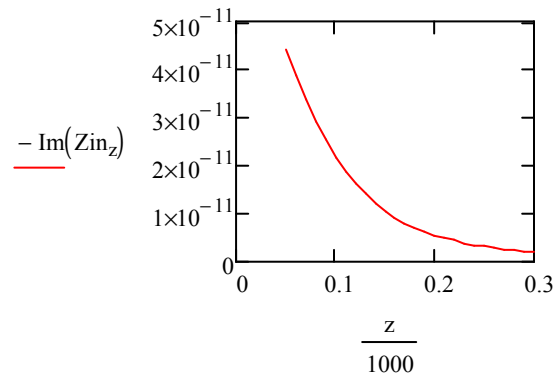
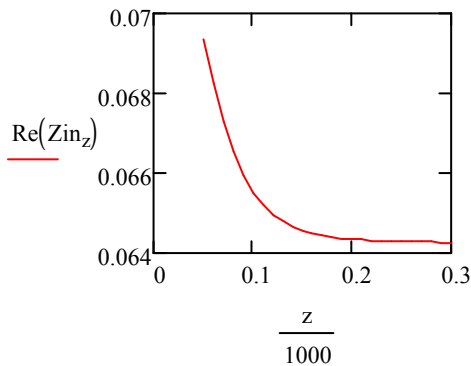
$$Y_{12b}_z := \frac{-Z_{12}_z}{Z_{11} \cdot Z_{22} - (Z_{12}_z)^2}$$

We will now assume a transmission line source will be connected to loop1, and then we can solve for I1 and V1

Assuming that loop 2 has a battery load we can solve the impedance matrix by "Collapsing a two-port to a one port network", and use this to calculate the reflection coefficient of the input terminal that the source will see. Then we will know V1 and I1 for power calculations:

ZinBy Schelkunoff:

$$Z_A := Z_{11} - \frac{Z_{12}^2}{Z_{22}} \quad Z_{in_z} := Z_{11} - \frac{(Z_{21_z})^2}{Z_{22}} \quad Z_{in2_z} := Z_{22} - \frac{(Z_{12_z})^2}{Z_{11}}$$



Impedance of the source matched to input of loop1, with loop2 at given distance:

$$Z_0 := \text{Re}(Z_{in_{50}}) + [-\text{Im}(Z_{in_{50}})i]$$

$$Z_0 = 0.069 + 4.406i \times 10^{-11}$$

And the reflection coefficient can now be seen as:

$$\Gamma_{\text{MZ}} := \frac{Z_{in_z} - Z_0}{Z_{in_z} + Z_0}$$

If the total voltage and current waves on the line can be written as :

$$V(x) := V_{\text{src}} \cdot (e^{-j \cdot \beta \cdot x} + \Gamma \cdot e^{j \cdot \beta \cdot x})$$

$$I(x) := \frac{V_{\text{src}}}{Z_0} \cdot (e^{-j \cdot \beta \cdot x} - \Gamma \cdot e^{j \cdot \beta \cdot x})$$

Since the distance of transmission line is nearly 0 (negligible), we can express the equations:

$$V_x := V_{\text{src}} \cdot (1 + \Gamma) \quad \text{and} \quad I_x := \frac{V_{\text{src}}}{Z_0} \cdot (1 - \Gamma)$$

Assume a source voltage:

$$V_{\text{src}} := 1$$

$$V1_z := V_{\text{src}} \cdot (1 + \Gamma_z) \quad \text{and, therefore} \quad I1_z := \frac{V_{\text{src}}}{Z_0} \cdot (1 - \Gamma_z)$$

Secondary loops is tuned in parallel, therefore we use expression.

$$V2_z := Z21_z \cdot I1_z$$

$$I2_z := Y21_z \cdot V1_z$$

Power Radiated (Schelkunoff Antennas p323):

NOTE: This is the power radiated by the primary loop antenna. Diaz stated to use Total Complex dipole moment of both antennas.

Power Radiated (Schelkunoff Antennas p323):

Loop 1 with 1amp assumed source:

$$\text{Prad1}_z := \frac{320 \pi^4 \cdot (\pi \cdot a^2)^2}{\lambda^4} \cdot \frac{(I1_z)^2}{2}$$

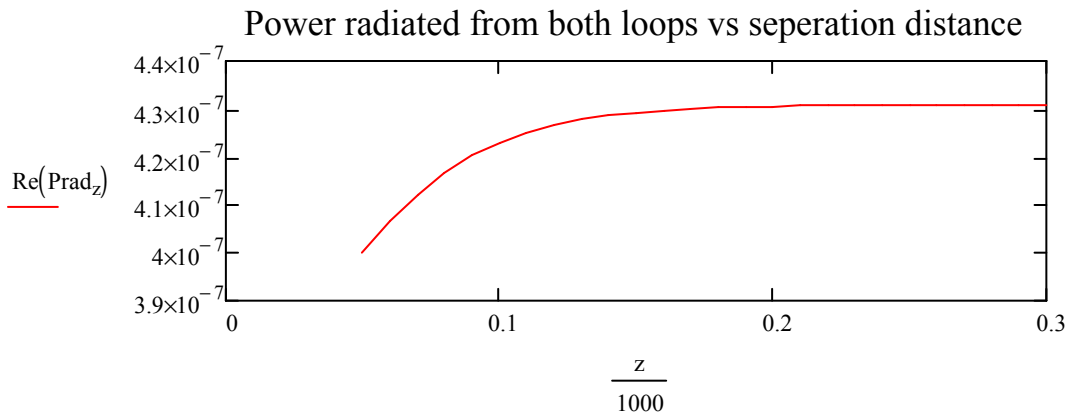
Loop 2 with calculated current (I2) using Linear Transducer Matrix:

$$\text{Prad2}_z := \frac{320 \pi^4 \cdot (\pi \cdot b^2)^2}{\lambda^4} \cdot \frac{(I2_z)^2}{2}$$

Total Complex Dipole Moment (Assuming they are so close and behave as one antenna):

$$I_{\text{tot}_z} := I1_z + I2_z$$

$$\text{Prad}_z := \frac{320 \pi^4 \cdot (\pi \cdot a^2)^2}{\lambda^4} \cdot \frac{(|I_{\text{tot}_z}|)^2}{2}$$



Series-Series Power due to copper at 1MHz:

Incident Power from  
Transmission Line Source

$$P_{inc_z} := \frac{(|V_{src}|)^2}{Re(Z_0)}$$

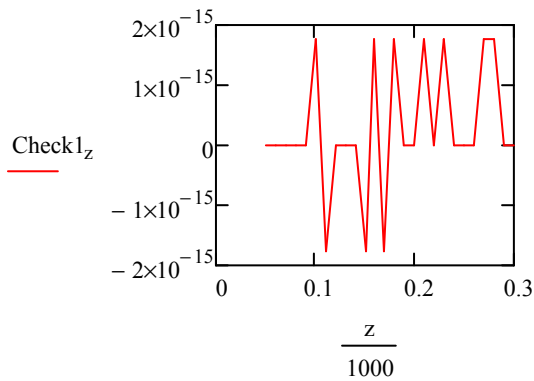
Reflected power to source

$$P_{refl_z} := \frac{(|V_{src}|)^2 \cdot (|\Gamma_z|)^2}{Re(Z_0)}$$

Power after reflection:

$$P_{tr_z} := \frac{(|V_{src}|)^2}{Re(Z_0)} \cdot [1 - (|\Gamma_z|)^2]$$

$$Check1_z := P_{inc_z} - P_{refl_z} - P_{tr_z}$$



## Power Calculations

Second loop is tuned in parallel, therefore power calcs are performed using following expressions.

$$P1ohm_z := \left( |I1_z| \right)^2 \cdot Z11$$

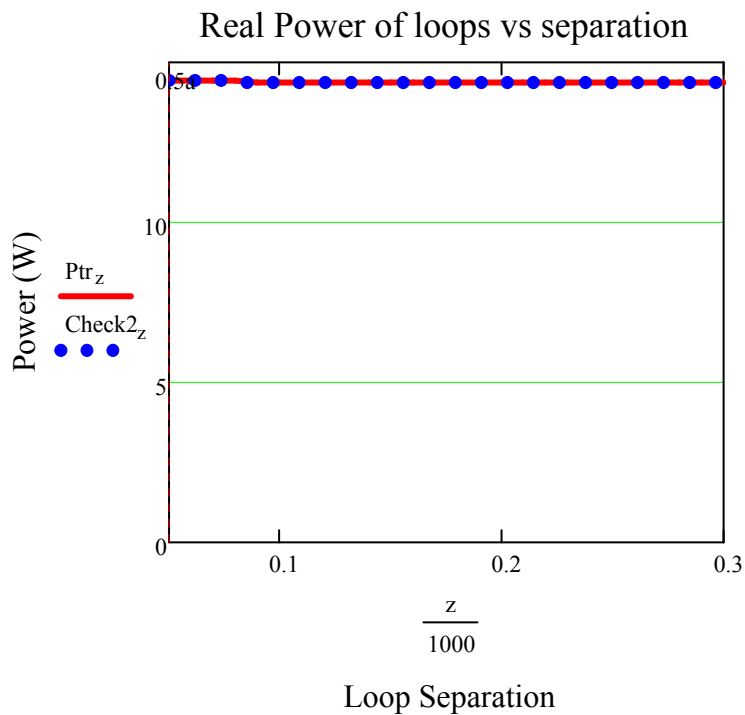
$$Pbatt_z := \frac{\left[ |V2_z| \cdot \left( \frac{Z_L}{Z22} \right) \right]^2}{Z_L}$$

$$P2res_z := \frac{\left[ |V2_z| \cdot \frac{(Z22 - Z_L)}{Z22} \right]^2}{Z22 - Z_L}$$

$$P2Volt_z := Pbatt_z + P2res_z$$

Compare power calculations to verify all Real Power is Accounted for in loop system:

$$Check2_z := P1ohm_z + Pbatt_z + P2res_z + Prad_z$$



$$Ptr_{50} = 14.415$$

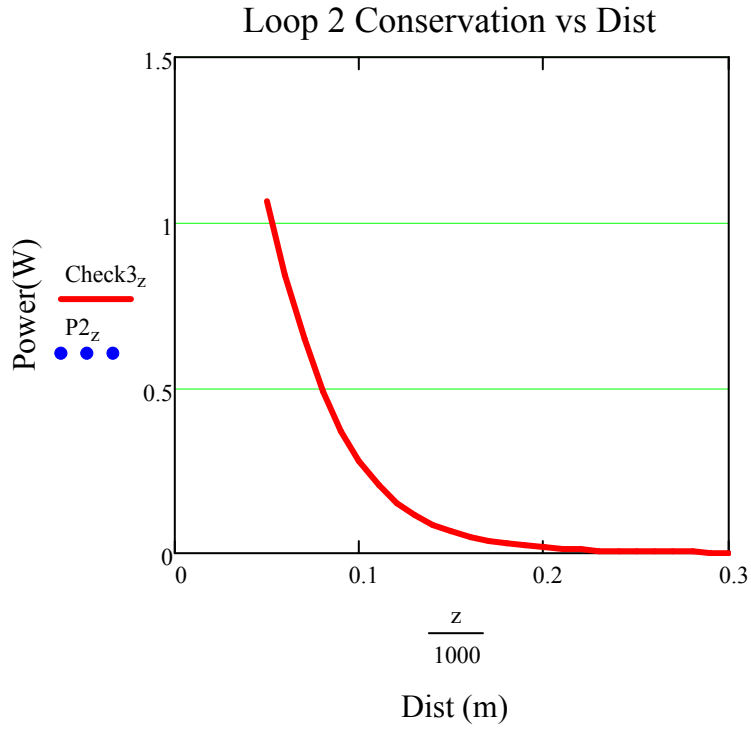
$$Pbatt_{50} = 2.114$$

$$Pbatt_{100} = 0.548$$

$$Pbatt_{200} = 0.036$$

Compare power calculations to verify all Real Power in Loop2 is Accounted for:

$$\text{Check3}_z := \text{Pbatt}_z + \text{P2res}_z$$

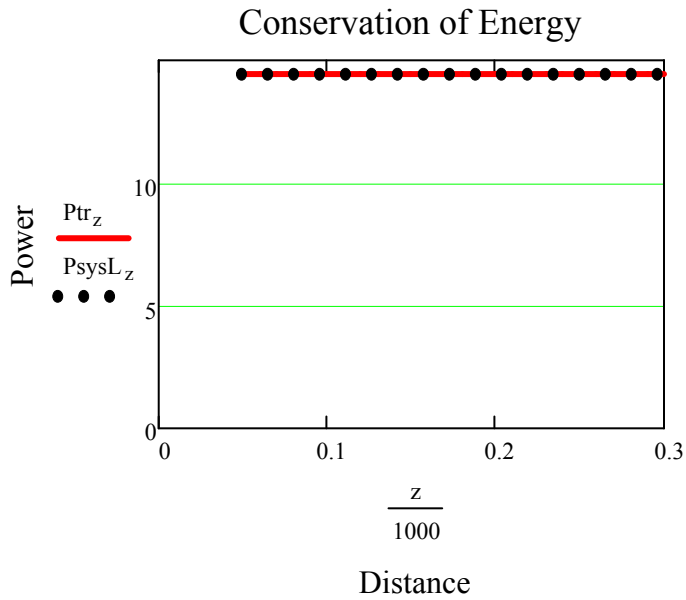


Check3<sub>z</sub> =

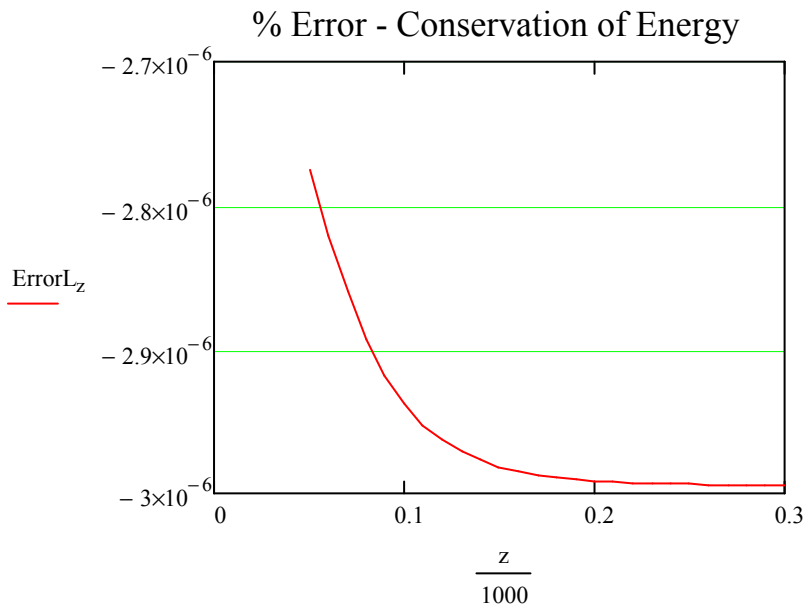
1.062
0.839
0.648
0.491
0.369
0.276
0.205
0.153
0.115
0.086
0.065
0.05
0.038
0.03
0.023
...

Compare power calculations of Matrix quantities and Copper Loss mechanisms to verify all Real Power is Accounted for:

$$P_{\text{sys}L_z} := (P_{1\text{ohm}_z}) + (P_{\text{batt}_z}) + (P_{2\text{res}_z}) + (P_{\text{rad}_z})$$



$$\text{Error}L_z := \left[ 1 - \frac{(P_{\text{sys}L_z})}{(P_{tr_z})} \right] \cdot 100$$



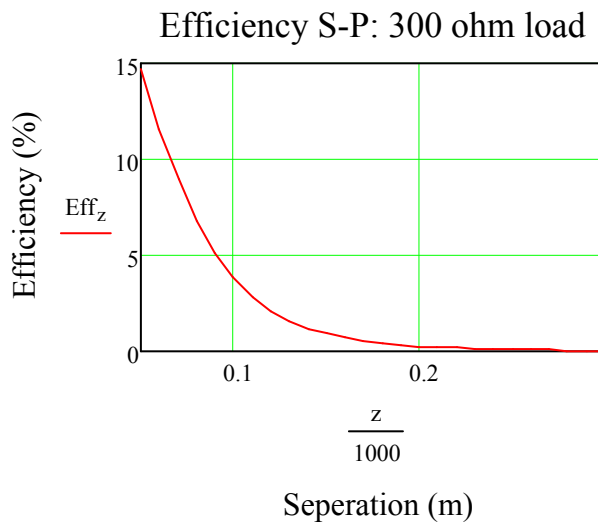
Let's see how much power at the source it requires for power to battery.

$$V_{\text{src}} = 1$$

$$\text{Eff}_z := \left( \frac{P_{\text{batt}_z}}{P_{\text{inc}_z}} \right) \cdot 100$$

$$\text{Eff}_z =$$

14.662
11.584
8.94
6.785
5.095
3.804
2.835
2.115
1.583
1.191
0.902
0.687
0.527
0.407
0.317
...



$$\text{Eff}_{50} = 14.662$$

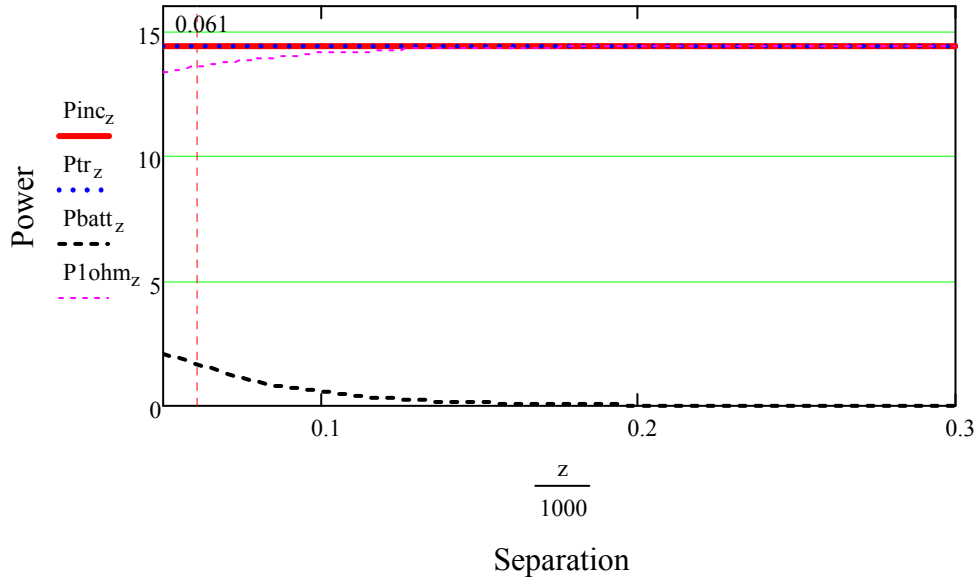
$$\text{Eff}_{100} = 3.804$$

$$\text{Eff}_{200} = 0.249$$

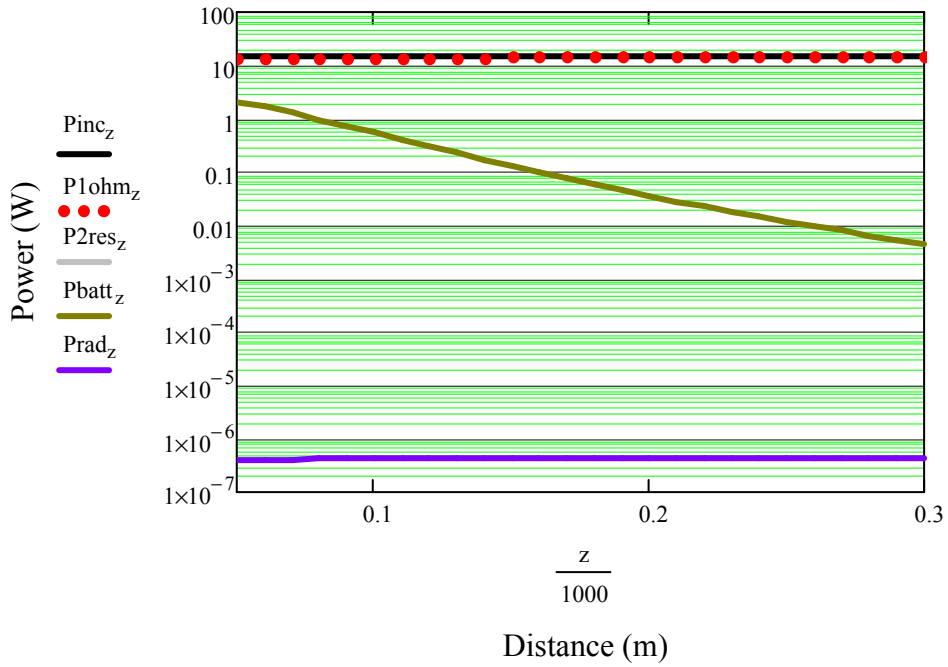
$$\text{Eff}_{300} = 0.031$$



S-P Match Source to Zin at Dist 0.5 Radius (1MHz)



Series-Parallel Power VS Separation (1MHz)



Coupling coefficient at half a radius (z=50):

For calculating equivalent circuit (NOTE must use Static Mutual and Self Inductances):

$$\text{If we know that: } M := k \cdot \sqrt{L_1 \cdot L_2} \quad M := 1.397 \cdot 10^{-7} \quad L_{p1} = 7.022 \times 10^{-7}$$

$$k := \frac{(M)}{\sqrt{L_{p1} \cdot L_{p2}}} \quad k = 0.199$$

#### Wireless Power Transfer Model: Parallel-Series

A wireless power transfer model for a two loops system was built. The tuning configuration consists of the first loop tuned in parallel for canceling reactance and the second loop tuned in series for canceling its reactance. Both loop reactance cancelation was performed assuming each loop was alone in free space.

By Duality and reference of RamoWhinnery, and Van Duzer (p.586) we can write the Magnetic field components of a magnetic dipole for Hr and Hθ , and express them here with the Magnetic Dipole Moment seen as ρ m.

$$\rho_m := I \cdot \pi \cdot a^2 \quad I := j \cdot \omega \cdot q \quad f := 1 \cdot 10^6 \quad \epsilon_r := 1 \quad \mu_0 := 4\pi \cdot 10^{-7} \quad \epsilon_0 := 8.85 \cdot 10^{-12}$$

$$\omega := 2 \cdot \pi \cdot (f)$$

Parallel - Series Program

$$\eta := \sqrt{\frac{\mu_0}{\epsilon_0 \cdot \epsilon_r}} \quad k_0 := \omega \cdot \sqrt{\mu_0 \cdot \epsilon_0 \cdot \epsilon_r} \quad k_0 = 0.021$$

Position of source as the center of the coordinate system (Cartesian):

$$x_{src} := 0 \quad y_{src} := 0 \quad z_{src} := 0$$

Radius of larger loop:  $a := 0.1$

Radius of equivalent loop:  $b := 0.1$

Unit Area dimensions:  
drop into equations after everything  
is  
working.

$$dx := \frac{a}{20} \quad dy := \frac{a}{20} \quad dz := 0$$

$$dx = 5 \times 10^{-3} \quad dy = 5 \times 10^{-3} \quad dz = 0$$

Position coordinates of  
loop observer (Large Loop).

$$x_{c\_obs} := 0$$

$$y_{c\_obs} := 0$$

$$z_{c\_obs} := 0$$

Planar from  $b+2 \cdot a$  to  $N \cdot b$ :  $N_x := 200$   $(b + 2a) = 0.3$   $N \cdot b = 200$

$$z := 50, 60.. 300$$

$$h_z := \frac{z}{1000}$$

Build a Raster Function :

$$p := 0.. 1595$$

Row:

Column:

$$m_p := \text{floor}\left(\frac{p}{40}\right) \quad n_p := p - (40 \cdot m_p)$$

Define the X and Y positions as observers for an 10 x 10 square mesh of loop (Add +/- a/10 for center square).

$$X_{obs_p} := \left( xc_{obs} - a + \frac{m_p}{199} + \frac{a}{80} \right)$$

$$Y_{obs_p} := \left( yc_{obs} + a - \frac{n_p}{199} - \frac{a}{80} \right)$$

$$Z_{obs_z} := -(h_z + zc_{obs})$$

R - distance from source to center of Observer loop:

$$R_{p,z} := \sqrt{(xsrc - X_{obs_p})^2 + (ysrc - Y_{obs_p})^2 + (zsrc - Z_{obs_z})^2}$$

This is an A-matrix for storing the positions of Unit Areas:

$$A_{p,z} := \sqrt{(X_{obs_p} - xc_{obs})^2 + (Y_{obs_p} - yc_{obs})^2}$$

Member of circle Matrix: Use the Heavyside step function to keep all Unit Area squares that compose the area of the Loop observer for a matrix that shapes the loop observer:

$$Member_{p,z} := \Phi(a - A_p)$$

$$\rho_m := \mathbf{I}_1 \cdot \pi \cdot b^2$$

$$B_{p,z}^{\theta} := \frac{j \cdot \omega \cdot \mu_0^2 \cdot l \cdot b^2}{4} \cdot e^{-j \cdot k_0 \cdot R_{p,z}} \cdot \left[ \frac{j \cdot \omega \cdot \epsilon_0 \cdot \epsilon_r}{R_{p,z}} + \frac{1}{\eta \cdot (R_{p,z})^2} + \frac{1}{j \cdot \omega \cdot \mu_0 \cdot (R_{p,z})^3} \right] \cdot \sqrt{1 - \left[ \frac{(zsrc - Z_{obs_z})}{R_{p,z}} \right]^2}$$

$$B_{p,z}^r := \frac{j \cdot \omega \cdot \mu_0^2 \cdot l \cdot b^2}{2} \cdot e^{-j \cdot k_0 \cdot R_{p,z}} \cdot \left[ \frac{1}{\eta \cdot (R_{p,z})^2} + \frac{1}{j \cdot \omega \cdot \mu_0 \cdot (R_{p,z})^3} \right] \cdot \frac{(zsrc - Z_{obs_z})}{R_{p,z}}$$

Unit Area defined:

$$dx = 5 \times 10^{-3} \quad dy = 5 \times 10^{-3} \quad dz = 0$$

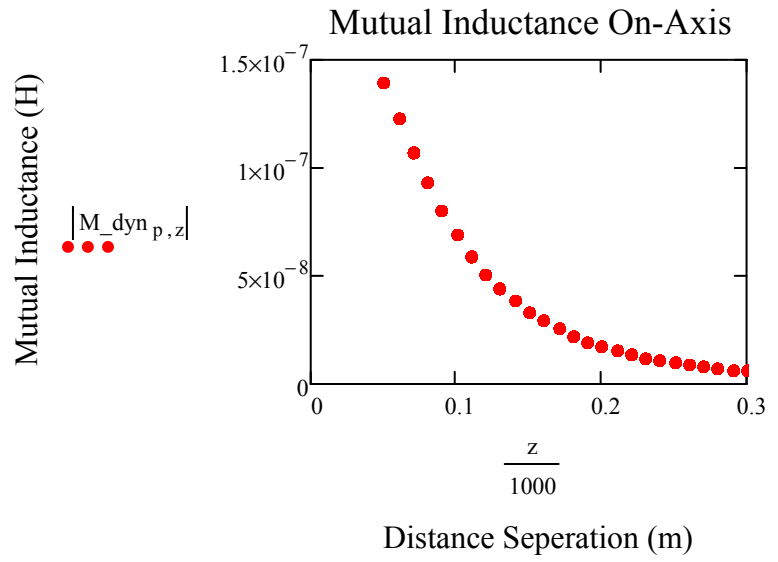
$$dS_z := dx \cdot dy$$

$$dS_{r,p,z} := dS_z \cdot \frac{(zsrc - Z_{obs_z})}{R_{p,z}} \quad dS_{\theta,p,z} := -dS_z \cdot \sqrt{1 - \left[ \frac{(zsrc - Z_{obs_z})}{R_{p,z}} \right]^2}$$

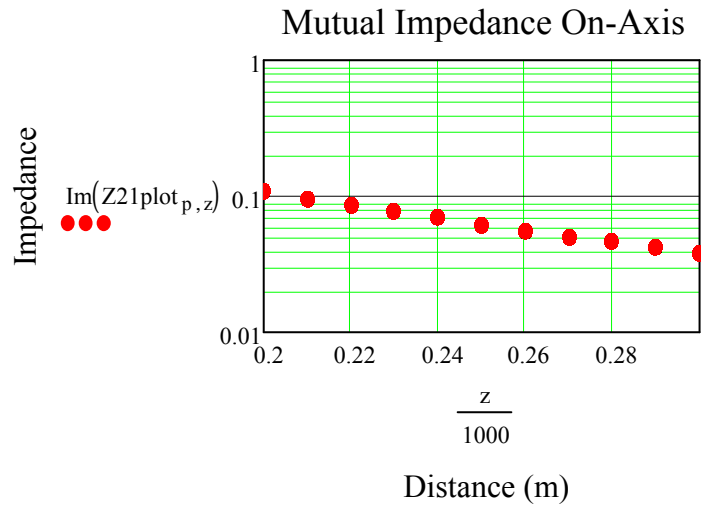
Flux: B-field components dotted with Unit Area components; All in spherical coordinates.

$$\Psi_{p,z}^{21} := (B_{p,z}^r \cdot dS_{r,p,z} + B_{p,z}^{\theta} \cdot dS_{\theta,p,z}) \cdot (Member_{p,z}) \quad \mathbf{I}_1 = \blacksquare$$

$$M_{\text{dyn}}_{p,z} := \frac{\sum_{p=0}^{1599} \Psi_{21}_{p,z}}{1}$$



$$Z_{21\text{plot}}_{p,z} := j \cdot \omega \cdot M_{\text{dyn}}_{p,z}$$



$$Z_{21_z} := j \cdot \omega \cdot \frac{\sum_{p=0}^{1599} \Psi_{21}_{p,z}}{1}$$

Assume wire is copper Twin-Lead line (20 gauge): Diameter=0.812mm, Dist\_apart=7.5mm

$$\sigma := 5.8 \cdot 10^7 \quad \rho_{\text{Cu}} := 1.724 \cdot 10^{-8}$$

Temperature coefficient per 1deg Celsius (Human temp ~ 37C):

$$\alpha := 4.29 \cdot 10^{-3} \quad \alpha_{37} := \alpha \cdot 37 \quad dR / R_s = \alpha \cdot dT, dR = \text{change in resistance (ohm)}, R_s = \text{standard resistance according, reference tables (ohm)}, \alpha = \text{temperature coefficient of resistance, } dT = \text{change in temperature (K)}$$

$$dR_{37} := \alpha \cdot dT \cdot R_s \quad dR_{37} := \alpha_{37} \rho_{\text{Cu}}$$

$$dR_{37} = 2.737 \times 10^{-9}$$

Large Loop Length:

$$L_{1g} := 2 \cdot \pi \cdot a$$

$$L_{1g} = 0.628$$

Second Loop Length:

$$L_{2nd} := 2 \cdot \pi \cdot b$$

$$L_{2nd} = 0.628$$

Skin Depth (Weeks p372): Surface Resistance (Weeks p373): Schelkunoff (p339)

$$\delta := \sqrt{\frac{2}{(2 \cdot \pi \cdot f) \cdot \mu_0 \cdot \sigma}} \quad R_s := \frac{1}{\sigma \cdot \delta} \quad R_{2s} := \sqrt{\frac{\pi \cdot f \cdot \mu_0}{\sigma}} \quad R_{3s} := 2.61 \cdot 10^{-7} \cdot \sqrt{f}$$

$$R_s = 2.609 \times 10^{-4} \quad R_{2s} = 2.609 \times 10^{-4} \quad R_{3s} = 2.61 \times 10^{-4}$$

Ramo uses Low-Frequency for ratios up to 1 (or lower), High Frequency calcs are > 1. Therefore, High Frequency resistance calculations are needed:

Radius of 20 awg wire:

$$r_{\text{Cu20awg}} := 0.000401$$

$$\frac{r_{\text{Cu20awg}}}{\delta} = 6.144$$

High Frequency (Ramo p182, Schelkunoff p339):

$$R_{\text{hf}} := \frac{R_s}{2 \cdot \pi \cdot r_{\text{Cu20awg}}} \quad R_{\text{hf}} = 0.102 \quad \text{Units are } \Omega / \text{m}$$

Clearly, the battery load (ZL) has significant impact on efficiency. If assumed 1 ohm, efficiency is very high !!!

Assume Ohmic resistance for loop1.

$$R_{\text{hf1st}} := R_{\text{hf}}(L_{1g}) + dR_{37}$$

$$R_{\text{hf1st}} = 0.064$$

$$R_{\text{hf2nd}} := R_{\text{hf}}(L_{2nd}) + dR_{37}$$

$$R_{\text{hf2nd}} = 0.064$$

$$Z_L := 300$$

The Total Mhos conductance may be found by taking the inverse of the total series resistance.

$$\sqrt{G_{lp1} := \frac{1}{Rhf_{1st}}} \quad G_{lp1} = 15.562 \quad \sqrt{G_{lp2} := \frac{1}{Rhf_{2nd}}} \quad G_{lp2} = 15.562$$

Use Schelkunoff Radiation conductance instead of Rrad

$$\lambda := \frac{2.99 \cdot 10^8}{f} \quad \lambda = 299$$

----- Magneto-Statics Capacitance of a small loop -----

(Schelkunoff p 321-322)

$$C_{av} := \frac{\pi \cdot \epsilon_0}{\log\left(\frac{b}{a}\right)} \quad \text{Average capacitance between two halves of loop per unit length along the circumference (Voltage distribution across loop).}$$

$$C_{loop} := \frac{1}{3} \cdot C_{av} \cdot b \cdot \pi \quad \text{Loop capacitance:}$$

$$C_{lp1} := \frac{\pi^2 \cdot \epsilon_0 \cdot a}{3 \cdot \ln\left(\frac{a}{r_{cu20awg}}\right)} \quad C_{lp1} = 5.287 \times 10^{-13} \quad \frac{1}{j \cdot \omega \cdot C_{lp1}} = -3.01i \times 10^5$$

$$C_{lp2} := \frac{\pi^2 \cdot \epsilon_0 \cdot b}{3 \cdot \ln\left(\frac{b}{r_{cu20awg}}\right)} \quad C_{lp2} = 5.287 \times 10^{-13}$$

----- Magneto Static Inductance (loop) -----

Internal inductance contribution (Balanis p245):

$$Li1 := \frac{a}{\omega \cdot r_{cu20awg}} \cdot \sqrt{\frac{\omega \cdot \mu_0}{2 \cdot \sigma}} \quad Li2 := \frac{b}{\omega \cdot r_{cu20awg}} \cdot \sqrt{\frac{\omega \cdot \mu_0}{2 \cdot \sigma}}$$

$$Li1 = 1.023 \times 10^{-8} \quad Li2 = 1.023 \times 10^{-8}$$

(Schelkunoff p 321) Small, single turn loop with substantially uniform current (approximate inductance).

$$L_{lp1} := \mu_0 \cdot a \cdot \ln\left(\frac{a}{r_{cu20awg}}\right) + Li1 \quad L_{lp1} = 7.022 \times 10^{-7} \quad j \cdot \omega \cdot L_{lp1} = 4.412i$$

$$L_{lp2} := \mu_0 \cdot b \cdot \ln\left(\frac{b}{r_{cu20awg}}\right) + Li2 \quad L_{lp2} = 7.022 \times 10^{-7}$$

Conductance - Using Ohmic resistance and the Radiation Resistance::  $\eta = 376.819$

$$G1 := \frac{3 \cdot \pi}{2\eta} \quad G1 = 0.013 \quad G2 := \frac{3 \cdot \pi}{2\eta} \quad G2 = 0.013$$

$$G1 := 320 \pi^4 \cdot \frac{(\pi \cdot a)^2}{\lambda^4} \quad G1 = 0.013 \quad G2 := G1 \quad G2 = 0.013$$

Admittance looking in on equivalent loop circuit, prematching capacitor:

$$Y_{pre1} := \frac{1 + \frac{j \cdot \omega \cdot C_{lp1}}{2} \cdot \left( j \cdot \omega \cdot L_{lp1} + \frac{1}{G_{lp1}} \right)}{j \cdot \omega \cdot L_{lp1} + \frac{1}{G_{lp1}}} + \frac{j \cdot \omega \cdot C_{lp1}}{2 + j \cdot \omega \cdot C_{lp1} \cdot \frac{1}{G1}} \quad Y_{pre1} = 3.3 \times 10^{-3} - 0.227i$$

$$Z_{pre1} := \frac{1}{Y_{pre1}} \quad Z_{pre1} = 0.064 + 4.412i$$

Assume a variable capacitive element that can cancel the complex conjugate:

$$C_{match} := -\text{Im}(Y_{pre1}) \cdot i \quad C_{match} = 0.227i$$

The complex conjugate will add in Parallel in the Admittance(Impedance) model circuit.

$$Y_{in1} := Y_{pre1} + C_{match} \quad Y_{in1} = 3.3 \times 10^{-3}$$

$$Z_{11} := \frac{1}{Y_{in1}} \quad Z_{11} = 302.997$$

$$C := \frac{L}{(R)^2 + \omega^2 \cdot L^2}$$

$$C_{ptune} := \frac{L_{lp2}}{(R_{hf1st})^2 + \omega^2 \cdot L_{lp2}^2}$$

$$C_{ptune} = 3.606 \times 10^{-8}$$



$$Y_{pre2} := \left[ \frac{1 + \frac{j \cdot \omega \cdot C_{lp2}}{2} \cdot \left( j \cdot \omega \cdot L_{lp2} + \frac{1}{G_{lp2}} \right)}{j \cdot \omega \cdot L_{lp2} + \frac{1}{G_{lp2}}} + \frac{j \cdot \omega \cdot C_{lp2}}{2 + j \cdot \omega \cdot C_{lp2} \cdot \frac{1}{G_2}} \right]$$

$$Y_{pre2} = 3.3 \times 10^{-3} - 0.227i$$

$$Z_{pre2} := \frac{1}{Y_{pre2}}$$

$$Z_{pre2} = 0.064 + 4.412i$$

Assume a variable capacitive element that can cancel the complex conjugate:

$$C_{match2} := -\text{Im}(Z_{pre2}) \cdot i \quad C_{match2} = -4.412i$$

The complex conjugate will add in Series in the Admittance model circuit.

ASSUMPTION: After the Loop has been matched (since battery R changes with charging), then we can add the load to Z22.

$$Z_{22} := (Z_{pre2} + C_{match2}) + Z_L$$

$$Z_{22} = 300.064$$

$$Y_{in2} := \frac{1}{Z_{22}}$$

$$Y_{in2} = 3.333 \times 10^{-3}$$

Now we have the following impedances of the system.

$$Z_{12} := Z_{21}$$

$$Z_{11} = 302.997$$

If we know:

$$\omega := \frac{1}{\sqrt{L \cdot C}}$$

Then, the tuning capacitance is:

$$C_{tune} := \left[ \frac{1}{\omega^2 \cdot (L_{lp2})} \right]$$

$$C_{tune} = 3.607 \times 10^{-8}$$

Mutual Z at 0.5 Radii  $Z_{21}_{50} = 3.783 \times 10^{-9} + 0.878i$

Mutual Z at 1.0 Radii  $Z_{21}_{100} = 3.783 \times 10^{-9} + 0.435i$

Mutual Z at 2.0 Radii  $Z_{21}_{200} = 3.783 \times 10^{-9} + 0.11i$

In the case of two loops in proximity, such that they can be modeled as a Linear Transducer. Loop1 and Loop2, each with two terminals for pos and neg bias. (Schelkunoff p291)

$$V_1 := Z_{11} \cdot I_1 + Z_{12} \cdot I_2$$

$$V_2 := Z_{21} \cdot I_1 + Z_{22} \cdot I_2$$

In matrix form:

$$\begin{pmatrix} V_1 \\ V_2 \end{pmatrix} := \begin{pmatrix} Z_{11} & Z_{12} \\ Z_{21} & Z_{22} \end{pmatrix} \cdot \begin{pmatrix} I_1 \\ I_2 \end{pmatrix}$$

For Admittance:

- Current at terminals are short circuited
- Yinternalcalc when all generators are open circuited.

Now, let D be:

$$D := (Z_{11} \cdot Z_{22} - Z_{12} \cdot Z_{21})$$

$$D_z := (Z_{11} \cdot Z_{22} - Z_{12}_z \cdot Z_{21}_z)$$

Next, we can solve the Matrix and re-write as such:

$$\begin{pmatrix} I_1 \\ I_2 \end{pmatrix} := \begin{pmatrix} \frac{Z_{22}}{D} & \frac{-Z_{12}}{D} \\ \frac{-Z_{21}}{D} & \frac{Z_{11}}{D} \end{pmatrix} \cdot \begin{pmatrix} V_1 \\ V_2 \end{pmatrix}$$

Writing current with respect to admittance gives us:

$$\begin{pmatrix} I_1 \\ I_2 \end{pmatrix} := \begin{pmatrix} Y_{11} & Y_{12} \\ Y_{21} & Y_{22} \end{pmatrix} \cdot \begin{pmatrix} V_1 \\ V_2 \end{pmatrix}$$

$$Y_{11}_z := \frac{Z_{22}}{D_z}$$

$$Y_{12}_z := \frac{-Z_{12}_z}{D_z}$$

$$Y_{21}_z := \frac{-Z_{21}_z}{D_z}$$

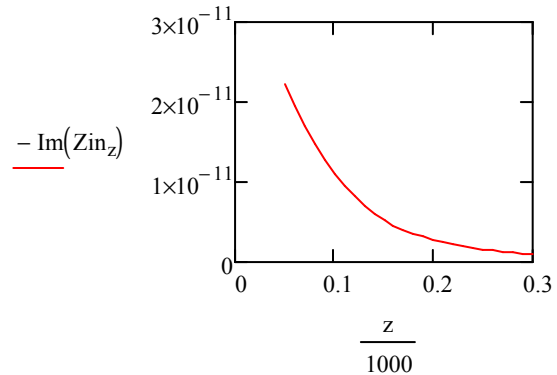
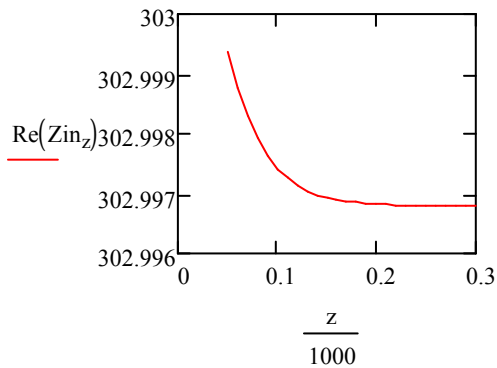
$$Y_{22}_z := \frac{Z_{11}}{D_z}$$

We will now assume a transmission line source will be connected to loop1, and then we can solve for I1 and V1

Assuming that loop 2 has a battery load we can solve the impedance matrix by "Collapsing a two-port to a one port network", and use this to calculate the reflection coefficient of the input terminal that the source will see. Then we will know V1 and I1 for power calculations:

ZinBy Schelkunoff:

$$Z_A := Z_{11} - \frac{Z_{12}^2}{Z_{22}} \quad Z_{in_z} := Z_{11} - \frac{(Z_{21_z})^2}{Z_{22}} \quad Z_{in2_z} := Z_{22} - \frac{(Z_{12_z})^2}{Z_{11}}$$



Impedance of the source matched to input of loop1, with loop2 at given distance:

$$Z_0 := \text{Re}(Z_{in_{50}}) + j \cdot \text{Im}(Z_{in_{50}}) \quad \text{Re}(Z_0) = 302.999$$

And the reflection coefficient can now be seen as:

$$\Gamma_z := \frac{Z_{in_z} - Z_0}{Z_{in_z} + Z_0}$$

If the total voltage and current waves on the line can be written as :

$$V(x) := V_{src} \cdot (e^{-j \cdot \beta \cdot x} + \Gamma \cdot e^{j \cdot \beta \cdot x}) \quad I(x) := \frac{V_{src}}{Z_0} \cdot (e^{-j \cdot \beta \cdot x} - \Gamma \cdot e^{j \cdot \beta \cdot x})$$

Since the distance of transmission line is nearly 0 (negligible), we can express the equations:

$$V_x := V_{\text{src}} \cdot (1 + \Gamma) \quad \text{and} \quad I_x := \frac{V_{\text{src}}}{Z_0} \cdot (1 - \Gamma)$$

Assume a source voltage:

$$V_{\text{src}} := 1$$

$$V1_z := V_{\text{src}} \cdot (1 + \Gamma_z) \quad \text{and, therefore} \quad I1_z := \frac{V_{\text{src}}}{Z_0} \cdot (1 - \Gamma_z)$$

$$V2_z := Z21_z \cdot I1_z$$

$$I2_z := Y21_z \cdot V1_z$$

Power Radiated (Schelkunoff Antennas p323):

NOTE: This is the power radiated by the primary loop antenna. Diaz stated to use Total Complex dipole moment of both antennas.

Power Radiated (Schelkunoff Antennas p323):

Loop 1 with 1 amp assumed source:

$$\text{Prad1}_z := \frac{320 \pi^4 \cdot (\pi \cdot a^2)^2 \cdot (I1_z)^2}{\lambda^4 \cdot 2}$$

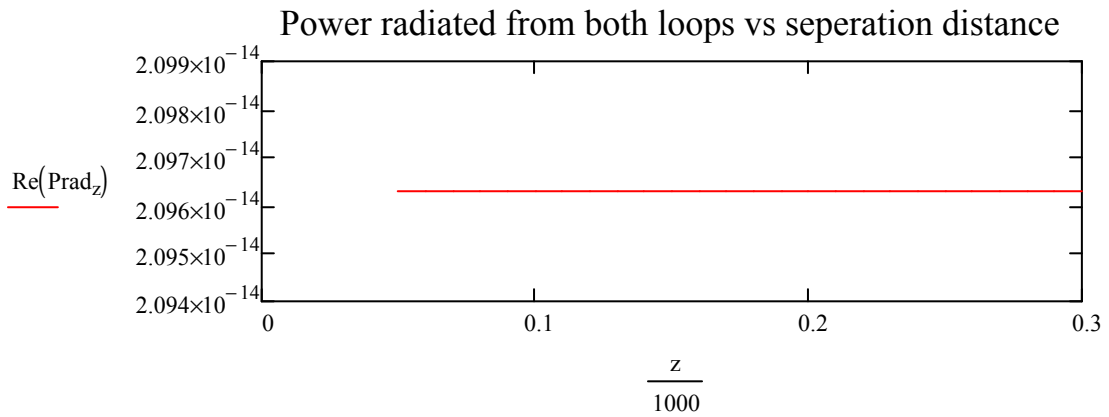
Loop 2 with calculated current (I2) using Linear Transducer Matrix:

$$\text{Prad2}_z := \frac{320 \pi^4 \cdot (\pi \cdot b^2)^2 \cdot (I2_z)^2}{\lambda^4 \cdot 2}$$

Total Complex Dipole Moment (Assuming they are so close and behave as one antenna):

$$I_{\text{tot}_z} := I1_z + I2_z$$

$$\text{Prad}_z := \frac{320 \pi^4 \cdot (\pi \cdot a^2)^2 \cdot (|I_{\text{tot}_z}|)^2}{\lambda^4 \cdot 2}$$



Series-Series Power due to copper at 1MHz:

Incident Power from  
Transmission Line Source

$$P_{inc_z} := \frac{(|V_{src}|)^2}{Re(Z_0)}$$

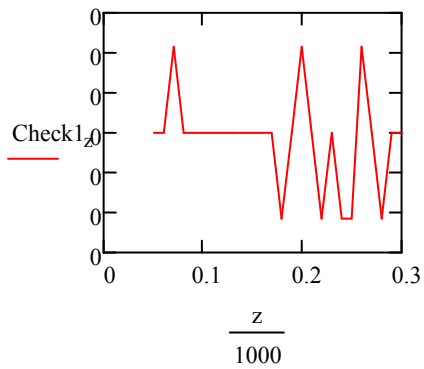
Reflected power to source

$$P_{refl_z} := \frac{(|V_{src}|)^2 \cdot (|\Gamma_z|)^2}{Re(Z_0)}$$

Power after reflection:

$$P_{tr_z} := \frac{(|V_{src}|)^2}{Re(Z_0)} \cdot [1 - (|\Gamma_z|)^2]$$

$$Check1_z := P_{inc_z} - P_{refl_z} - P_{tr_z}$$



Power Calculations broken up according to Copper loading:

Second loop is tuned in parallel, therefore power calcs are performed using following expressions.

$$P1ohm_z := \frac{\left( |V1_z| \cdot \frac{Z11}{\text{Re}(Zin_z)} \right)^2}{Z11}$$

$$P2Rbatt_z := \left( |I2_z| \right)^2 \cdot Z_L$$

$$P2ohm_z := \left( |I2_z| \right)^2 \cdot Rhf_{2nd}$$

$$Pbatt_z := \frac{\left[ |Z21_z \cdot I1_z| \cdot \left( \frac{Z_L}{Z_L + Rhf_{2nd}} \right) \right]^2}{Z_L}$$

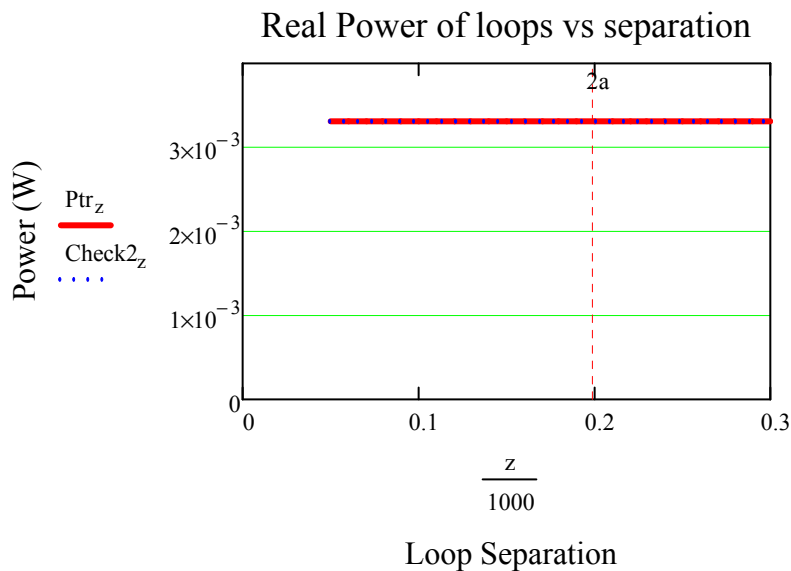
$$P2res_z := \frac{\left[ |Z21_z \cdot I1_z| \cdot \left( \frac{Rhf_{2nd}}{Rhf_{2nd} + Z_L} \right) \right]^2}{Rhf_{2nd}}$$

$$P2Volt_z := Pbatt_z + P2res_z$$

$$P2_z := \left( |I2_z| \right) \cdot |V2_z|$$

Compare power calculations to verify all Real Power is Accounted for in loop system:

$$Check2_z := P1ohm_z + Pbatt_z + P2res_z + Prad_z$$



$$Ptr_{50} = 3.3 \times 10^{-3}$$

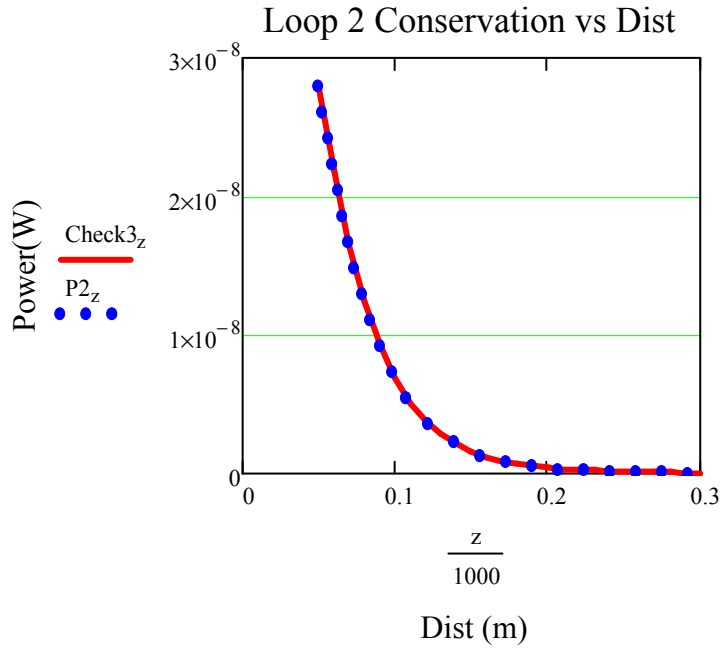
$$P2Rbatt_{50} = 2.796 \times 10^{-8}$$

$$P2Rbatt_{100} = 6.856 \times 10^{-9}$$

$$P2Rbatt_{200} = 4.407 \times 10^{-10}$$

Compare power calculations to verify all Real Power in Loop2 is Accounted for:

$$\text{Check3}_z := \text{Pbatt}_z + \text{P2res}_z$$



Check3<sub>z</sub> =

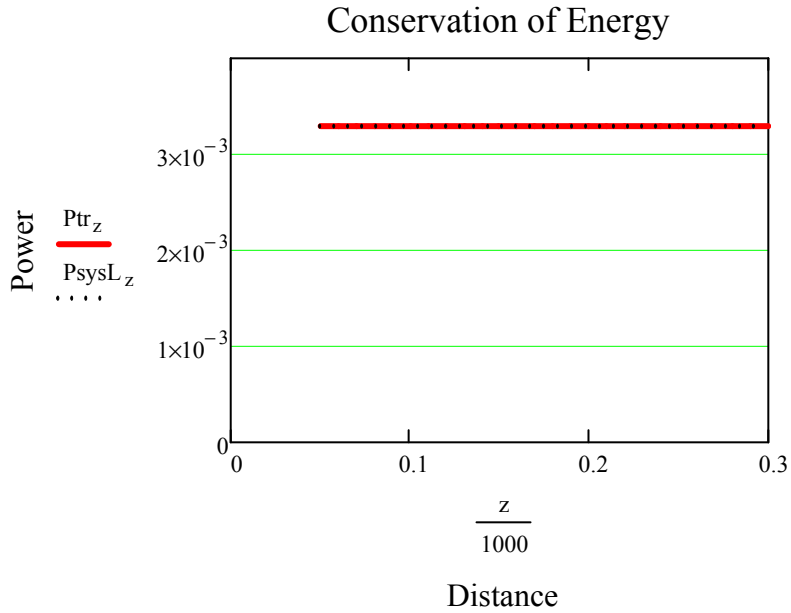
2.797·10 <sup>-8</sup>
2.174·10 <sup>-8</sup>
1.654·10 <sup>-8</sup>
1.242·10 <sup>-8</sup>
9.245·10 <sup>-9</sup>
6.857·10 <sup>-9</sup>
5.086·10 <sup>-9</sup>
3.781·10 <sup>-9</sup>
2.823·10 <sup>-9</sup>
2.12·10 <sup>-9</sup>
1.602·10 <sup>-9</sup>
1.22·10 <sup>-9</sup>
9.352·10 <sup>-10</sup>
7.224·10 <sup>-10</sup>
5.622·10 <sup>-10</sup>
...

P2<sub>z</sub> =

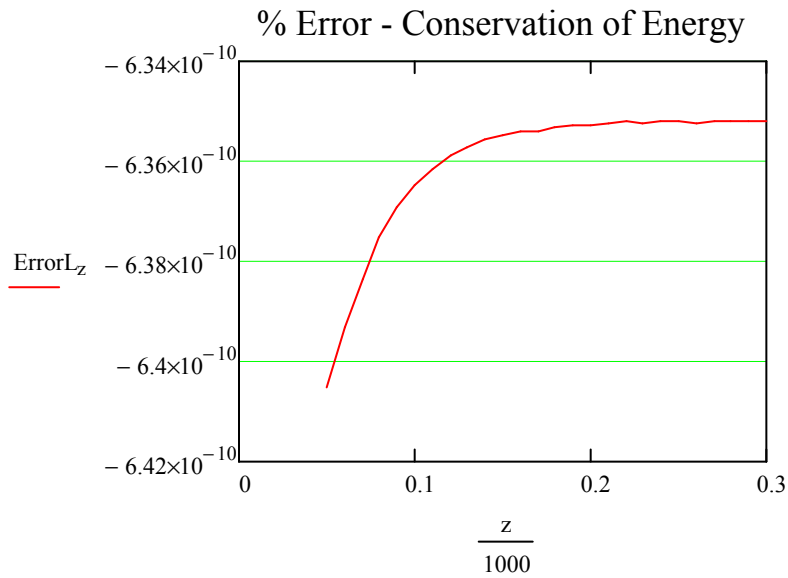
2.797·10 <sup>-8</sup>
2.174·10 <sup>-8</sup>
1.654·10 <sup>-8</sup>
1.242·10 <sup>-8</sup>
9.245·10 <sup>-9</sup>
6.857·10 <sup>-9</sup>
5.086·10 <sup>-9</sup>
3.781·10 <sup>-9</sup>
2.823·10 <sup>-9</sup>
2.12·10 <sup>-9</sup>
1.602·10 <sup>-9</sup>
1.22·10 <sup>-9</sup>
9.352·10 <sup>-10</sup>
7.224·10 <sup>-10</sup>
5.622·10 <sup>-10</sup>
...

Compare power calculations of Matrix quantities and Copper Loss mechanisms to verify all Real Power is Accounted for:

$$P_{\text{sys}L_z} := (P_{1\text{ohm}_z}) + (P_{\text{batt}_z}) + (P_{2\text{res}_z}) + (P_{\text{rad}_z})$$



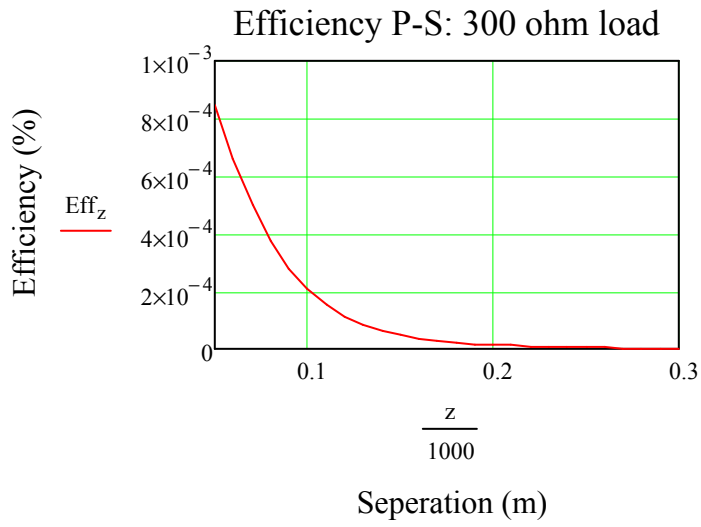
$$\text{Error}L_z := \left[ 1 - \frac{(P_{\text{sys}L_z})}{(P_{\text{tr}_z})} \right] \cdot 100$$





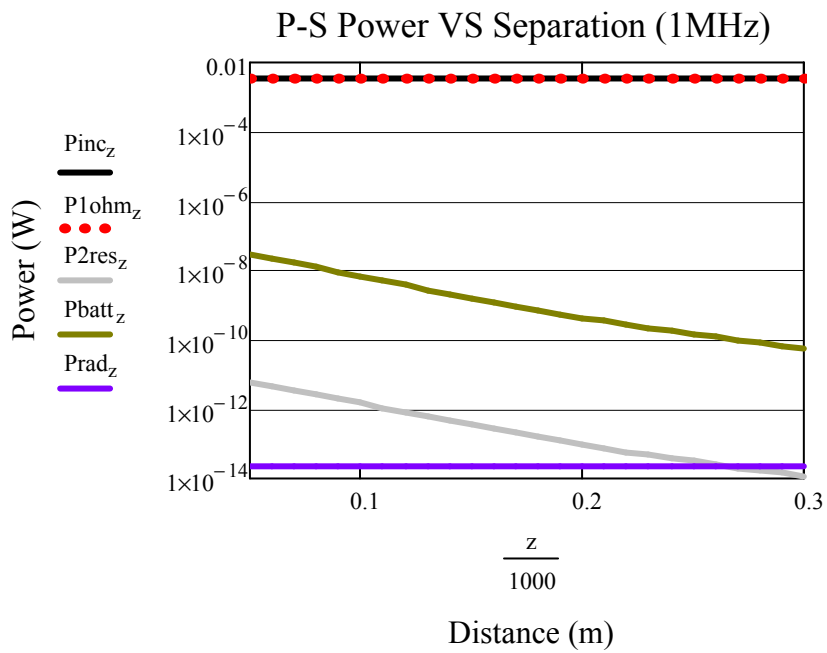
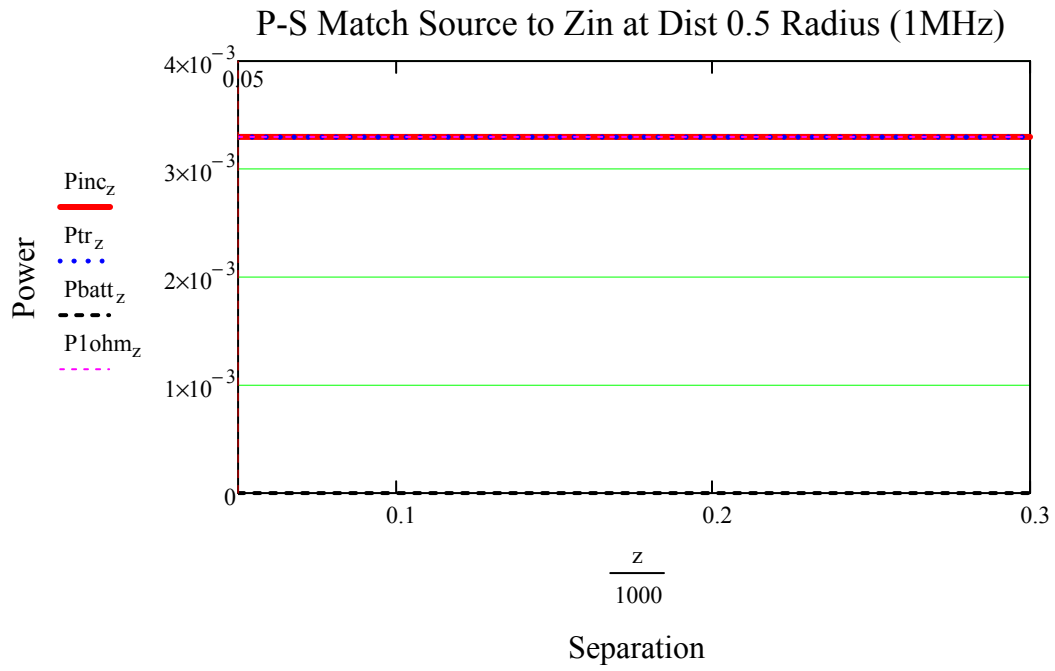
Let's see how much power at the source it requires for power to battery.

$$V_{\text{src}} = 1 \quad \text{Eff}_z := \left( \frac{P_{\text{batt}_z}}{P_{\text{inc}_z}} \right) \cdot 100$$



$$\text{Eff}_z =$$

$8.472 \cdot 10^{-4}$
$6.585 \cdot 10^{-4}$
$5.012 \cdot 10^{-4}$
$3.762 \cdot 10^{-4}$
$2.8 \cdot 10^{-4}$
$2.077 \cdot 10^{-4}$
$1.541 \cdot 10^{-4}$
$1.145 \cdot 10^{-4}$
$8.553 \cdot 10^{-5}$
$6.423 \cdot 10^{-5}$
$4.854 \cdot 10^{-5}$
$3.695 \cdot 10^{-5}$
$2.833 \cdot 10^{-5}$
$2.188 \cdot 10^{-5}$
$1.703 \cdot 10^{-5}$
...



Coupling coefficient at half a radius (z=50):

For calculating equivalent circuit (NOTE must use Static Mutual and Self Inductances):

$$\text{If we know that: } M := k \cdot \sqrt{L_1 \cdot L_2} \quad M := 1.397 \cdot 10^{-7} \quad L_{p1} = 7.022 \times 10^{-7}$$

$$k := \frac{(M)}{\sqrt{L_{p1} \cdot L_{p2}}} \quad k = 0.199$$

#### Wireless Power Transfer Model: Parallel-Parallel

A wireless power transfer model for a two loops system was built. The tuning configuration consists of the first loop tuned in parallel for canceling reactance and the second loop tuned in parallel for canceling its reactance. Both loop reactance cancelation was performed assuming each loop was alone in free space.

By Duality and reference of RamoWhinnery, and Van Duzer (p.586) we can write the Magnetic field components of a magnetic dipole for Hr and Hθ , and express them here with the Magnetic Dipole Moment seen as ρ m.

$$\rho_m := I \cdot \pi \cdot a^2 \quad I := j \cdot \omega \cdot q \quad f := 1 \cdot 10^6 \quad \epsilon_r := 1 \quad \mu_0 := 4\pi \cdot 10^{-7} \quad \epsilon_0 := 8.85 \cdot 10^{-12}$$

$$\omega := 2 \cdot \pi \cdot (f)$$

Parallel - Parallel Program

$$\eta := \sqrt{\frac{\mu_0}{\epsilon_0 \cdot \epsilon_r}} \quad k_0 := \omega \cdot \sqrt{\mu_0 \cdot \epsilon_0 \cdot \epsilon_r} \quad k_0 = 0.021$$

Position of source as the center of the coordinate system (Cartesian):

$$x_{src} := 0 \quad y_{src} := 0 \quad z_{src} := 0$$

Radius of larger loop:  $a := 0.1$

Radius of equivalent loop:  $b := 0.1$

Unit Area dimensions:  
drop into equations after everything  
is  
working.

$$dx := \frac{a}{20} \quad dy := \frac{a}{20} \quad dz := 0$$

$$dx = 5 \times 10^{-3} \quad dy = 5 \times 10^{-3} \quad dz = 0$$

Position coordinates of  
loop observer (Large Loop).

$$x_{c\_obs} := 0$$

$$y_{c\_obs} := 0$$

$$z_{c\_obs} := 0$$

Planar from  $b+2 \cdot a$  to  $N \cdot b$ :  $N_x := 200$   $(b + 2a) = 0.3$   $N \cdot b = 200$

$$z := 50, 60 \dots 400$$

$$h_z := \frac{z}{1000}$$

Build a Raster Function :

$$p := 0 \dots 1595$$

Row:

Column:

$$m_p := \text{floor}\left(\frac{p}{40}\right) \quad n_p := p - (40 \cdot m_p)$$

Define the X and Y positions as observers for an 10 x 10 square mesh of loop (Add +/- a/10 for center square).

$$X_{obs_p} := \left( xc_{obs} - a + \frac{m_p}{199} + \frac{a}{80} \right)$$

$$Y_{obs_p} := \left( yc_{obs} + a - \frac{n_p}{199} - \frac{a}{80} \right)$$

$$Z_{obs_z} := -(h_z + zc_{obs})$$

R - distance from source to center of Observer loop:

$$R_{p,z} := \sqrt{(xsrc - X_{obs_p})^2 + (ysrc - Y_{obs_p})^2 + (zsrc - Z_{obs_z})^2}$$

This is an A-matrix for storing the positions of Unit Areas:

$$A_{p,z} := \sqrt{(X_{obs_p} - xc_{obs})^2 + (Y_{obs_p} - yc_{obs})^2}$$

Member of circle Matrix: Use the Heavyside step function to keep all Unit Area squares that compose the area of the Loop observer for a matrix that shapes the loop observer:

$$Member_{p,z} := \Phi(a - A_p) \quad \rho_m := \mathbf{I}_1 \cdot \pi \cdot b^2$$

$$B\theta_{p,z} := \frac{j \cdot \omega \cdot \mu_0^2 \cdot 1 \cdot b^2}{4} \cdot e^{-j \cdot k_0 \cdot R_{p,z}} \cdot \left[ \frac{j \cdot \omega \cdot \epsilon_0 \cdot \epsilon_r}{R_{p,z}} + \frac{1}{\eta \cdot (R_{p,z})^2} + \frac{1}{j \cdot \omega \cdot \mu_0 \cdot (R_{p,z})^3} \right] \cdot \sqrt{1 - \left[ \frac{(zsrc - Z_{obs_z})}{R_{p,z}} \right]^2}$$

$$Br_{p,z} := \frac{j \cdot \omega \cdot \mu_0^2 \cdot 1 \cdot b^2}{2} \cdot e^{-j \cdot k_0 \cdot R_{p,z}} \cdot \left[ \frac{1}{\eta \cdot (R_{p,z})^2} + \frac{1}{j \cdot \omega \cdot \mu_0 \cdot (R_{p,z})^3} \right] \cdot \frac{(zsrc - Z_{obs_z})}{R_{p,z}}$$

Unit Area defined:

$$dx = 5 \times 10^{-3} \quad dy = 5 \times 10^{-3} \quad dz = 0$$

$$dS_z := dx \cdot dy$$

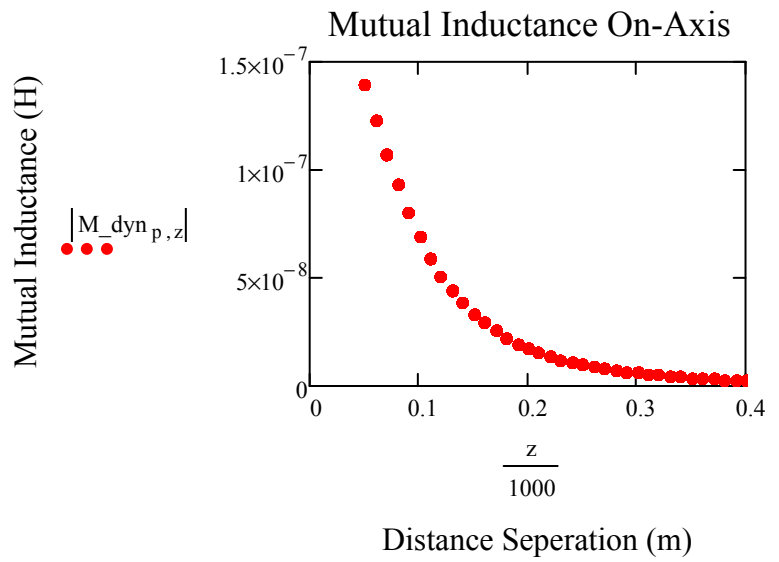
$$dS_{-r_{p,z}} := dS_z \cdot \frac{(zsrc - Z_{obs_z})}{R_{p,z}}$$

$$dS_{-\theta_{p,z}} := -dS_z \cdot \sqrt{1 - \left[ \frac{(zsrc - Z_{obs_z})}{R_{p,z}} \right]^2}$$

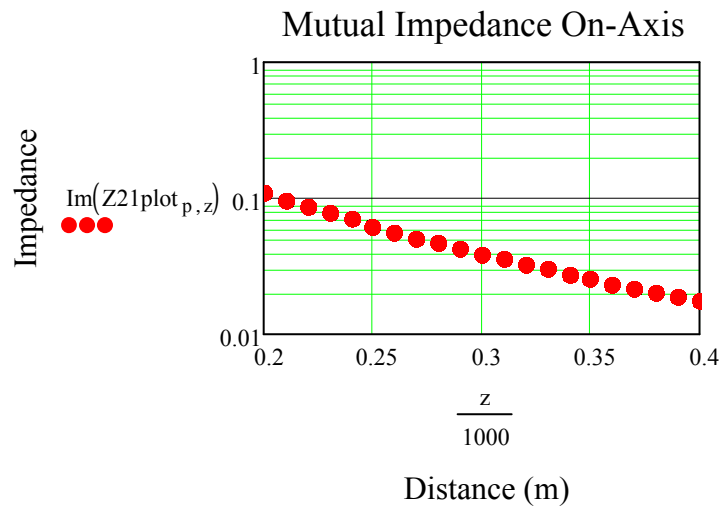
Flux: B-field components dotted with Unit Area components; All in spherical coordinates.

$$\Psi_{21_{p,z}} := (Br_{p,z} \cdot dS_{-r_{p,z}} + B\theta_{p,z} \cdot dS_{-\theta_{p,z}}) \cdot (Member_{p,z}) \quad \mathbf{I}_1 = \blacksquare$$

$$M_{\text{dyn}}_{p,z} := \frac{\sum_{p=0}^{1599} \Psi_{21}_{p,z}}{1}$$



$$Z_{21\text{plot}}_{p,z} := j \cdot \omega \cdot M_{\text{dyn}}_{p,z}$$



$$Z_{21_z} := j \cdot \omega \cdot \frac{\sum_{p=0}^{1599} \Psi_{21}_{p,z}}{1}$$

Assume wire is copper Twin-Lead line (20 gauge): Diameter=0.812mm, Dist\_apt=7.5mm

$$\sigma := 5.8 \cdot 10^7 \quad \rho_{\text{cu}} := 1.724 \cdot 10^{-8}$$

Temperature coefficient per 1deg Celsius (Human temp ~ 37C):

$$\alpha := 4.29 \cdot 10^{-3} \quad \alpha_{37} := \alpha \cdot 37 \quad \begin{array}{l} dR / R_s = \alpha \cdot dT, dR = \text{change in resistance (ohm)}, R_s = \\ \text{standard resistance according, reference tables (ohm)}, \alpha \\ \text{= temperature coefficient of resistance, } dT = \text{change in} \\ \text{temperature (K)} \end{array}$$

$$dR_{37} := \alpha \cdot dT \cdot R_s \quad dR_{37} := \alpha_{37} \rho_{\text{cu}}$$

$$dR_{37} = 2.737 \times 10^{-9}$$

Large Loop Length:

$$L_{1g} := 2 \cdot \pi \cdot a$$

$$L_{1g} = 0.628$$

Second Loop Length:

$$L_{2nd} := 2 \cdot \pi \cdot b$$

$$L_{2nd} = 0.628$$

Skin Depth (Weeks p372): Surface Resistance (Weeks p373): Schelkunoff (p339)

$$\delta := \sqrt{\frac{2}{(2 \cdot \pi \cdot f) \cdot \mu_0 \cdot \sigma}} \quad R_s := \frac{1}{\sigma \cdot \delta} \quad R_{2s} := \sqrt{\frac{\pi \cdot f \cdot \mu_0}{\sigma}} \quad R_{3s} := 2.61 \cdot 10^{-7} \cdot \sqrt{f}$$

$$R_s = 2.609 \times 10^{-4} \quad R_{2s} = 2.609 \times 10^{-4} \quad R_{3s} = 2.61 \times 10^{-4}$$

Ramo uses Low-Frequency for ratios up to 1 (or lower), High Frequency calcs are > 1. Therefore, High Frequency resistance calculations are needed:

Radius of 20 awg wire:

$$r_{\text{cu20awg}} := 0.00040$$

$$\frac{r_{\text{cu20awg}}}{\delta} = 6.144$$

High Frequency (Ramo p182, Schelkunoff p339):

$$R_{\text{hf}} := \frac{R_s}{2 \cdot \pi \cdot r_{\text{cu20awg}}} \quad R_{\text{hf}} = 0.102 \quad \text{Unis are } \Omega / \text{m}$$

Assume Ohmic resistance for loop1.

$$R_{\text{hf1st}} := R_{\text{hf}} \cdot (L_{1g}) + dR_{37}$$

$$R_{\text{hf1st}} = 0.064$$

$$R_{\text{hf2nd}} := R_{\text{hf}} \cdot (L_{2nd}) + dR_{37}$$

$$R_{\text{hf2nd}} = 0.064$$

$$Z_L := 300$$

The Total Mhos conductance may be found by taking the inverse of the total series resistance.

$$\sqrt{G_{lp1} := \frac{1}{R_{hf1st}}} \quad G_{lp1} = 15.562 \quad \sqrt{G_{lp2} := \frac{1}{R_{hf2nd}}} \quad G_{lp2} = 15.562$$

Use Schelkunoff Radiation conductance instead of Rrad  $\lambda := \frac{2.99 \cdot 10^8}{f}$   $\lambda = 299$

----- Magneto-Statics Capacitance of a small loop -----  
(Schelkunoff p 321-322)

$$C_{av} := \frac{\pi \cdot \epsilon_0}{\log\left(\frac{b}{a}\right)} \quad \text{Average capacitance between two halves of loop per unit length along the circumference (Voltage distribution across loop).}$$

$$C_{loop} := \frac{1}{3} \cdot C_{av} \cdot b \cdot \pi \quad \text{Loop capacitance:}$$

$$C_{lp1} := \frac{\pi^2 \cdot \epsilon_0 \cdot a}{3 \cdot \ln\left(\frac{a}{r_{cu20awg}}\right)} \quad C_{lp1} = 5.287 \times 10^{-13} \quad \frac{1}{j \cdot \omega \cdot C_{lp1}} = -3.01i \times 10^5$$

$$C_{lp2} := \frac{\pi^2 \cdot \epsilon_0 \cdot b}{3 \cdot \ln\left(\frac{b}{r_{cu20awg}}\right)} \quad C_{lp2} = 5.287 \times 10^{-13}$$

----- Magneto Static Inductance (loop) -----

Internal inductance contribution (Balanis p245):

$$Li1 := \frac{a}{\omega \cdot r_{cu20awg}} \cdot \sqrt{\frac{\omega \cdot \mu_0}{2 \cdot \sigma}} \quad Li2 := \frac{b}{\omega \cdot r_{cu20awg}} \cdot \sqrt{\frac{\omega \cdot \mu_0}{2 \cdot \sigma}}$$

$$Li1 = 1.023 \times 10^{-8} \quad Li2 = 1.023 \times 10^{-8}$$

(Schelkunoff p 321) Small, single turn loop with substantially uniform current (approximate inductance).

$$L_{lp1} := \mu_0 \cdot a \cdot \ln\left(\frac{a}{r_{cu20awg}}\right) + Li1 \quad L_{lp1} = 7.022 \times 10^{-7} \quad j \cdot \omega \cdot L_{lp1} = 4.412i$$

$$L_{lp2} := \mu_0 \cdot b \cdot \ln\left(\frac{b}{r_{cu20awg}}\right) + Li2 \quad L_{lp2} = 7.022 \times 10^{-7}$$



Conductance - Using Ohmic resistance and the Radiation Resistance::  $\eta = 376.819$

$$G1 := \frac{3 \cdot \pi}{2\eta} \quad G1 = 0.013 \quad G2 := \frac{3 \cdot \pi}{2\eta} \quad G2 = 0.013$$

$$G1 := 320 \pi^4 \cdot \frac{(\pi \cdot a)^2}{\lambda^4} \quad G1 = 0.013 \quad G2 := G1 \quad G2 = 0.013$$

Admittance looking in on equivalent loop circuit, prematching capacitor:

$$Y_{pre1} := \frac{1 + \frac{j \cdot \omega \cdot C_{lp1}}{2} \cdot \left( j \cdot \omega \cdot L_{lp1} + \frac{1}{G_{lp1}} \right)}{j \cdot \omega \cdot L_{lp1} + \frac{1}{G_{lp1}}} + \frac{j \cdot \omega \cdot C_{lp1}}{2 + j \cdot \omega \cdot C_{lp1} \cdot \frac{1}{G1}} \quad Y_{pre1} = 3.3 \times 10^{-3} - 0.227i$$

$$Z_{pre1} := \frac{1}{Y_{pre1}} \quad Z_{pre1} = 0.064 + 4.412i$$

Assume a variable capacitive element that can cancel the complex conjugate:

$$C_{match} := -\text{Im}(Y_{pre1}) \cdot i \quad C_{match} = 0.227i$$

The complex conjugate will add in Parallel in the Admittance(Impedance) model circuit.

$$Y_{in1} := Y_{pre1} + C_{match} \quad Y_{in1} = 3.3 \times 10^{-3}$$

$$Z_{11} := \frac{1}{Y_{in1}} \quad Z_{11} = 302.997$$

$$C := \frac{L}{(R)^2 + \omega^2 \cdot L^2}$$

$$C_{ptune} := \frac{L_{lp2}}{(R_{hf1st})^2 + \omega^2 \cdot L_{lp2}^2}$$

$$C_{ptune} = 3.606 \times 10^{-8}$$

Assume a battery Load and re-derive the equation need for modeling the admittance of the second loop. With Battery adding to the loading of the loop2, the Zin equation should change. Power calculation will have to be based on drop across battery loading, not just Ohmic resistance due to wire:

$$Y_{pre2} := \left[ \frac{1 + \frac{j \cdot \omega \cdot C_{lp2}}{2} \cdot \left( j \cdot \omega \cdot L_{lp2} + \frac{1}{G_{lp2}} \right)}{j \cdot \omega \cdot L_{lp2} + \frac{1}{G_{lp2}}} + \frac{j \cdot \omega \cdot C_{lp2}}{2 + j \cdot \omega \cdot C_{lp2} \cdot \frac{1}{G_2}} \right]$$

$$Y_{pre2} = 3.3 \times 10^{-3} - 0.227i$$

$$Z_{pre2} := \frac{1}{Y_{pre2}}$$

$$Z_{pre2} = 0.064 + 4.412i$$

Assume a variable capacitive element that can cancel the complex conjugate:

$$C_{match2} := -\text{Im}(Y_{pre2}) \cdot i \quad C_{match2} = 0.227i$$

$$C := \frac{L}{(R)^2 + \omega^2 \cdot L^2}$$

$$C_{\text{tune}} := \frac{L_{lp2}}{(\text{Rhf}_{1st} + Z_L)^2 + \omega^2 \cdot L_{lp2}^2}$$

$$C_{\text{tune}} = 7.797 \times 10^{-12}$$

The complex conjugate will add in Parallel in the Admittance model circuit.

$$Y_{in2} := (Y_{pre2} + C_{match2}) + \frac{1}{Z_L}$$

$$Y_{in2} = 6.634 \times 10^{-3}$$

$$Z_{22} := \frac{1}{Y_{in2}}$$

$$Z_{22} = 150.745$$

Now we have the following impedances of the system.

$$Z_{12_z} := Z_{21_z}$$

$$Z_{11} = 302.997$$

Mutual Z at 0.5 Radii  $Z_{21_{50}} = 3.783 \times 10^{-9} + 0.878i$

Mutual Z at 1.0 Radii  $Z_{21_{100}} = 3.783 \times 10^{-9} + 0.435i$

Mutual Z at 2.0 Radii  $Z_{21_{200}} = 3.783 \times 10^{-9} + 0.11i$

In the case of two loops in proximity, such that they can be modeled as a Linear Transducer. Loop1 and Loop2, each with two terminals for pos and neg bias. (Schelkunoff p291)

$$V_1 := Z_{11} \cdot I_1 + Z_{12} \cdot I_2$$

$$V_2 := Z_{21} \cdot I_1 + Z_{22} \cdot I_2$$

In matrix form:

$$\begin{pmatrix} V_1 \\ V_2 \end{pmatrix} := \begin{pmatrix} Z_{11} & Z_{12} \\ Z_{21} & Z_{22} \end{pmatrix} \cdot \begin{pmatrix} I_1 \\ I_2 \end{pmatrix}$$

For Admittance:

- Current at terminals are short circuited
- Yinternalcalc when all generators are open circuited.

Now, let D be:

$$D := (Z_{11} \cdot Z_{22} - Z_{12} \cdot Z_{21})$$

$$D_z := (Z_{11} \cdot Z_{22} - Z_{12}_z \cdot Z_{21}_z)$$

Next, we can solve the Matrix and re-write as such:

$$\begin{pmatrix} I_1 \\ I_2 \end{pmatrix} := \begin{pmatrix} \frac{Z_{22}}{D} & \frac{-Z_{12}}{D} \\ \frac{-Z_{21}}{D} & \frac{Z_{11}}{D} \end{pmatrix} \cdot \begin{pmatrix} V_1 \\ V_2 \end{pmatrix}$$

Writing current with respect to admittance gives us:

$$\begin{pmatrix} I_1 \\ I_2 \end{pmatrix} := \begin{pmatrix} Y_{11} & Y_{12} \\ Y_{21} & Y_{22} \end{pmatrix} \cdot \begin{pmatrix} V_1 \\ V_2 \end{pmatrix}$$

$$Y_{11}_z := \frac{Z_{22}}{D_z}$$

$$Y_{12}_z := \frac{-Z_{12}_z}{D_z}$$

$$Y_{21}_z := \frac{-Z_{21}_z}{D_z}$$

$$Y_{22}_z := \frac{Z_{11}}{D_z}$$

verification using Schelkunoff p 407:

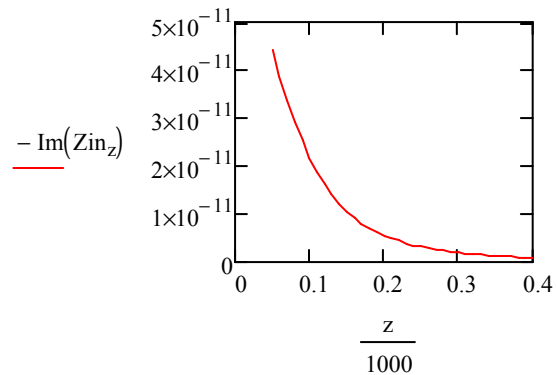
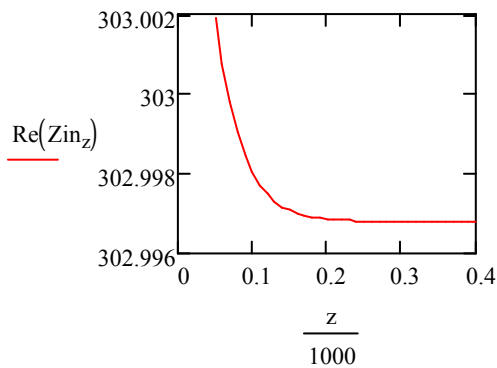
$$Y_{12b}_z := \frac{-Z_{12}_z}{Z_{11} \cdot Z_{22} - (Z_{12}_z)^2}$$

We will now assume a transmission line source will be connected to loop1, and then we can solve for I1 and V1

Assuming that loop 2 has a battery load we can solve the impedance matrix by "Collapsing a two-port to a one port network", and use this to calculate the reflection coefficient of the input terminal that the source will see. Then we will know V1 and I1 for power calculations:

ZinBy Schelkunoff:

$$Z_A := Z_{11} - \frac{Z_{12}^2}{Z_{22}} \quad Z_{in_z} := Z_{11} - \frac{(Z_{21_z})^2}{Z_{22}} \quad Z_{in2_z} := Z_{22} - \frac{(Z_{12_z})^2}{Z_{11}}$$



Impedance of the source matched to input of loop1, with loop2 at given distance:

$$Z_0 := \text{Re}(Z_{in_{50}}) + -(\text{Im}(Z_{in_{50}})) \quad Z_0 = 303.002$$

And the reflection coefficient can now be seen as:

$$\Gamma_{\text{avg}} := \frac{Z_{in_z} - Z_0}{Z_{in_z} + Z_0}$$

If the total voltage and current waves on the line can be written as :

$$V(x) := V_{\text{src}} \cdot (e^{-j \cdot \beta \cdot x} + \Gamma \cdot e^{j \cdot \beta \cdot x}) \quad I(x) := \frac{V_{\text{src}}}{Z_0} \cdot (e^{-j \cdot \beta \cdot x} - \Gamma \cdot e^{j \cdot \beta \cdot x})$$

Since the distance of transmission line is nearly 0 (negligible), we can express the equations:

$$V_x := V_{\text{src}} \cdot (1 + \Gamma) \quad \text{and} \quad I_x := \frac{V_{\text{src}}}{Z_0} \cdot (1 - \Gamma)$$

Assume a source voltage:

$$V_{\text{src}} := 1$$

$$V_{1_z} := V_{\text{src}} \cdot (1 + \Gamma_z) \quad \text{and, therefore} \quad I_{1_z} := \frac{V_{\text{src}}}{Z_0} \cdot (1 - \Gamma_z)$$

Secondary loops is tuned in parallel, therefore we use expression.

$$V_{2_z} := Z_{21_z} \cdot I_{1_z} \quad I_{2_z} := Y_{21_z} \cdot V_{1_z}$$

Power Radiated (Schelkunoff Antennas p323): NOTE: This is the power radiated by the primary loop antenna. Diaz stated to use Total Complex dipole moment of both antennas.

Power Radiated (Schelkunoff Antennas p323):

Loop 1 with 1 amp assumed source:

$$\text{Prad}_{1_z} := \frac{320 \pi^4 \cdot (\pi \cdot a^2)^2 \cdot (I_{1_z})^2}{\lambda^4 \cdot 2}$$

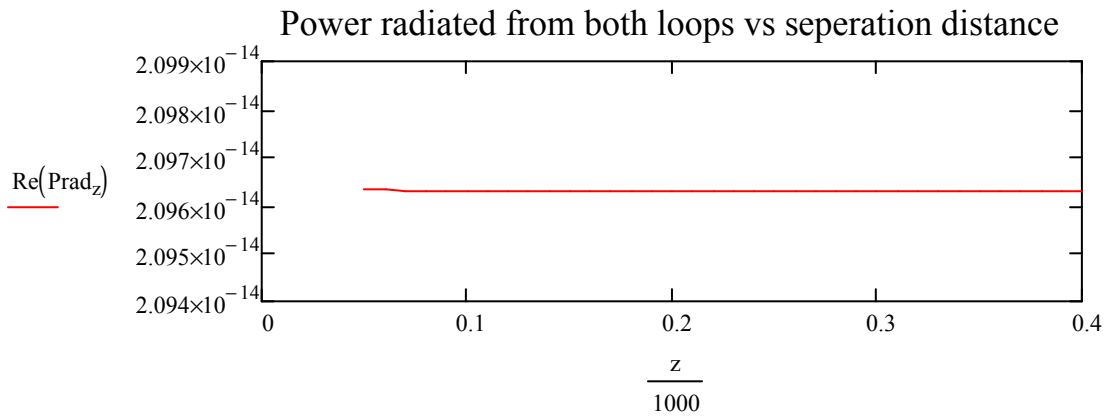
Loop 2 with calculated current (I2) using Linear Transducer Matrix:

$$\text{Prad}_{2_z} := \frac{320 \pi^4 \cdot (\pi \cdot b^2)^2 \cdot (I_{2_z})^2}{\lambda^4 \cdot 2}$$

Total Complex Dipole Moment (Assuming they are so close and behave as one antenna):

$$I_{\text{tot}_z} := I_{1_z} + I_{2_z}$$

$$\text{Prad}_z := \frac{320 \pi^4 \cdot (\pi \cdot a^2)^2 \cdot (|I_{\text{tot}_z}|)^2}{\lambda^4 \cdot 2}$$



Series-Series Power due to copper at 1MHz:

Incident Power from  
Transmission Line Source

$$P_{\text{inc}_z} := \frac{(|V_{\text{src}}|)^2}{\text{Re}(Z_0)}$$

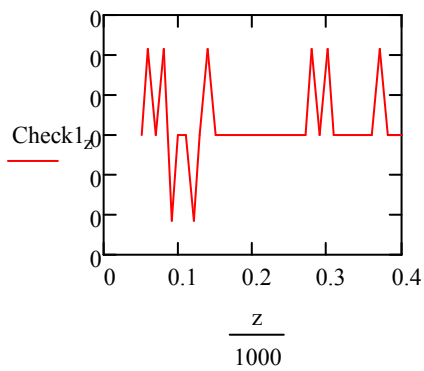
Reflected power to source

$$P_{\text{refl}_z} := \frac{(|V_{\text{src}}|)^2 \cdot (|\Gamma_z|)^2}{\text{Re}(Z_0)}$$

Power after reflection:

$$P_{\text{tr}_z} := \frac{(|V_{\text{src}}|)^2}{\text{Re}(Z_0)} \cdot [1 - (|\Gamma_z|)^2]$$

$$\text{Check1}_z := P_{\text{inc}_z} - P_{\text{refl}_z} - P_{\text{tr}_z}$$



Power Calculations broken up according to Copper loading:

$$P1ohm_z := \frac{\left( \left| V1_z \right| \cdot \frac{Z11}{\operatorname{Re}(Zin_z)} \right)^2}{Z11}$$

Second loop is tuned in parallel, therefore power calcs are performed using following expressions.

$$Pbatt_z := \frac{\left[ \left| V2_z \right| \cdot \left( \frac{Z_L}{Z22} \right) \right]^2}{Z_L}$$

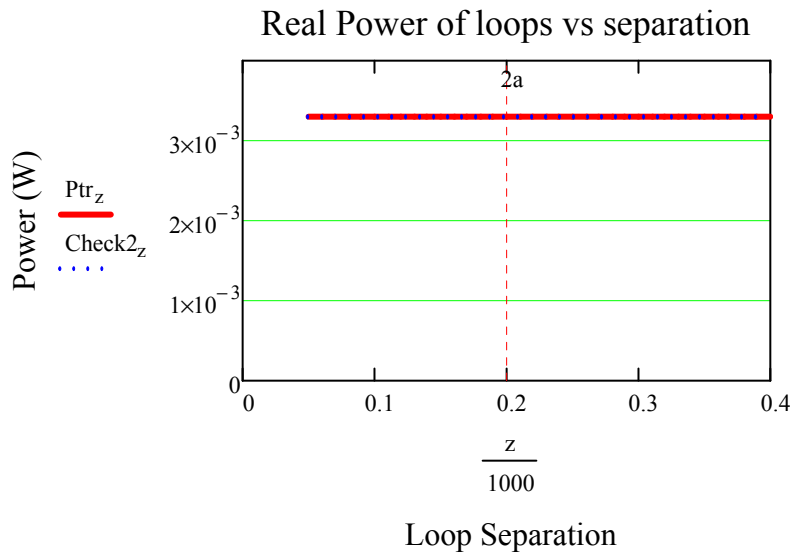
$$P2res_z := \frac{\left( \left| V2_z \right| \cdot \frac{Z22 - Z_L}{Z22} \right)^2}{Z22 - Z_L}$$

$$P2_z := \left( \left| I2_z \right| \right) \cdot \left| V2_z \right|$$

$$P2Volt_z := Pbatt_z + P2res_z$$

Compare power calculations to verify all Real Power is Accounted for in loop system:

$$Check2_z := P1ohm_z + Pbatt_z + P2res_z + Prad_z$$



$$Ptr_{50} = 3.3 \times 10^{-3}$$

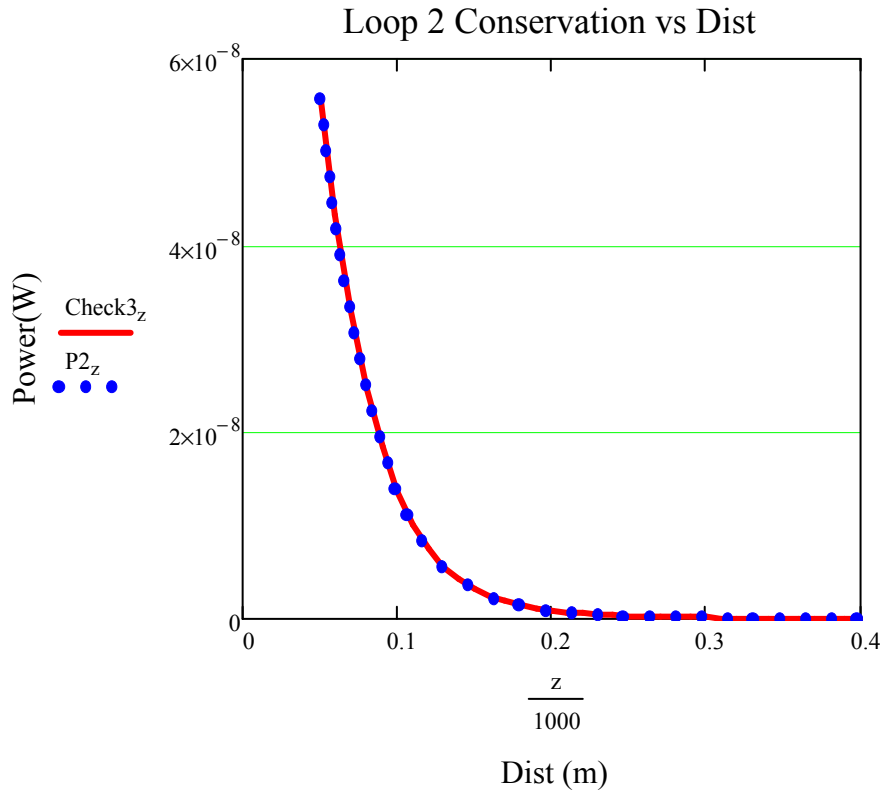
$$Pbatt_{50} = 1.108 \times 10^{-7}$$

$$Pbatt_{100} = 2.716 \times 10^{-8}$$

$$Pbatt_{200} = 1.746 \times 10^{-9}$$

Compare power calculations to verify all Real Power in Loop2 is Accounted for:

$$\text{Check3}_z := \text{Pbatt}_z + \text{P2res}_z$$



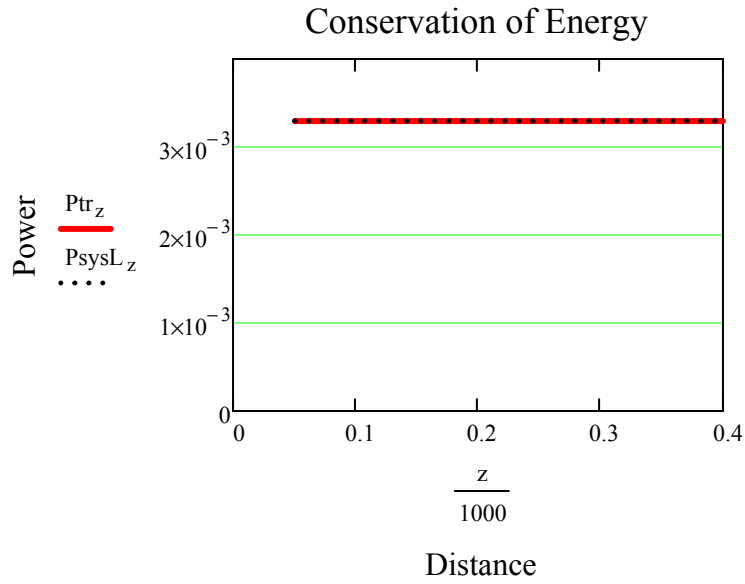
Check3<sub>z</sub> =

5.567·10 <sup>-8</sup>
4.327·10 <sup>-8</sup>
3.293·10 <sup>-8</sup>
2.472·10 <sup>-8</sup>
1.84·10 <sup>-8</sup>
1.365·10 <sup>-8</sup>
1.012·10 <sup>-8</sup>
7.527·10 <sup>-9</sup>
5.62·10 <sup>-9</sup>
4.22·10 <sup>-9</sup>
3.19·10 <sup>-9</sup>
2.428·10 <sup>-9</sup>
1.862·10 <sup>-9</sup>
1.438·10 <sup>-9</sup>
1.119·10 <sup>-9</sup>
...

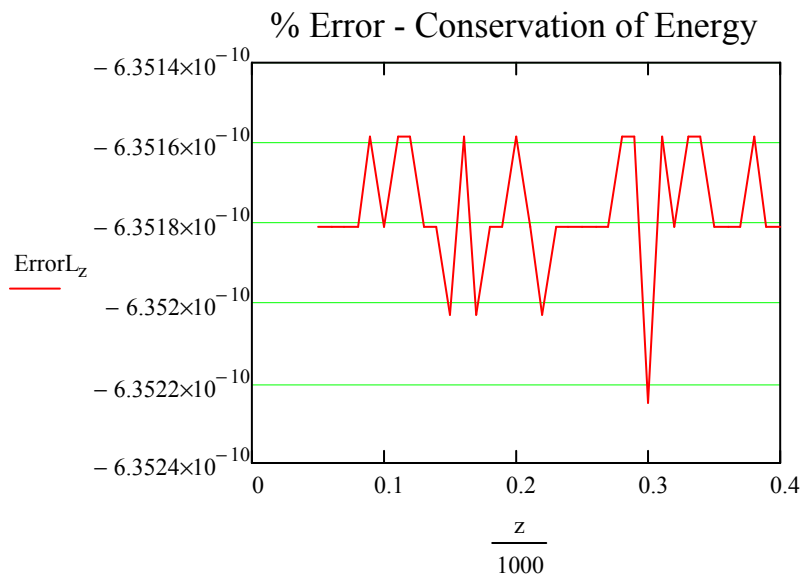


Compare power calculations of Matrix quantities and Copper Loss mechanisms to verify all Real Power is Accounted for:

$$P_{\text{sys}L_z} := (P_{1\text{ohm}_z}) + (P_{\text{batt}_z}) + (P_{2\text{res}_z}) + (P_{\text{rad}_z})$$



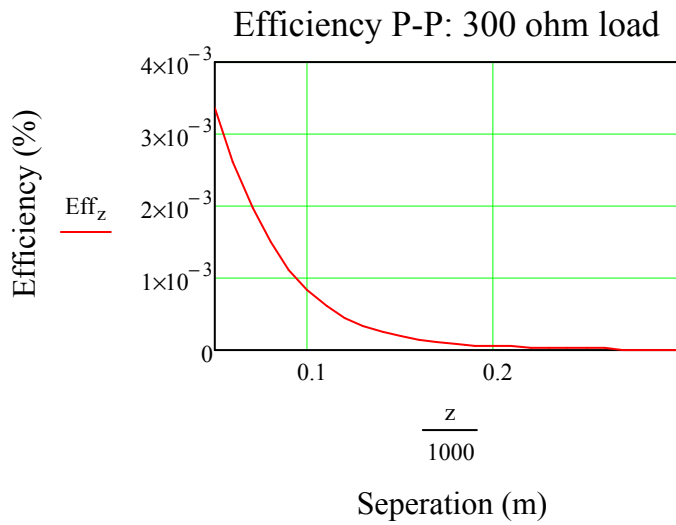
$$\text{Error}L_z := \left[ 1 - \frac{(P_{\text{sys}L_z})}{(P_{\text{tr}_z})} \right] \cdot 100$$



Let's see how much power at the source it requires for power to battery.

$$V_{\text{src}} = 1$$

$$\text{Eff}_z := \left( \frac{P_{\text{batt}_z}}{P_{\text{inc}_z}} \right) \cdot 100$$

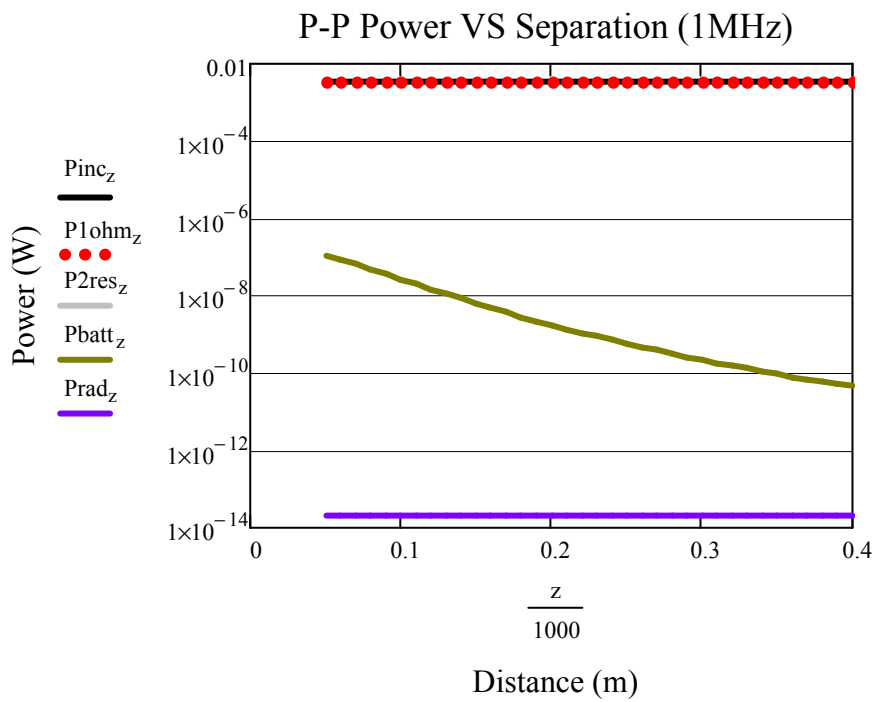
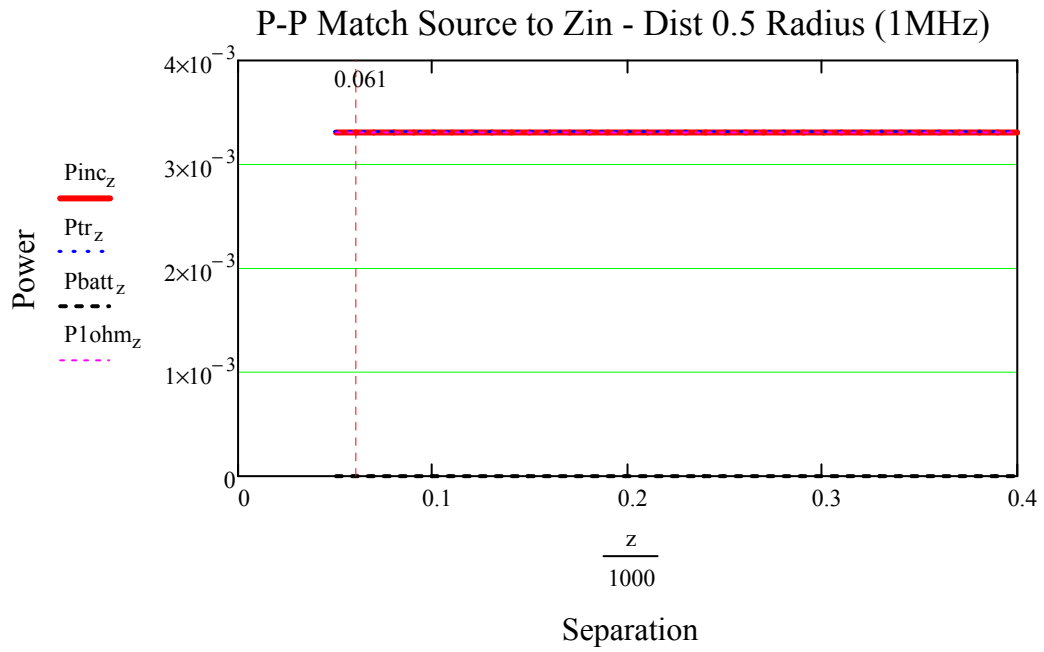


$$\text{Eff}_z =$$

$3.357 \cdot 10^{-3}$
$2.609 \cdot 10^{-3}$
$1.986 \cdot 10^{-3}$
$1.49 \cdot 10^{-3}$
$1.11 \cdot 10^{-3}$
$8.231 \cdot 10^{-4}$
$6.105 \cdot 10^{-4}$
$4.539 \cdot 10^{-4}$
$3.389 \cdot 10^{-4}$
$2.545 \cdot 10^{-4}$
$1.923 \cdot 10^{-4}$
$1.464 \cdot 10^{-4}$
$1.123 \cdot 10^{-4}$
$8.671 \cdot 10^{-5}$
$6.748 \cdot 10^{-5}$
...

$$\text{Eff}_{50} = 3.357 \times 10^{-3} \quad \text{Eff}_{100} = 8.231 \times 10^{-4}$$

$$\text{Eff}_{200} = 5.29 \times 10^{-5} \quad \text{Eff}_{300} = 6.622 \times 10^{-6}$$



Coupling coefficient at half a radius ( $z=50$ ):

For calculating equivalent circuit (NOTE must use Static Mutual and Self Inductances):

If we know that:  $M := k \cdot \sqrt{L_1 \cdot L_2}$        $M := 1.397 \cdot 10^{-7}$        $L_{lp1} = 7.022 \times 10^{-7}$

$$k := \frac{(M)}{\sqrt{L_{lp1} \cdot L_{lp2}}} \quad k = 0.199$$

